Max-Planck-Institut für Kolloid- und Grenzflächenforschung

Structure and dynamics of amorphous carbonates related to biomineralization

A neutron diffraction study

Max-Planck-Institut für Kolloid- und Grenzflächenforschung

Department of biomaterials

Univ.-Diss.

zur Erlangung des akademischen Grades
"doctor rerum naturalium"
(Dr. rer. nat.)
in der Wissenschaftsdisziplin physikalische Chemie

eingereicht an der
Mathematisch-Naturwissenschaftlichen Fakultät
der Universität Potsdam

von
Anders Christian Solberg Jensen

Potsdam, den 03.01.2018

Table of content

Abstract (English)

Amorphous calcium carbonate(ACC) is a wide spread biological material found in many organisms, such as sea Urchins and mollusks, where it serves as either a precursor phase for the crystalline biominerals or is stabilized and used in the amorphous state. As ACC readily crystallizes, stabilizers such as anions, cations or macromolecules are often present to avoid or delay unwanted crystallization. Furthermore, additives often control the properties of the materials to suit the specific function needed for the organism. E.g. cystoliths in leaves that scatter light to optimize energy uptake from the sun or calcite/aragonite crystals used in protective shells in mussels and gastropods. Lifetime of the amorphous phase is controlled by the kinetic stability against crystallization. This has often been linked to water which plays a role in the mobility of ions and hence the probability of forming crystalline nuclei to initiate crystallization. However, it is unclear how the water molecules are incorporated within the amorphous phase, either as liquid confined in pores, as structural water binding to the ions or as a mixture of both. It is also unclear how this is perturbed when additives are added, especially Mg^{2+}, one the most common additives found in biogenic samples. Mg^{2+} are expected to have a strong influence on the water incorporated into ACC, given the high energy barrier to dehydration of magnesium ions compared to calcium ions in solution.

During the last 10-15 years, there has been a large effort to understand the local environment of the ions/molecules and how this affects the properties of the amorphous phase. But only a few aspects of the structure have so far been well-described in literature. The reason for this is partly caused by the low stability of ACC if exposed to air, where it tends to crystallize within minutes and by the limited quantities of ACC produced in traditional synthesis routes. A further obstacle has been the difficulty in modeling the local structure based on experimental data. To solve the problem of stability and sample size, a few studies have used stabilizers such as Mg^{2+} or OH^- and severely dehydrated samples so as to stabilize the amorphous state, allowing for combined neutron and x-ray analysis to be performed. However, so far, a clear description of the local environments of water present in the structure has not been reported.

In this study we show that ACC can be synthesized without any stabilizing additives in quantities necessary for neutron measurements and that accurate models can be derived with the help of empirical-potential structural refinement. These analyses have shown that there is a wide range of local environments for all of the components in the system suggesting that the amorphous phase is highly inhomogeneous, without any phase separation between ions and water. We also showed that the water in ACC is mainly structural and that there is no confined or liquid-like water present in the system. Analysis of amorphous magnesium carbonate also showed that there is a large difference in the local structure of the two cations and that Mg^{2+} surprisingly interacts with significantly less water molecules then Ca^{2+} despite the higher dehydration energy. All in all, this shows that the role of water molecules as a structural component of ACC, with a strong binding to cat- and anions probably retard or prevents the crystallization of the amorphous phase.

Abstract (English)

Abstract (Deutsch)

Amorphes Calciumcarbonat (ACC) ist ein weit verbreitetes biologisches Material, das in vielen Organismen zu finden ist, beispielsweise in Seeigeln und Mollusken, wo es als Präkursorphase für kristalline Biomaterialien dient oder stabilisiert wird und im amorphen Zustand genutzt wird. Da ACC leicht kristallisiert, sind oft Stabilisatoren wie Anionen, Kationen und Makromoleküle zugegen, die eine ungewollte Kristallisation verzögern oder verhindern können. Zusätzlich kontrollieren Additive oftmals die Materialeigenschaften, um spezielle Funktionen erfüllen zu können, die der Organismus benötigt. Z.B. Zystolithen in Blättern, die das Licht streuen, um die Energieaufnahme durch das Sonnenlicht zu optimieren oder den Calcit-/Aragonitkristallen, die in den schützenden Schalen von Muscheln und Schnecken verwendet werden. Die Lebensdauer der amorphen Phase ist kontrolliert von der kinetischen Stabilität gegenüber der Kristallisation. Dies wurde oft mit Wasser verbunden, welches eine Rolle spielt für die Mobilität der Ionen und demzufolge für die Wahrscheinlichkeit der Bildung von Kristallisationskernen, die eine Kristallisation einleiten. Es ist jedoch unklar, wie die Wassermoleküle in die amorphe Phase integriert sind, ob als Flüssigkeit eingeschlossen in Poren, als strukturiertes Wasser gebunden an Ionen oder als Mischung aus beidem. Es ist ebenfalls unklar, wie dies gestört wird durch die Zugabe von Additiven, insbesondere Mg^{2+}, eines der häufigsten Additive in biogenen Proben. Von Mg^{2+} wird ein starker Einfluss auf das in ACC integrierte Wasser vermutet, vergleicht man die hohe Energiebarriere gegen Dehydration von Magnesiumionen gegenüber Calciumionen in Lösung.

Im Verlauf der letzten 10-15 Jahre wurden große Anstrengungen unternommen, um die lokale Umgebung der Ionen/Moleküle zu verstehen und wie diese die Eigenschaften der amorphen Phase beeinflusst. Jedoch wurden bisher nur wenige Aspekte der Struktur gut in der Literatur beschrieben. Dies wird zum Teil von der geringen Stabilität von ACC verursacht, wenn es der Luft ausgesetzt wird, wo es nach wenigen Minuten zur Kristallisation neigt und zum Teil von den begrenzten Mengen an ACC, welches auf traditionellen Synthesewegen produziert wird. Ein weiteres Hindernis stellte die Schwierigkeit dar, die lokale Struktur anhand von experimentellen Daten zu modellieren. Um das Problem der Stabilität und der Probenmenge zu beheben, haben einige Studien Stabilisatoren wie Mg^{2+} oder OH^- und hochgradig dehydrierte Proben verwendet und dadurch den amorphen Zustand stabilisiert, welches eine kombinierte Neutronen- und Röntgenanalyse ermöglichte. Dennoch liegt bis jetzt keine klare Beschreibung der lokalen Umgebung von Wasser in der Struktur vor.

In dieser Arbeit zeigen wir, dass ACC ohne stabilisierende Additive in Mengen hergestellt werden kann, wie sie für Neutronenmessungen benötigt werden und dass akkurate Modelle durch *empirical-potential structural refinement* abgeleitet werden können. Diese Analysen haben gezeigt, dass es eine große Bandbreite lokaler Umgebungen für alle Systemkomponenten gibt, was zu der Vermutung führt, dass die amorphe Phase hochgradig imhomogen ist ohne Phasentrennung zwischen Wasser und Ionen. Wir konnten ebenfalls zeigen, dass das Wasser in ACC hauptsächlich strukturiert ist und dass kein eingeschlossenes oder flüssigkeitsähnliches Wasser im System vorliegt. Die Analyse von amorphem Magnesiumcarbonat zeigte ebenfalls, dass es große Unterschiede in den lokalen Strukturen der beiden Kationen gibt und dass Mg^{2+} überraschenderweise mit signifikant weniger Wassermolekülen als Ca^{2+} interagiert, trotz der höheren Dehydrationsenergie. Zusammenfassend zeigt dies, dass die Wassermoleküle in der Rolle als strukturelle Komponenten von ACC, mit einer starken Bindung zu Kat- und Anionen wahrscheinlich die Kristallisation der amorphen Phase verzögern oder verhindern.

Curriculum Vitae

Anders Christian Solberg Jensen
Email: acsjensen@gmail.com
Orchid id: 0000-0003-2366-6051
Born: 05.10.1988

Education:

- July 2007 – general student exam of Horsens Gymnasium (mathematic major) with chemistry A and Mathematics A. Grade average: 8.6(Danish 13 scale, ECTS grade: C)
- September 2009-september 2012: B. Sc. Chem. Kemisk Institut, Aarhus Universitet. Grade Average: 8.6(Danish 12 scale, ECTS grade: C)
  - Bachelors (group of Henrik Birkedal) project grade: 7(Danish 12 scale, ECTS grade: C)
    - Title: Transparent aggregates of nanocrystalline hydroxyapatite that self-assemble under evaporation
- September 2012-December 2014: MSc. Chem, Kemisk Institut, Aarhus Universitet: Grade Average: 11.25 (Danish 12 scale, ECTS grade: A)
  - Chemical project (group of Henrik Birkedal) project grade: 12 (Danish 12 scale, ECTS grade: A)
    - Title: Citrate mediated self-assembly of hydroxyapatite nanoparticles
  - Master thesis September 2013-December 2014(group of Henrik Birkedal) project grade: 12 (Danish 12 scale, ECTS grade: A)
    - Title: Bio-inspired Crystal Design: Modifying inorganic materials using polymer additives
- January 2015-present: PhD student at Max Planck institute of colloids and interfaces, Potsdam Germany, Department of Biomaterials(Group of Peter Fratzl)

Summer schools:

Oxford school of Neutron science, September 2015
Niels Bohr international academy workshop on ESS Science, November 2015

Science related work:

- Student aid at Aarhus University: October 2013-December 2014
  - Teaching high school student in practical and theoretical exercises
- Student aid at teknologisk institut: October 2013-September 2014
  - Assisting the development of surface coatings for industrial applications

Awards:

- Science as Art at iNANO 2014: 3[ed] Place
- Science Slam, Tag der Wissenshaft Potsdam 2017: 2nd Place
- Excellent Oral presentation at the Fifth Annual Niels Bohr International Academy

Presentations:

Number of articles published: 4published and 3 in prep at the moment of writing
Number of Poster presentations at conferences: 12
Number of Oral presentations: 5

Publication list

Published based on my bachelor thesis:

Transparent aggregates of nanocrystalline hydroxyapatite, Cryst, Growth. Des. 2014,
A.C.S. Jensen, CJS Ibsen, D. Sutherland, H. Birkedal

Published based on my Master thesis:

Calcite nucleation on the surface of PNIPAM–PAAc micelles studied by time resolved in situ PXRD, Crystengcomm. 2015
A.C.S. Jensen, M. Hinge, H. Birkedal

Morphology-preserving transformation of minerals mediated by a temperature-responsive polymer membrane: calcite to hydroxyapatite, Crystengcomm. 2016
A.C.S. Jensen, A. Brif, B. Pokroy, M. Hinge, H. Birkedal

Published based on my doctoral thesis:

Calcite nucleation on the surface of PNIPAM–PAAc micelles studied by time resolved in situ PXRD, Chem. Mater. 2015
Z. Zou, ACS. Jensen, Y. Politi, S. Weiner, L. Addadi, P. Fratzl, WJEM, Habraken

Hydrogen Bonding in Amorphous Calcium Carbonate and Molecular Reorientation Induced by Dehydration, In review
ACS. Jensen, S. Imberti, S. Parker, E. Schneck, Y. Politi, P. Fratzl, L. Bertinetti, WJEM. Habraken

Mobility of hydrous species in amorphous calcium/magnesium carbonate, In preparation
ACS. Jensen, I. Rodriguez, Y. Politi, WJEM. Habraken, P. Fratzl, L. Bertinetti

On the structure of amorphous magnesium carbonate and mixed calcium/magnesium carbonate, In preparation
ACS. Jensen, S. Imberti, I. Rodriguez, Y. Politi, WJEM. Habraken, P. Fratzl, L. Bertinetti

Outline

The thesis has been organized into five main chapters covering the following areas:

Chapter 1 General introduction: The first chapter contains a short literature review covering the known structural information on the amorphous carbonate phases and compares some of the short coming of previous attempts to describe the structure.

Chapter 2 Principles behind Methods: This chapter covers the underlying principles behind the EPSR method and both the inelastic and elastic neutron scattering techniques used in this study.

Chapter 3 Results and discussion: This chapter covers the synthesis and structural analysis of ACC, ACMC and AMC from pdf analysis and a dynamic analysis based on inelastic neutron scattering, it also cover the discussion putting the results into context of the current literature on the subject.

Chapter 4 Summary and conclusion: Here the results are summaries and a concise final conclusion is given.

Chapter 5 Outlook: This chapter discusses some of the future prospects of structural analysis of amorphous carbonates using neutron diffraction and the opportunities now available from the high yield synthesis reported in this work.

Abbreviations

ACC	Amorphous calcium carbonate
ACMC	Amorphous calcium magnesium carbonate
AMC	Amorphous magnesium carbonate
CW	constant wavelength
EPSR	Empirical potential structural refinement
EXAFS	Extended X-ray absorption fine structure
FTIR	Fourier transformed infrared spectroscopy
FWHM	Full with at half maximum
HWHM	half with at half maximum
ICP-OES	inductively couples plasma-optical emission spectroscopy
IINS	Incoherent inelastic neutron scattering
NMR	nuclear magnetic resonance
n-pdf	Neutron pair distribution function
pdf	Pair distribution function
ppdf	Partial pair distribution function
QENS	Quasi elastic neutron scattering
SDF	Spherical density function
TGA/DSC	Thermogravimetric analysis/differential scanning calorimetry
TOF	Time of flight
x-pdf	X-ray pair distribution function

1   General introduction

In this chapter the general literature relating to this study is reviewed and key findings reported in the literature are presented in more detail. The first part gives a short introduction into the field of biomineralization and described the main materials and control mechanisms reported for in the biogenic systems. Emphasis is placed on the calcium carbonate systems as this is the main focus of this study. The second part highlights the role of amorphous calcium carbonate (ACC) in biogenic systems and the roles it plays in both biomineral formation and as a biomineral in itself. After this we delve into the literature regarding the structure and stability of synthetic ACC and the role of magnesium ions as an additive in ACC. Special interest should be given to chapter 1.3.1 as this deals with the structure of ACC which will be elaborated on in chapter 3 where the results of this study are presented. Finally a brief discussion is given on the structural analysis of disordered material.

1.1   Biomineralization

Biomineralization involves the formation of minerals in various organisms. It is described by Mann[1] as the selective extraction and uptake of elements from the local environment and subsequent incorporation into functional materials, with the whole process controlled by the organism. The biominerals found in nature are mainly composed of a small group of highly abundant minerals e.g. calcium phosphate[1] (vertebrates skeleton), silica[1] (plants, sponges, algae[2]), iron oxides (bacteria[3], limpet teeth[4]) and the main focus of this work calcium carbonate, found in the protective shells of many mollusks[5] and snails[6], in plants leaves[7], ear stones[8-9] and more. However, more exotic biominerals such as gold[10] and uranyl[11] minerals also exists. The high degree of biological control exerted on the crystallization process has allowed the organism to tailor crystals with specific polymorphs, morphology and composition to suit the needs of that specific species[1]. The ability to produce specific polymorphs is seen in several animal that can produce ACC[12], vaterite[13] or aragonite[14] instead of the thermodynamically stable polymorph calcite[15]. More detailed control can also be observed were several polymorphs are produces in close proximity of each other, e.g. in otolith of lake trout which is composed of a mixture of vaterite and aragonite[9] or in the attachment of the bivalve anomia simplex where the byssus is made of calcite and aragonite with a complex three dimensional architecture[5]. Morphological control is exhibited by most organism producing calcium carbonate minerals as seen in figure 1.1. The *habitus* of geological calcite is defined by the 104 crystal plane forming a rhombohedral shape whereas aragonite naturally forms needles (figure 1.1). This is in sharp contrast to the morphology of biogenic calcite as seen in the sea urchin (figure 1.1), where the teeth[16] and spines[17] of the sea urchin are mainly composed of calcite. The teeth are composed of highly aligned calcite crystal[18] and each spine is a single crystal with clearly different morphology from the naturally thermodynamically favored one seen in the geological calcite[19]. This is also seen in

nacre (biogenic aragonite) where the aragonite crystals are plates[20] rather than needles as observed for geological samples (figure 1.1).

The high performances of these materials are a result of the highly controlled formation mechanism performed by the organism during mineralization. How these minerals are formed is still a highly debated field, but it has been shown that ACC is commonly associated with calcium carbonate formation[21-23] and several formation mechanism involving amorphous phases have been suggested[24-25].
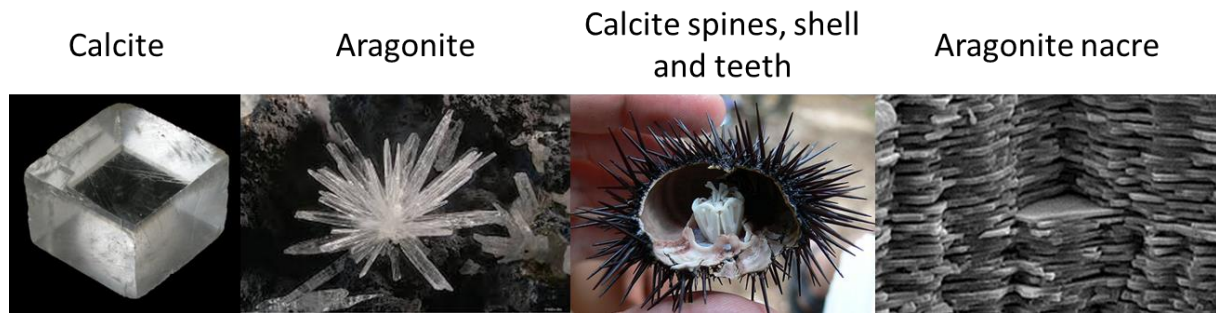

Figure 1.1 On the left the two most common geological calcium carbonate minerals calcite and aragonite are shown. On the right are two examples of biogenic mineral from the sea urchin, showing the inner tooth, the shell and spines all made from calcite, and nacre from a blue mussel showing the plate shaped aragonite crystals.

1.2 ACC in biomineralization

As mentioned in the previous section ACC plays a central role in biogenic calcium carbonate formation[1, 21-22, 26]. The amorphous nature of ACC gives several advantages over the crystalline counterpart of the calcium carbonate phase[21]. Amorphous phases often show an increased solubility[27] over the crystalline phases, making them easier to dissolve and reprecipitate when needed or to use as a precursor material that can easily be transported and crystallized at a desired site[21]. This transport can takes place with the ACC granules encased in a membrane to avoid unwanted mineralization[28]. The amorphous phase is also isotropic resulting in no preferred growth orientation or high energy facets making molding presumably easier for the ACC phase compared to the crystalline phases[21].

The biogenic ACCs are generally divided into two groups transient and stable biogenic ACC[21]. The transient form is rare in adult animals, but higher purity samples (i.e. non-crystalline) can be found in e.g. early stages of the sea urchin[29]. Several transformation mechanisms have been suggested for transient ACC[6]. The earlier studies suggested that the crystalline structure was premade in the amorphous phase based on extended x-ray absorption fine structure (EXAFS) measurements[6]. More recent studies have suggested that these minerals form via a particle accretion mechanism[25], here ACC particles are attached to the parent mineral and transforms via epitaxial growth[25]. In this case the parent crystal determines

the orientation and polymorph of the final mineral. Evidence for this mechanism has been seen in several calcium carbonate forming organisms[25, 30]. Stable biogenic ACC on the other hand remains ACC presumably indefinitely if kept under the right conditions[21]. It is especially well known from gastroliths[12] and cystoliths[7], the former functioning as calcium storage in crustaceans and the latter a light scatterer found in plant leaves[31]. This type of ACC has been shown to be structurally very similar to the synthetic ACC[32], although there are minor structural differences in the varies biogenic ACC's depending on the species[33].

The stability of both groups of biogenic ACC is suspected to arise from the multitude of additives associated with the amorphous phase and while there are many additives described for different species producing ACC, two additives are commonly used, namely magnesium and phosphate ions[21].

1.3   Structure and stability of synthetic ACC

The structure and stability of ACC have been extensively studied and several reviews have been published on the subject[15, 21-22, 34]. However, they all come to the conclusion that the structure is still not particularly well understood, nor is the role of additives. One review points out that the local environment and dynamics of water are especially poorly described as neutron scattering experiments are difficult to carry out on ACC[34]. The lack of consistent composition of the ACC reported in literature further complicates these types of studies.

1.3.1   Structure of ACC

Much like the biogenic ACC the synthetic counterparts have been grouped into two main types, disordered and proto-structured. The proto structured ACC has been described as having a local environment similar to one of the crystalline polymorphs[15, 35], while the disordered ACC does not show any resemblances to the crystal phases[36-37]. In this study the focus has been placed on the disordered ACC for several reasons:

- This type of ACC has been shown to be very similar to the stable biogenic ACC[32].
- It has been widely used in various studies on the effects of additives, especially magnesium[38-44].
- Finally it is possible to scale the synthesis to produce the large amounts of materials needed for neutron scattering experiments which are necessary in order to understand the role of water in this system (see chapter 1.5).

Henceforth the notation ACC will refer to the synthetic disordered ACC phase unless otherwise stated.

The early structural studies on ACC have relied heavily on the Ca-EXAFS measurements[6, 29, 33, 45-49]. These studies have mainly revealed the calcium-oxygen bond distance of 2.2-2.44 Å and mean coordination numbers around 7. The bond distance here strongly resembles that found in the crystalline polymorphs of 2.36-2.65 Å[50-54]. The range of mean coordination numbers reported in literature is quite wide. However, most studies suggest a coordination

number ~7 with a few studies suggesting a coordination number as low as 3.8[55] and the highest number reported is 9.0[6, 49]. The coordination number in the crystalline calcium carbonates range from six (calcite)[50] to nine (aragonite)[51] making a mean coordination number of ~4 in the amorphous phase unlikely given the size of the calcium cation[a].

The role of water has so far been studied using solid state ^{1}H-neuclear magnetic resonance (NMR) spectroscopy[36, 56-59]. This has suggested that the hydrous species in ACC consists of a mixture of rigid, mobile and fluid-like water and hydroxides[59]. However, the NMR spectra seems to differ significantly depending on the synthesis conditions at which the ACC was made, with two sharp features present for some samples[56-58] and a broad feature present for all samples[36, 59]. All the NMR spectroscopy studies agree that several hydrogen species are present in the sample and that they show different mobility. However, it is not clear if this indicates that the water exhibits confined motion (i.e. water rotating or reorientation in its local environment) or translational motion (i.e. long range diffusion) and on what time scale this occurs. ^{13}C-NMR measurements on ACC have also been reported that mainly rely on comparing with the spectrum of the crystalline calcium carbonate phases. This has shown a broad peak with a chemical shift between that of the calcite and vaterite phases suggesting a highly disordered system as expected from an amorphous phase[36-37].

While EXAFS and NMR spectroscopy have provided significant insight into the structure of ACC, it is highly specific and lack the more holistic view provided by pair distribution function (pdf) analysis[60-62], especially when both neutron and x-ray pdfs are used in combination. However, the pdf is notoriously difficult to interpret and even when this is done well, a unique structural solution can only be made for simple systems[60] (see chapter 1.5). This is also reflected in the studies that have reported on the x-ray pdf[32, 36, 38, 43, 63-66] of ACC and even on the few reporting on the neutron pdf[43, 66] that so far have not provided a clear picture of the local structure of ACC. However, several important aspects have been described. Using a combination of pdf analysis, EXAFS, XANES and NMR spectroscopy Michel et al.[36] compared the structure of ACC with the known crystalline polymorphs of $CaCO_3$ and the hydrated mineral monohydrocalcite ($CaCO_3 \cdot H_2O$). Figure 1.2A shows the comparison of the peaks found in the pdf of ACC with those of the crystalline compounds. This showed that three peaks at 2.3, 4 and 6 Å are present in all the pdfs, these correspond to the first calcium to oxygen distance, first and second calcium to calcium distances (taken from the calcite crystal structure[50]). The peaks at 2.9, 9 and 12 Å are less frequent in the crystalline phases, but still present in several of the pdfs. Based on the pdf analysis and the other mentioned techniques Michel et al. concluded that ACC could not distinctly be described by anyone of the known crystalline structure of calcium carbonate[36]. The work of Michel et al.[36] showed that a more advanced data analysis method was needed to better understand the pdf of ACC. This was attempted by Goodwin et al.[63] using the big box approach Reverse Monte-Carlo (RMC, for details on RMC, see chapter 1.5.1) on the x-ray pdf (x-pdf) of ACC. To validate the RMC method for calcium carbonate system Goodwin et al.[63] showed that they could successfully determine the structure of calcite from experimental data and has at the moment of writing published the best fit to the experimental data of ACC. This study revealed

---

[a] Not saying that four coordinated Ca cannot exist in the amorphous phases but that a mean coordination number of four is unlikely as Ca seems to prefer higher coordination number at least in the crystalline phases.

a high degree of disorder in ACC with a wide range of coordination numbers from 3 to 9 for oxygen coordinating to calcium (figure 1.2B) consistent with the amorphous nature of ACC. However the RMC method also produced large scale structures in the system, specifically a charged separated system with adjacent calcium and carbonate rich pores with a diameter of ~1 nm. This of course violates the need for charge neutrality that one would expect to be present even on the nanometer scale and indeed the structure was shown to be highly unstable using molecular dynamics simulation[64].
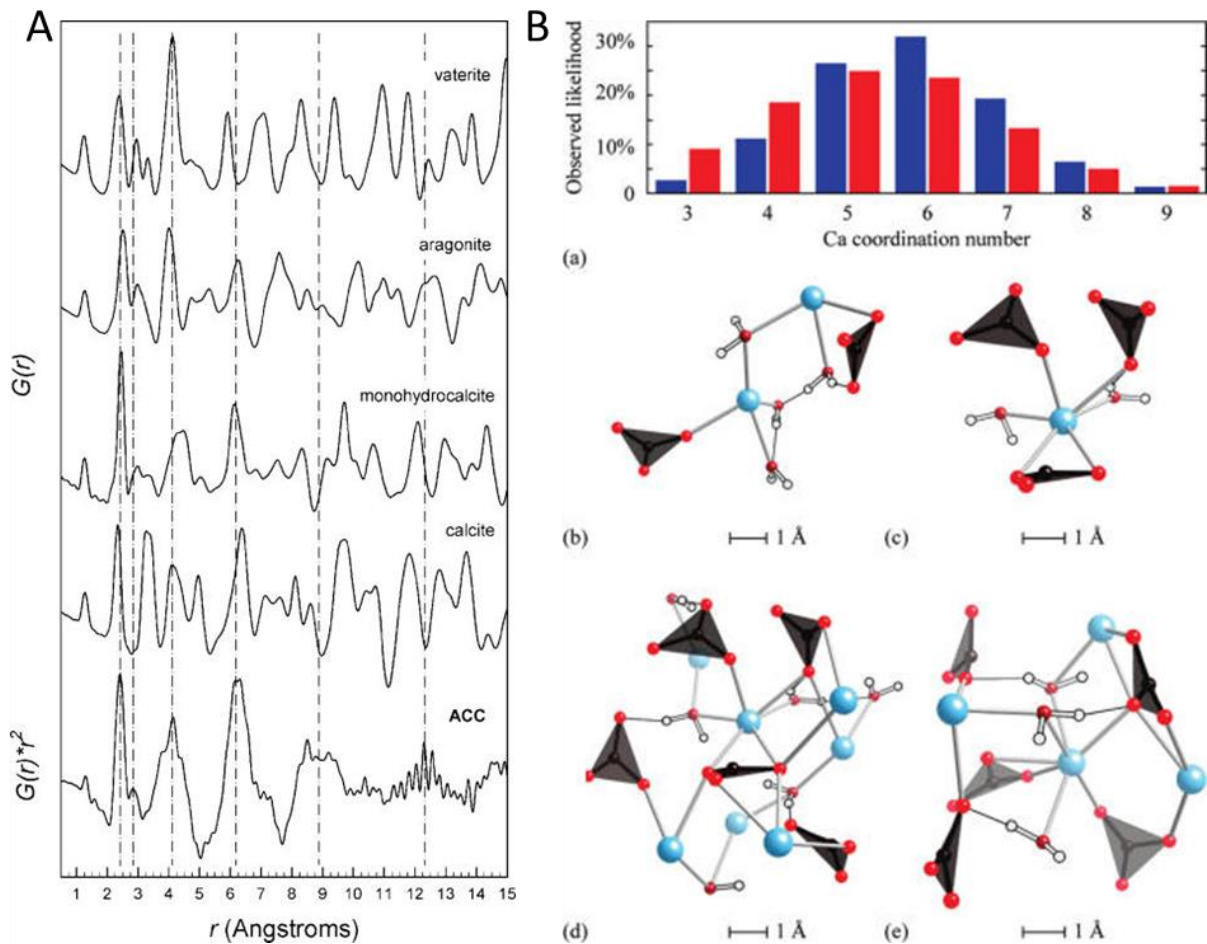
Figure 1.2: A) comparison of the pdf of ACC with the pdf of calcite (CaCO₃), vaterite (CaCO₃), aragonite (CaCO₃) and monohydrocalcite (CaCO₃·H₂O) taken from Michel et al.[36]. B) Distribution of coordination number for oxygen around calcium (a) and examples of local environments for calcium from low to high coordination number (b-e) extracted from RMC analysis of the x-ray pdf of ACC. Taken from Goodwin et al.[63]. Permissions to reprinting these figures can be found in Appendix I.

To overcome the problems with the RMC method Cobourne et al.[43] used the empirical potential structural refinement (EPSR) routine on both x-pdf and neutron pdf (n-pdf) of ACC. Since the EPSR method relies on a reference potential it can avoid high energy structure like that reported by Goodwin et al[63]. Given that neutron diffraction requires a large sample size and low exposure time they used magnesium substituted ACC with 5% Mg/(Ca+Mg) and dehydrated the sample to a hydration level of 0.25 H₂O/(Ca+Mg) to avoid crystallization.

Despite the addition of the neutron data and the more sophisticated analysis the pdf was not reproduced very well beyond the 2.4 Å peak of the Ca-O nearest neighbor distances and even here the position and intensity are slightly off (figure 1.3). As a result the model suggested some unlikely interatomic distances such as a hydrogen bond distance of 1.2 Å. Unfortunately the interatomic potentials used for this study was not published so it is unclear why EPSR did not fit the structure in this case, but as seen in chapter 3.2 EPSR is capable of reproducing the pdf and structure factor (for details on the structure factor see chapter 2.2) of ACC given the right reference potential.
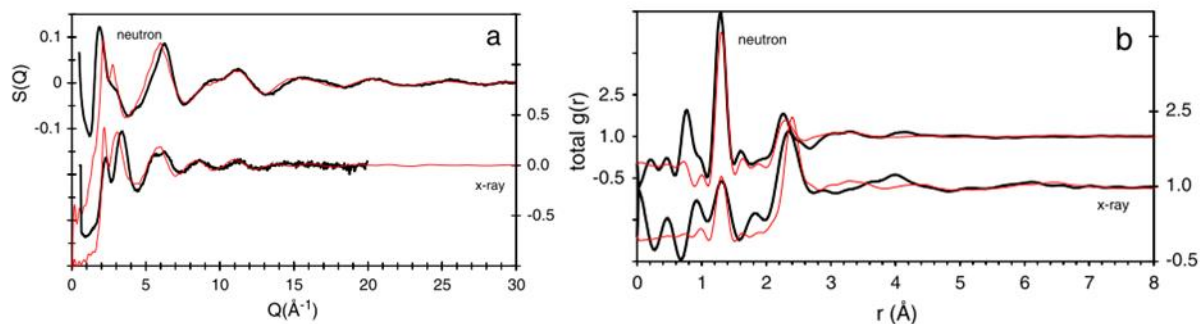

Figure 1.3: EPSR fit to the structure factor (a) and pdf (b) of ACC using both neutrons and x-rays sources taken from Cobourne et al.[63]. Permissions to reprinting these figures can be found in Appendix I.

Despite the large effort to describe the structure of ACC, most structural aspects are still unknown and the attempts to describe the pdf have so far produced models involving unrealistic structural motifs[43, 63]. However, three main results are in agreement with most structural studies mentioned above[34]:

- Nearest neighbor calcium to oxygen distance is 2.2-2.44 Å.
- Mean coordination number of oxygen around calcium in the first coordination sphere ranges from 6 to 8.
- Multiple binding sites exist for hydrous species with different mobility.

To further elucidate the structure of ACC several theoretical studies have been made[64, 67-71] dealing with both proto-structured ACC[67-68, 71] and disordered ACC[64, 69-70]. Two theoretical studies[69-70] are highlighted here as they deal with the role of water in disordered ACC, which is a key aspect of the results given in chapter 3. Malini et al[70] used molecular dynamic simulations to generated a model for ACC ($CaCO_3 \cdot H_2O$) with a density in the range of 2.54-2.63 g/cm^3 and the structure was in agreement with the three main results from experimental work as mentioned above. They reported that the Ca-O mean coordination number is composed of 1.2-1.7 oxygen from water (O_w) and 5.9-6.2 oxygen from carbonate (O_c) with a Ca-C mean coordination number of 5.2-5.5. They also reported on the diffusion constant of the water molecules, but found that it depends highly on the starting configuration of the model, giving a wide range of diffusion constants ranging from 10^{-12} to 10^{-15} m$^2 \cdot$s^{-1} based on four different starting configurations.

This was elaborated on by Bushuev et al.[69] who studied the hydration level of ACC by varying the n=H_2O/Ca ratio from 0 to 6. They found that above a hydration level of 0.9 percolations started to appear (figure 1.4). However, this was determined by the O_w-O_w distance being below a cut off value set to 3.8 Å, not taking hydrogen bonding into account. They showed that this was correlated to an increase in the water and ion mobility (figure 1.4) linking the water percolations to the stability of the amorphous phase.

It's clear that even with the addition of the theoretical studies there are still several important features that are still poorly described in the literature, especially moving from the qualitative results presented in many pdf studies[32, 36] to the quantitative results available from the more advanced analysis methods if reliable models can be produced[43, 63]. It's also clear that not only is the structure of ACC important but also the dynamics of the system are crucial to understand as these are likely to be paramount to the stability of the ACC.
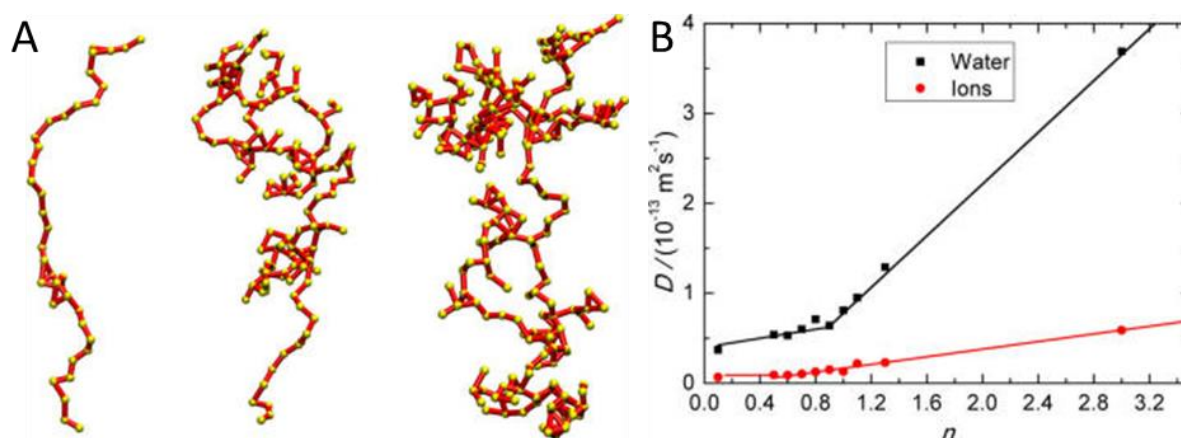

Figure 1.4: Example of percolations described by the molecular dynamics simulations and the diffusion constant for water and ions (i.e. Ca^{2+} and CO_3^{2-}) in the ACC above and below the percolation threshold of 0.9 H_2O/Ca taken from Bushuev et al.[69] Permissions to reprinting these figures can be found in Appendix I.

1.3.2 Stability of ACC

The stability of ACC generally refers to the fact that ACC is the thermodynamically least stable phase of calcium carbonate with calcite being the thermodynamically favored phase at ambient conditions[38]. However, it is also used to refer to the propensity of ACC to crystalize either in solution[27, 39-40, 65, 72-73], humidity[74], temperature[27, 59, 65, 75] or pressure[76-77] i.e. kinetic stabilization. Pure ACC ($CaCO_3 \cdot nH_2O$) is kinetically highly unstable and will crystallize within a few minutes in solution or at relatively low temperatures (~130 °C) if exposed to heat[27]. Immediately after extraction it has to be washed with ethanol in order to remove any surface water that could initiate crystallization[27, 78], but if stored under vacuum ACC will remain amorphous for several months[74].

There are many chemical and physical changes to the ACC phase that can influence the stability of the amorphous phase. Zou et al.[27] reported on the effect of particle size on the stability of ACC and found that smaller particle increased the crystallization temperature to 300 °C for the smallest particle size measured. In solution the particle size had the opposite

effect leading to faster crystallization due to an increased solubility of the ACC with decreasing particle size. The incorporation of hydroxide, often referred to as basic ACC, can also increase both the crystallization time in solution and the crystallization temperature (figure 1.5)[65, 75]. This method is especially popular for structural studies of ACC[56-58, 66], which may lead to some differences when comparing pure and basic ACC.
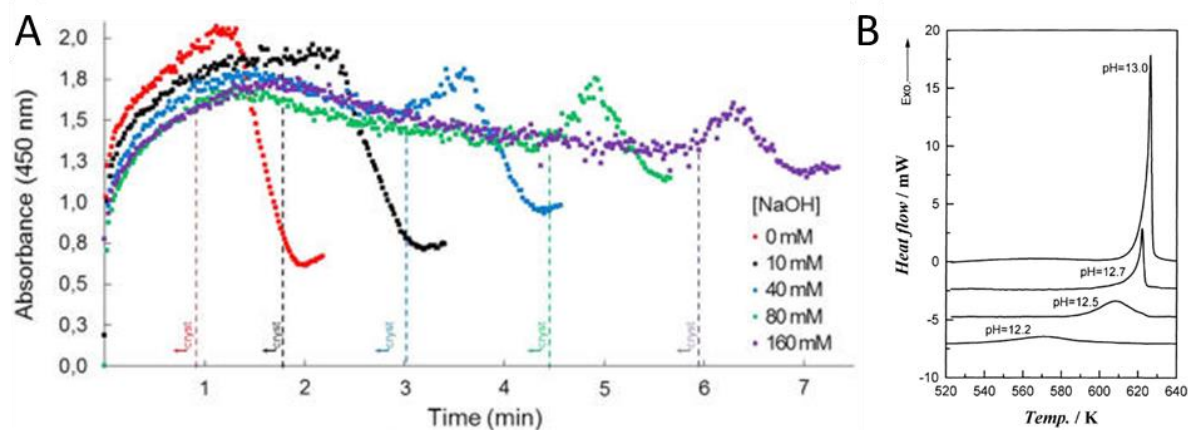

Figure 1.5: A) Nucleation time for calcite from ACC with increasing pH determined from turbidity measurements, the sudden drop in absorbance indicates crystallization, taken from Tobler et al. [65] and B) crystallization temperature of ACC with increasing pH of the carbonate solution prior to precipitation determined from differential scanning calorimetry (DSC) measurements, the exothermic peak in the DSC indicates crystallization. Taken from Koga et al.[75] Permissions to reprinting these figures can be found in Appendix I.

Similar to the hydroxide the incorporation of many organic[79-81] and inorganic compounds[39-40, 79, 81] or surface coating[56, 82] of the ACC particle will also greatly increase the stability of ACC both in solution and during heating. Of special interest to this is the effect of Mg^{2+} which is near omnipresent in the biogenic ACC samples and covered in the following section.

1.4 The role of Mg in ACC and its effect on calcium carbonate formation

The role of magnesium in calcium carbonate formation has mainly focused on synthetic samples[38-43, 83-87]. It has been shown that this follows a simple reaction scheme depending on the ratio of Magnesium to calcium given here as the Mg/(Mg+Ca) ratio.

At 0% Mg the following reaction occur[72-73]:

$$Na_2CO_3(aq) + CaCl_2(aq) \rightarrow ACC(s) \rightarrow vaterite(s) \rightarrow calcite(s)$$

Increasing the Mg concentration to 10 % inhibits the vaterite formation and Mg substituted calcite is formed directly from amorphous calcium/magnesium carbonate (ACMC)[39]:

$$Na_2CO_3(aq) + CaCl_2(aq) + MgCl_2(aq) \rightarrow ACMC(s) \rightarrow calcite(s)$$
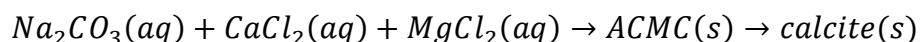
At 15%-25% Mg, calcite and vaterite formation is inhibited and the nucleation time is increased from ~5-10 min to ~2 hours given the following reaction[40, 83]:

$$Na_2CO_3(aq) + CaCl_2(aq) + MgCl_2(aq) \rightarrow ACMC(s) \rightarrow monohydrocalcite(s)$$
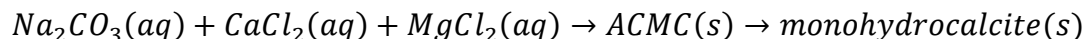
Above 25% Mg, hydromagnesite ($Mg_5(CO_3)_4(OH)_2 \cdot 4H_2O$) starts to form after monohydrocalcite formation, presumably via an amorphous magnesium carbonate (AMC) phase[40, 83]:

$$Na_2CO_3(aq) + CaCl_2(aq) + MgCl_2(aq) \rightarrow ACMC(s)$$

$$\rightarrow monohydrocalcite(s) + AMC(s) \rightarrow monohydrocalcite(s) + hydromagnesite(s)$$

As evident from the above reaction equations, Mg^{2+} has a complex interaction as inhibitor for the various calcium carbonate polymorphs. A more elaborate study by Nish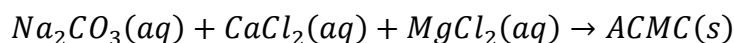iyama et al.[41] showed that this can be further complicated by varying the ratio of Ca/CO_3 (figure 1.6). It is unclear if the complex chemistry of the mixed calcium/magnesium carbonate systems originate in structural changes in the amorphous phase[67] or simply from crystal growth and nucleation inhibition of the calcite and vaterite phases[85, 88]. However, the ability of Mg to stabilize the ACC is clear[40, 81], which also plays a major role in the biogenic ACCs[47] and has been linked to the higher dehydration energy of magnesium compared to calcium[47, 87, 89].
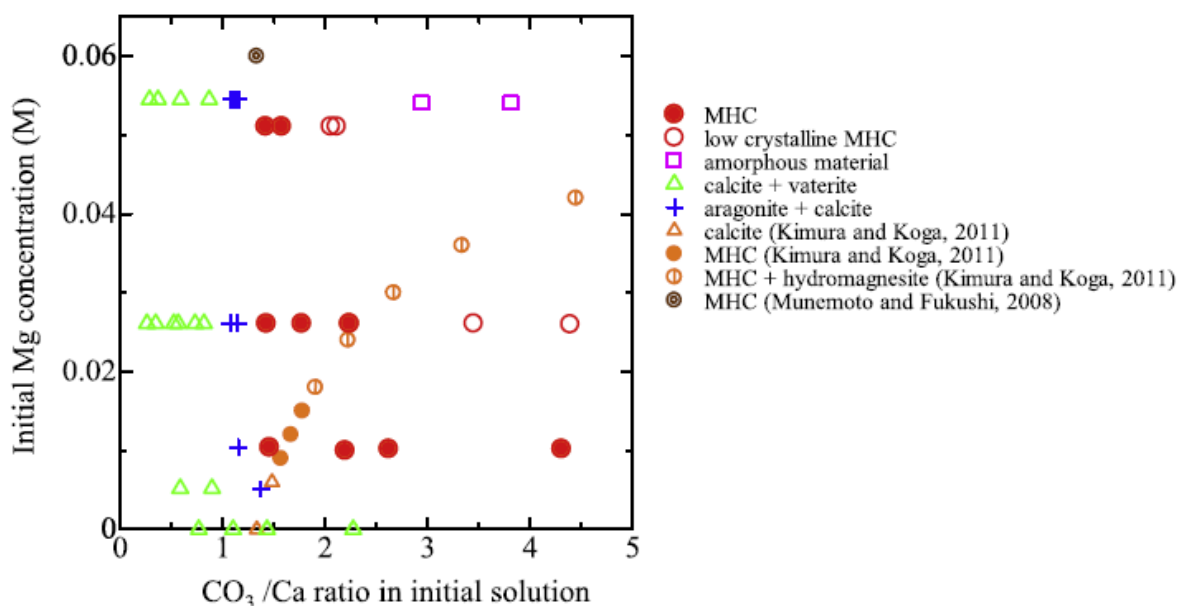
Figure 1.6: Distribution of various calcium carbonate minerals formed after 24 hours in solution by varying the Ca/CO₃ ratio and the magnesium concentration taken from Nishiyama et al[41] with references to Kimura et al.[83] and Munemoto et al.[90] Permissions to reprinting these figures can be found in Appendix I.

In the amorphous phases the local environment of magnesium is still poorly understood. EXAFS studies have shown that the Mg-O distance is ~2.1 Å with a coordination number around ~6[47] similar to what has been reported for the crystalline magnesium carbonates which all have a coordination number of 6 with a octahedral coordination[50, 91-94]. Detailed

Thermogravimetric analysis (TGA) and pdf analysis of amorphous $Ca_{1-x}Mg_xCO_3 \cdot nH_2O$ (0 < x <1; 0.25 < n < 1.8) suggested a solubility limit of 50% Mg in ACC with higher concentration resulting from a mix of AMC and ACMC with 50% Mg[38], although this has been disputed by NMR spectroscopy studies[42]. The pdf of AMC and ACMC did not reveal any insight into the structure as the pdf was too difficult to analyze beyond 2.3 Å of the Ca-O bond distance, without a detailed structural model of ACC and AMC[38]. The first detailed structural study of AMC was reported by White et al.[84] on $MgCO_3 \cdot 3H_2O$, which showed a distribution of coordination environments of Mg ranging from 4 to 6. They also found that small water pores were present in the structure but did not quantify the size or dynamic nature of the water in the pores.

The available structural information on AMC and ACMC are equivalent to that of ACC with the cation to nearest neighboring oxygen distance and coordination number well known, but structural details beyond the first cation-O coordination sphere have not been well-described. Only the study of White et al.[84] present some insight into the role of water in AMC, where they find small water pores at elevated hydration level (3 H_2O/Mg). Also, while for the ACC the ratio of Ca/CO_3 has been thoroughly investigated[27, 65], in the case of AMC, the actual composition of the solid has not been discussed in literature, as in most of these studies a rigorous stoichiometric analysis is absent. For example, at least two works report TGA measurements showing a CO_3/Mg ratio ~0.8[38, 95], while the composition is still indicated as $MgCO_3 \cdot nH_2O$. In other studies the TGA analysis has either not been performed or not reported. The cause of this low CO_3/Mg ratio is discussed in chapter 3 were it is shown that magnesium ions do not coprecipitate with carbonate ions alone but also coprecipitates with hydroxide ions and that this has to be taken into account for both AMC and ACMC.

1.5 Structural analysis of amorphous materials

We now changed gears a bit and move away from the structural studies that have already been published on the amorphous carbonates and instead discuss the methods which are available for performing structural analysis on disordered systems. Any structural study relating to an amorphous or crystalline material is faced with the same problem, how to represent the structure of the ~10^{23} atoms that make up a material as simple and clear as possible[62]. For the crystalline sample this is done very efficiently by the construction of the unit cell, where only the relative position of the unique atoms needs to be determined and the symmetry of the crystal. From this the entire crystal can be described via point and translational symmetry[96]. E.g in the case of calcite only the relative positions of one Ca, one O and one C are necessary to describe the entire structure (figure 1.7)[50].
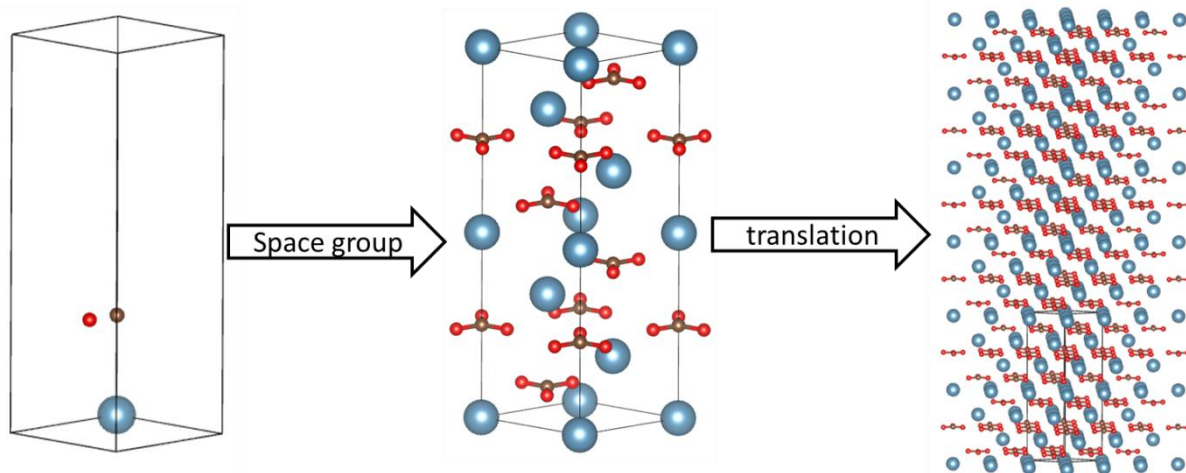
Figure 1.7: The three unique atoms of the calcite structure shown on the left (Ca=blue, O=red, C=Brown), via the space group R-3c the whole unit cell can be filled with atoms(middle) and then the translational symmetry, known from the unit cell dimensions, can generate the entire crystal, a subsection of which is shown on the right.

For an amorphous material this is more difficult as point and translational symmetries are absent. However, we still need to condense the structure down to the unique elements or to be more precise the statistically most likely structural motifs as every atom in an amorphous system are in principle unique compared to all other atoms[62]. For this there are three main techniques: EXAFS, NMR spectroscopy and pdf analysis. EXAFS analyses are specific to a given element and can provide bond distances and coordination numbers for the element in question. However, only the first few coordination spheres can generally be measured and for ACC only the first Ca-O coordination sphere has been well described using this method[29, 33, 45]. Similarly NMR spectroscopy is element specific, but unlike EXAFS works well for H and C. However, it is difficult to get quantitative information from NMR spectroscopy, but not impossible as shown by Singer et al.[64] who determined the Ca-O distance in ACC from ^{43}Ca-NMR spectroscopy. In contrast pdf analysis is in principle sensitive to all the elements at once and is a direct measurement of the interatomic distances[62]. Furthermore using advanced analysis techniques quantitative information can be extracted based on a computer model[60, 62, 97].

Several ways of interpreting the pdf of ACC have been attempted, the most common of which has been the comparison between the pdf of ACC and that of the crystalline compounds (figure 1.2A)[32, 36, 65]. This approach, while simplistic, has a high risk of misinterpreting the data as with the work of Tobler et al.[65] who reported an increase in a peak at 3.8 Å when adding hydroxide to ACC and correlated it with the Ca-Ca pair of vaterite present at ~4 Å[54] but could just as easily originate from the Ca-OH-Ca motif in $Ca(OH)_2$ with a Ca-Ca distance of 3.6 Å[98]. The other major drawback of this approach is that it is inherently qualitative.

To get quantitative results a more mathematical approach is needed[60, 62]. This involves deconvoluting the pdf into the partial pdfs (ppdf) of which there are:

$$N_{ppdf} = \frac{N_\alpha(N_\alpha+1)}{2} \tag{1.1}$$

Where N_{ppdf} is the number of ppdfs and N_α is the number of unique atoms in the system. For small N_α, it is possible to precisely determine the ppdfs by measuring N_e number of pdfs with different contrasts if $N_e > N_{ppdf}$[99]. Measuring the pdf with several contrasts can be done either by neutron diffraction with isotope substitution (NDIS) due to the change in the neutron scattering length of different isotopes and by anomalous x-ray diffraction (AXD) taking advantage of the change in x-ray scattering length close to an absorption edge. However, NDIS requires a large difference between the scattering length of different isotopes for the same element and AXD is only possible for element heavier then zinc in the periodic table as the diffraction pattern has to be measured to at least 10 $Å^{-1}$ which is limited by the energy associated with the absorption edge of the element in question[60]. As evident from equation 1.1 the number of pdf measurement needed to deconvolute the pdf for systems with $N_\alpha > 2$ is in practice difficult if not impossible as the number of NDIS experiments that can be made is limited by the availability of suitable isotopes and AXD will not be suitable for pdf analysis for many light elements[60].
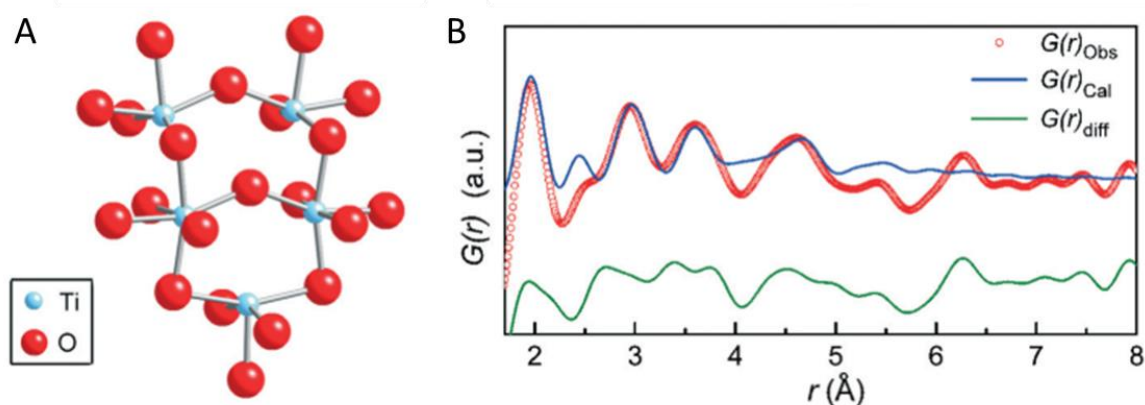
Figure 1.8: Example of a Small box model for amorphous TiO$_2$ precursor for anatase. With the proposed structure (A) and the fit to the experimental data (B). Taken from Mi et al.[100] Permissions to reprinting these figures can be found in Appendix I.

To overcome this challenge atomistic models are necessary[62]. These models all involve generating a box of atoms to represent the structure of the system using various methods to refine the structure against experimental data. These come in two forms, small box and big box approaches[62]. The small box approach is best known from PDFfit[101] which is essentially equivalent to a rietveld refinement as the atomic position, unit cell, atomic displacement parameters and more can be refined in a non-linear least square method to achieve the best fit to the experimental pdf[b]. This approach has been very successful when combined with time resolved pdf data measuring the crystallization process and extrapolating the structure of the crystal into the amorphous systems. This has mainly been performed for metal oxides[100, 102-103]. However, it does have several disadvantages, since the systems has to be very homogenous so that the structure can be represented by a unit cell sized model (a few cubic nanometers at the most, see figure 1.8). In order to utilize the time resolved data the system has to go from an amorphous to crystalline state in a homogenous manner and not via a point

---

[b] But using the total scattered signal (i.e. the pdf) and not just the Bragg peaks as in rietveld refinement

nucleation and growth process. For ACC[104] it is unclear if this is valid especially taking into account that ACC can crystallize in several ways[27, 72, 74, 76], none of which are clearly favored in the natural systems. Therefore this approach was deemed unfit for this study and a big box approach was preferred.

1.5.1 The big box approach

The Big box approach uses a large box of atoms, typically several thousand atoms, to represent the structure of the material (figure 1.9). The key of this method is to constrain the system as much as possible using data from additional techniques. The main constrain in any such method is the hard sphere assumption, insuring that atoms do not overlap. Experimental data can further constrain the system, especially density and composition are key constrains that must be placed on the model.
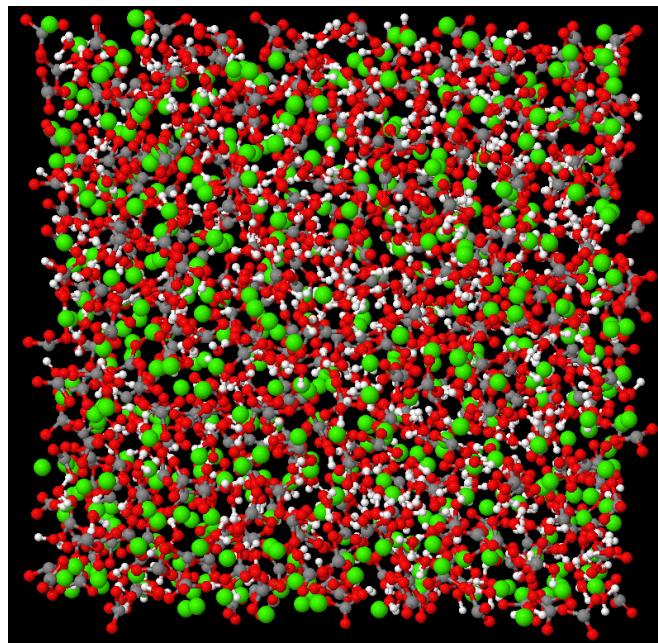
Figure 1.9: A typical big box size, in this case ACC with a composition of $CaCO_3\ 1.1H_2O$ containing 4150 atoms within a cube with a side length of 3.52 nm.

For reverse Monte-Carlo (RMC) these are the only constraints needed, the method then relies on the data to constrain the refinement to reach the correct solution[105]. The RMC method uses a standard Monte-Carlo approach to move atoms around in the box, i.e. random motion/rotation of a single particle/molecule. The move is then accepted if the χ^2 (goodness of fit) is lowered or if the move increases the χ^2 it may be rejected or accepted with a probability P given by:

For a regular Monte-Carlo:

$$P = \exp\left(-\frac{\Delta U}{kT}\right) \tag{1.2}$$

And for RMC:

$$P = \exp\left(-\frac{\Delta \chi}{kT}\right) \tag{1.3}$$

Where U is the energy of the system kT is the Boltzmann constant times the temperature and here determines how many "bad" moves are accepted and in RMC is usually set by the user to avoid local minima. This process is done iteratively and eventually the χ^2 becomes stable at the best possible fit given the constraints[105]. The strong reliance on the data in the RMC method makes it unbiased in its results. However, this strength is also a major weakness since unphysical results can be produced especially if the data is insufficient to constrain the refinement, which is especially the case when N_α in equation 1.1 is high[63-64]. To avoid unphysical results the model can be run alternatingly through a molecular dynamics or density function theory simulation and an RMC program to ensure that the system is minimizing both the energy and goodness of fit[84].

The most successful big box approach for liquids[106-108] and glasses[97, 109-110] is likely the empirical potential structural refinement program (EPSR)[61, 110-114]. EPSR works much like RMC, except that it uses equation 1.2 instead of 1.3 to accept or reject changes to the structure, described in detail in chapter 2.3. This introduces an extra constraint via the inter/intra-atomic potential insuring that the structural motifs present in the model are low energy structures (e.g. no direct contact between cations). Since the RMC introduces the data via equation 1.3 the EPSR program need an alternative route to refine the model against the data. This is done by generating an empirical potential via comparison of the structure factor *S(Q)* of the calculated structure and the experimentally determined *S(Q),* the math behind how this is done is explained in chapter 2.3. The main advantage of this is that all the refinement takes place in the same program at the same time, instead of generating a model that is first minimized in χ and then in energy, where the two methods may not converge on the same structure. However, this is not without disadvantages, since several significantly different structures may give equally good fits to the same data[109, 112] and comply with the same constraints making it is difficult to determine which one is the better model. At this point supporting information may be needed such as NMR or vibrational spectroscopy to determine if one is more valid compared to the other[109]. In any case supporting data should, when possible, be considered before drawing conclusions from big box models of any type. Since the EPSR model is used extensively in this study more details are presented in chapter 2.3 and will not be discussed further in this chapter.

1.6   Open questions on the structure and water dynamic of ACC and ACMC

The structural studies that have so far been made on ACC have left a large amount of unanswered questions, especially concerning the light elements such as hydrogen that are essential for hydrogen bonding and will be essential to adequately describe the water environment in the system. Given the large amount of stabilizers present in biogenic samples it is also important to understand how common additives such as magnesium ions affect the local structure of the ACC.

To address this problem combined neutron and x-ray total scattering with computer modeling was used. This allowed for a full deconvolution of the pdf into the partial pair distribution functions, making it possible to retrieve qualitative and quantitative information concerning the structure of ACC for all elements. A similar analysis was made for amorphous magnesium carbonate and a mixed amorphous calcium magnesium carbonate phase elucidating the effect of magnesium on the ACC structure and providing a clearer picture of the magnesium-water interaction that has been suspected to be responsible for the stabilizing effect of magnesium ions.

However, the pdf represents the time averaged structure and as such is only related to the structure of the material and not to the dynamics present in the structure. This can instead be addressed using the dynamic structure factor which is available for hydrous species from inelastic neutron scattering, revealing the timescale and geometry of motion on the ps time scale where atomic diffusion takes place. Using both the time averaged structure and the dynamic structure factor the state of water molecules in the system can be described in much greater detailed compared to only using one of the approaches.

Before these questions could be addressed some technical problems had to be resolved. Most importantly: is it possible to make large quantities of ACC needed for neutron diffraction without the addition of stabilizers and at a hydration level relevant to biogenic samples (i.e. 1 H_2O/Ca^{2+})? It turns out that this can be done with some optimization to existing protocols[27, 75] as described in chapter 3.1. The second problem we were faced with was: can big box models be used to describe the local structure without the presence of unphysical bond distance or charge separation that have been present in previous attempts to model this system? Using the ESPR program this turned out to be the case with an excellent fit to the experimental data of ACC comparable to the goodness of fit reported from the RMC analysis[63].

2 Principles behind methods

This chapter covers the theoretical background behind the methods used in this thesis. The first section is devoted to the pair distribution function (pdf) and describes the necessary steps to obtain the pdf from the diffraction measurement. Chapter 2.1.2 shortly discusses the difference between the available instruments for neutron pdf measurements and emphasis why time of flight neutron diffraction is preferable for the samples under investigation in this study. We then delve into the analysis routine EPSR and the routines used to extract results from the final structure. Finally the fundamentals behind the neutron spectroscopy techniques IINS and QENS are explained and the method to analysis these data is briefly discussed.

2.1 The pair distribution function: theory and experiment

Pdf analysis has become increasingly popular during the last decades, especially after the development of rapid acquisition x-pdf[62, 115]. The next two sections are dedicated to the theory behind pdf analysis, the definition used in this study and to the choice of beam line, which has little meaning for x-pdf but is very important for n-pdf.

2.1.1 From diffraction experiment to the pdf
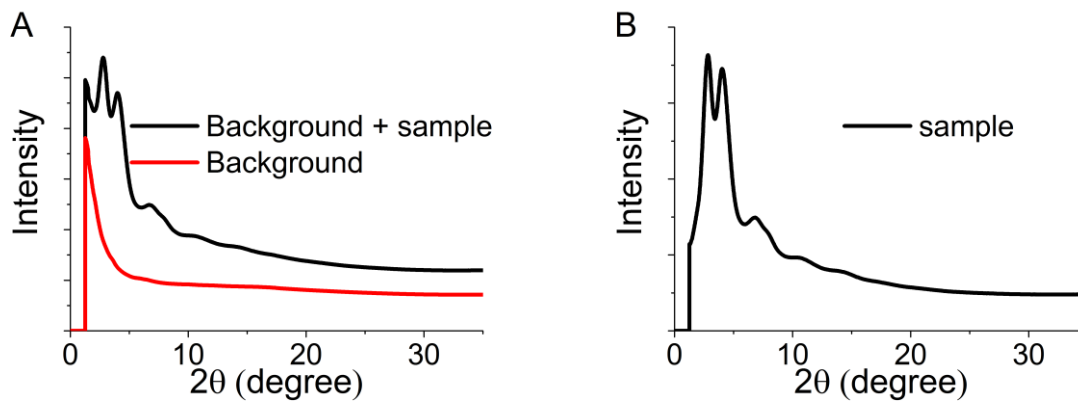
Figure 2.1: A) Plots of the total intensity (I(Q)) in black and background ($I_{nonsample}$) in red from equation 2.1 for ACC measured at the x-ray beamline ID11(ESRF). B) I_{sample} of ACC after subtraction of the background.

The data reduction transforming the data from the diffraction signal to the pdf varies between the available software[116], in this study the software GUDRUN[117] was used, since this is essential for data reduction for the SANDALS instrument which was used for the neutron experiments. The data reduction is described in detail by Hannon et al.[118] and Keen[116], the main steps are described in the following section

Any pdf measurement will always begin with a diffraction experiment, where the intensity I must be measured as a function of the scattering vector Q and is given by[c] (figure 2.1A):

$$I(Q) = I_{sample}(Q) + I_{nonsample}(Q) \qquad (2.1)$$

And:

$$Q = \frac{4\pi sin\theta}{\lambda} \qquad (2.2)$$

Here λ is the wavelength of the neutron or x-ray beam and θ is the scattering angle. Since any type of matter will diffract neutrons or x-ray, including air in the beam path, it is important to remove the background ($I_{nonsample}(Q)$) before any further data reduction can be performed. This leaves $I_{sample}(Q)$ (figure 2.1B) which can be written as equation 2.3 using the static approximation.
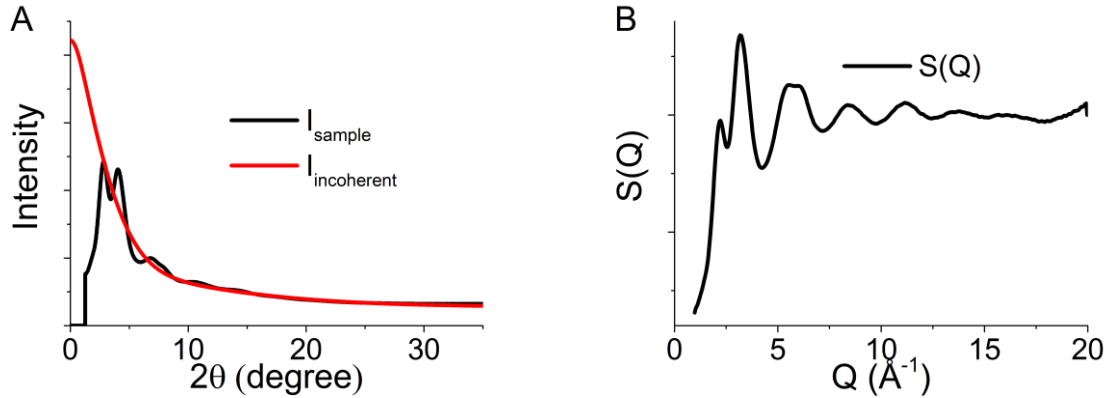
Figure 2.2: A) plot of the total scattered intensity I_{sample} from ACC and the incoherent term from equation 2.3. B) The final structure factor or S(Q) from equation 2.6 obtained by subtracting the incoherent term from the total scattering intensity shown in A. The S(Q) here is normalized to $\langle b^2 \rangle$. Note that the S(Q) is oscillating around zero, while the incoherent term is always positive.

Here the differential scattering cross section (figure 2.1B) is separated into the incoherent scattering term $S_i^S(Q)$ and the coherent scattering term $S_{ij}(Q)$, which is the part that relates to the pdf.

$$I_{sample}(Q) = \frac{1}{N}\frac{d\sigma}{d\Omega} = \sum_{i=1}^{n}\left(\overline{b_i^2} - \overline{b_i}^2\right)S_i^S(Q) + \sum_{i,j=1}^{n}\overline{b_i}\,\overline{b_j}S_{ij}(Q) \qquad (2.3)$$

Where N is the number of atoms in the material, σ is the scattering cross section, Ω is the solid angle, b_i is the scattering length of the ith atom, $\sigma_i^{coh} = 4\pi\overline{b_i}^2$ and $\sigma_i = 4\pi\overline{b_i^2}$ is the coherent and total scattering cross section respectively with $\sigma_i^{inc} = \sigma_i^{tot} - \sigma_i^{coh}$, $S_i^S(Q)$ is equal to the proportion of the ith species in the material c_i and the coherent scattering term can be written as:

---

[c] In theory $I(Q)$ should be measured to infinitely high Q. However, in practice the $I(Q)$ has to be measured to at least 10 Å^{-1}, but higher is preferable.

$$S_{ij}(Q) = c_i c_j \left[A_{ij}(Q) - 1 \right] + c_i \delta_{ij} \tag{2.4}$$

Where $A_{ij}(Q)$ are the partial structure factors and δ_{ij} is a dirac delta function. Equation 2.3 can then be rewritten as:

$$\frac{1}{N} \frac{d\sigma}{d\Omega} = \sum_{i,j=1}^{n} c_i c_j \overline{b_i}\, \overline{b_j} \left[A_{ij}(Q) - 1 \right] + \sum_{i=1}^{n} c_i \overline{b_i^2} \tag{2.5}$$

If c_i and b_i are known, the incoherent term ($\sum_{i=1}^{n} c_i \overline{b_i^2}$) can be corrected for (figure 2.2A) and this leaves the coherent scattering term also known as the total scattering structure factor (figure 2.2B).

$$S(Q) = \sum_{i,j=1}^{n} c_i c_j \overline{b_i}\, \overline{b_j} \left[A_{ij}(Q) - 1 \right] \tag{2.6}$$

S(Q) can then be converted into the pdf, *G(r)* via Fourier transform and vice versa.

$$S(Q) = \rho_0 \int_0^{\infty} 4\pi r^2 G(r) \frac{\sin(Qr)}{Qr} dr \tag{2.7}$$

and

$$G(r) = \frac{1}{(2\pi)^3 \rho_0} \int_0^{\infty} 4\pi Q^2 S(r) \frac{\sin(Qr)}{Qr} dQ \tag{2.8}$$

The pdf is related to the ppdf, $g_{ij}(r)$ as

$$G(r) = \sum_{i,j=1}^{n} c_i c_j \overline{b_i}\, \overline{b_j} \left[g_{ij}(r) - 1 \right] \tag{2.9}$$

with

$$g_{ij}(r) = \frac{n_{ij}(r)}{2\pi r^2 dr \rho_j} \tag{2.10}$$

Where n_{ij} is the number of atoms of type *j* between distance *r* and *r+dr* from an atom of type *i* and $\rho_j = c_j \rho_0$, with ρ_0 being the atomic density of the material.

The ppdf is essential for any pdf analysis as interpretation of the pdf at distances above 2-3 Å is exceedingly difficult due to overlapping pair correlations. Equation 2.1-2.10 summerize the data reduction needed for converting the *I(Q)* to *G(r)* for the elastic scattering and is similar for both x-ray and neutrons, except that the *b* values are different for the two[d]. However, there are several corrections that must be made for inelastic effects for both neutrons and x-rays[60, 117, 119], but since these are not important for this study they will not be discussed here.

---

[d] The scattering length b for x-ray is Q and λ dependent, whereas b for neutrons is mostly independent of Q and λ.

2.1.2 Choice of neutron beamline

The choice of beam line may seem trivial; a beam line capable of performing a pdf measurement should give the same result as any other beam line. While this is generally true the quality of the n-pdf can vary significantly depending on the instrument. This is mainly due to the incoherent scattering length of H which is an order of magnitude more intense than most other scattering lengths coherent or incoherent (see table 2.1 for scattering lengths for the elements relevant for this study).

Table 2.1: scattering lengths for the elements relevant for this study

b	H	C	O	Mg	Ca
Neutron Coherent	-3.739	6.646	5.803	5.375	4.7
Neutron Incoherent	80.26	0	0	0	0
X-ray*	1	6	8	12	20

*given as the number of electrons as $b_{x-ray} \propto number\ if\ electrons$

The first choice to make when planning a neutron total scattering experiment is to decide to use constant wavelength (CW) or time-of-flight (TOF) diffraction (figure 2.3).
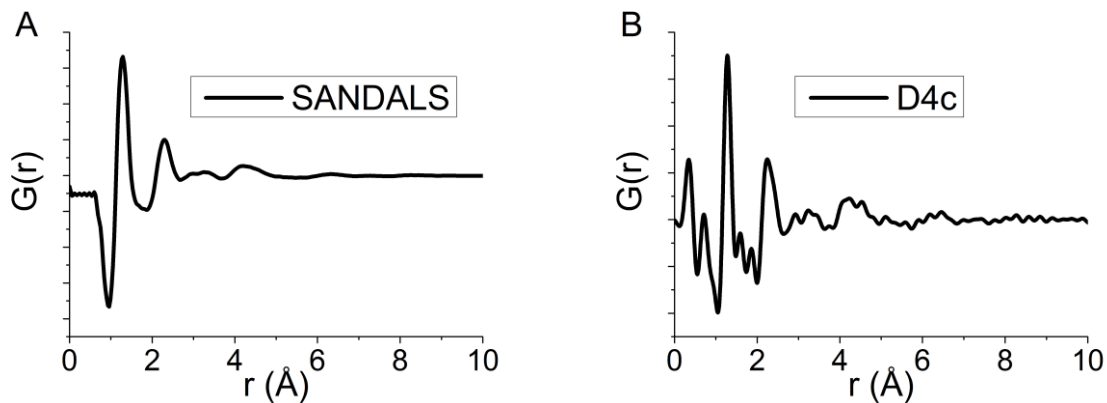
Figure 2.3: A) pdf of ACC measured at the SANDALS[120] TOF-diffractometer using a sample size of 5 g and an exposure time of 8 h and B) same sample measured at the D4c[121] CW-diffractometer at ILL using 0.25 g of sample and 36 h exposure time.

CW diffraction is analogous with a standard x-ray experiment where the detector is moved to cover as much of the scattering angle as possible. This has two main disadvantages. First most of the neutrons are discarded by a monochromator without reaching the sample. The second disadvantage is that the detectors have to be moved at several intervals to cover the entire scattering range. However, CW diffraction can be essential if working with isotopes that have absorption edges (e.g, Gd), where the λ can be chosen to avoid the absorption edge. TOF

diffraction offers several advantages, especially for hydrogen containing samples. If the instrument is placed on a pulsed neutron source such as ISIS, all of the neutrons can be used as Q can be probed by varying λ in equation 2.2 at a known angle. Several detectors are then be placed at different angles and combined to increase counting rates. This results in a Q range of 0.1-50 Å^{-1} for the SANDALS[120] instrument which is nearly impossible to reach using a CW diffractometer. The other main advantage is that the inelastic (energy dependent) and elastic scattering (Q dependent) can be deconvoluted since a given λ will have the same energy but different Q for each detector. This is especially important for hydrogen containing samples, where the inelastic[e] scattering can be comparable to the elastic scattering[60]. For the SANDALS instrument the diffraction data can also be normalized on an absolute scale using a vanadium standard, if the sample density and composition is known[117]. This results in the $S(Q)$ being in the units of barns/steradian/atom, meaning that any fit to the data has to fit the shape and the intensity of the $S(Q)$. Figure 2.3 shows the pdf of ACC measured at the CW D4c instrument at ILL and at the TOF SANDALS instrument at ISIS. The quality of the pdf measured at SANDALS is clearly superior. However, this instrument also allowed for bigger sample size compared to the D4c.

2.2   Empirical potential structural refinement

Define atomistic box

⇩

Monte Carlo simulation to get the energy minimized state

⇩

Introduce data via empirical potential

⇩

Generate ensample

⇩

Extract results
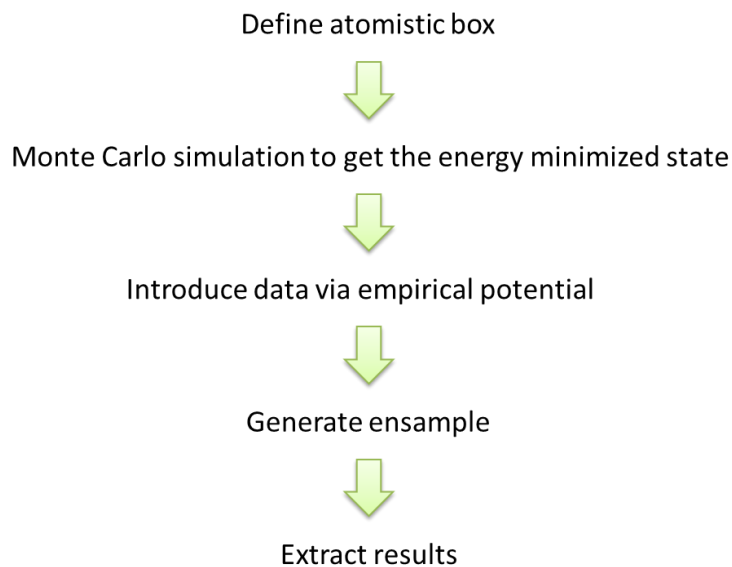
Figure 2.4: Flow chart showing the necessary steps in an EPSR analysis

The EPSR analysis follows a simple flow chart as shown in figure 2.4. This is explained in detail by Soper[61, 110-114] and the main points are summarized in the following. The first step is to define an atomistic box to represent the sample in question. This requires significant previous knowledge of the sample, specifically density, molecular structure and composition.

---

[e] The inelastic scattering is mainly dependent on the incoherent scattering length as therefore can be very high for hydrogen containing samples

In this study the molecular structure is rather simple as carbonate, water and hydroxide molecules have well known geometries. The composition was determined in this study by ICP-OES to determine the calcium and magnesium content and TGA to determine the water, hydroxide and carbonate levels. The density is significantly more difficult to determine, requiring a gas-pycnometer and significant volumes of sample[f]. The second step involves a Monte Carlo simulation based on a usual metropolis condition for move acceptance (equation 1.2). The simulation is based on an intramolecular reference potential (figure 2.5A), defined as follows.

$$U_{intra} = C \sum_i \sum_{\alpha\beta>\alpha} \frac{\left(r_{\alpha_i\beta_i}-d_{\alpha\beta}\right)^2}{2w_{\alpha\beta}^2} \qquad (2.11)$$
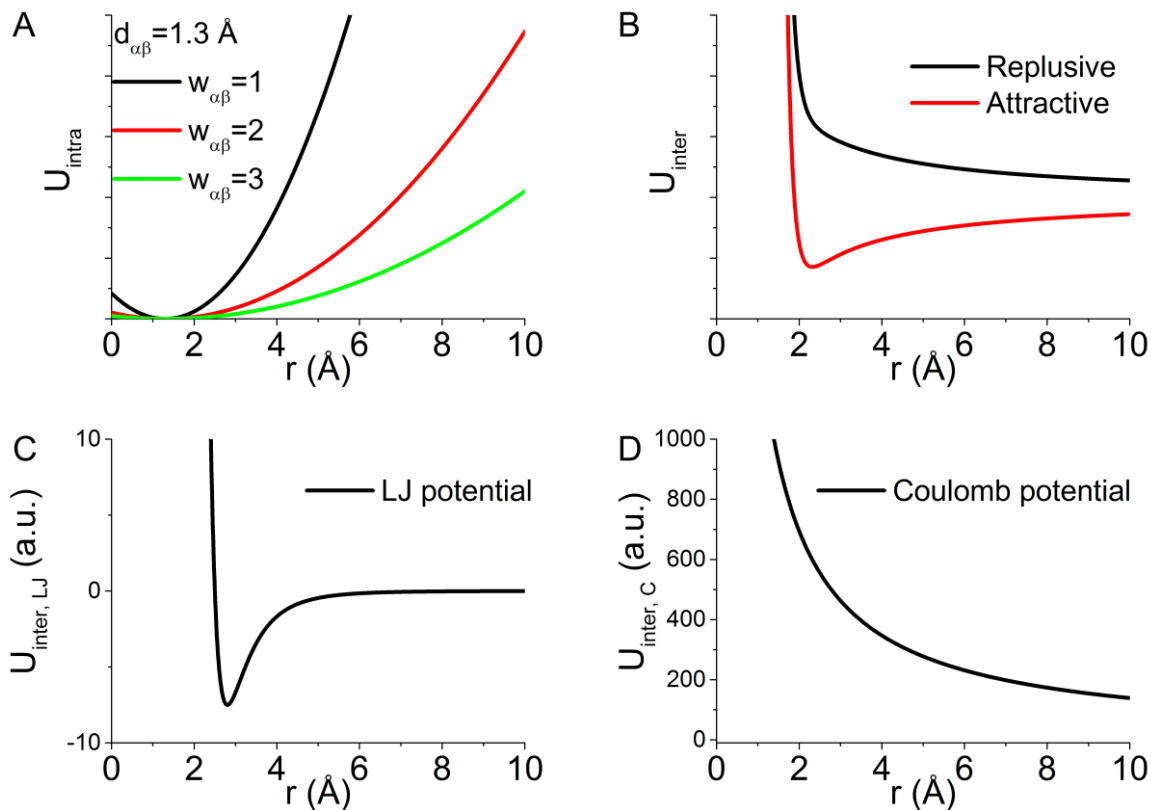
Figure 2.5: The atomic potentials used by the EPSR program: A) The intra-molecular potential plotted at three different $w_{\alpha\beta}$ values from equation 2.11, notice that with increasing $w_{\alpha\beta}$ (i.e. decreasing weight, equation 2.12) the energy penalty for molecular vibration is decreased (i.e. lighter elements vibrate at a higher frequency than heavier elements). B) Attractive and repulsive inter-atomic/molecular potential composed of a Lennard-Jones potential (C) and a coulomb potential (D, only shown for a repulsive pair) as shown in equation 2.13. Here the attractive potential in B is given by the LJ potential in C and a negative coulomb potential (from particle of opposite charge) while the repulsive potential has a positive coulomb potential as shown in D (particle of like charge).

---

[f] Luckily not a problem in this study due to the large quantities already prepared for the neutron experiment.

Where $r_{\alpha_i \beta_i}$ is the actual separation between α and β atoms, $d_{\alpha\beta}$ is the average distance between the atoms, C is a constant set to 65 $\text{Åamu}^{0.5}$, $w_{\alpha\beta}^2$ is a broadening function replacing the Debye Waller factors (i.e. intramolecular vibrations) given by:

$$w_{\alpha\beta}^2 = \frac{d_{\alpha\beta}}{\sqrt{M_\alpha M_\beta / M_\alpha + M_\beta}} \tag{2.12}$$

The interatomic potential (figure 2.5 B-D) is given by a Lennard jones potential with a point charge given as:

$$U_{\alpha\beta}^{ref}(r_{ij}) = 4\epsilon_{\alpha\beta}\left[\left(\frac{\sigma_{\alpha\beta}}{r_{ij}}\right)^{12} - \left(\frac{\sigma_{\alpha\beta}}{r_{ij}}\right)^{6}\right] + \frac{q_\alpha q_\beta}{4\pi\epsilon_0 r_{ij}} \tag{2.13}$$

with

$$\epsilon_{\alpha\beta} = \left(\epsilon_\alpha \epsilon_\beta\right)^{\frac{1}{2}} \tag{2.14}$$

and

$$\sigma_{\alpha\beta} = \frac{1}{2}\left(\sigma_\alpha + \sigma_\beta\right) \tag{2.15}$$

Where $U_{\alpha\beta}^{ref}(r_{ij})$ the inter-atomic potential between α and β atoms, ε is the well depth parameter and σ is the range parameter, q is the elemental charge, ε_0 is the vacuum permittivity and r_{ij} is the interatomic distance. These potentials are used in the Monte-Carlo simulation to obtain the energy minimized structure. After a minimum energy structure is obtained the data can be introduced via the empirical potential.
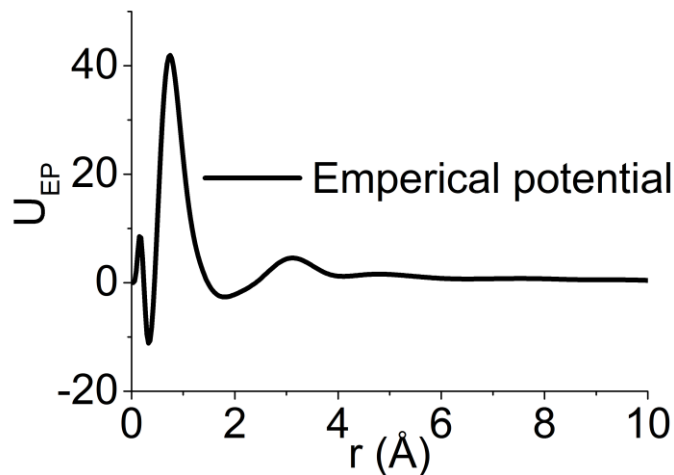

Figure 2.6: Example of an empirical potential derived using EPSR. Notice that the oscillations are dampened with increasing r mimicking the shape of an atomic potential.

The empirical potential (figure 2.6) is implemented in the form of a series of power exponential function given by:

$$U^{EP}(r) = kT \sum_i C_i P_{n_i}(r, \sigma_r) \tag{2.16}$$

with

$$P_n(r, \sigma_r) = \frac{1}{4\pi\rho\sigma_r^3(n+2)!} \left(\frac{r}{\sigma_r}\right)^n \exp\left(-\frac{r}{\sigma_r}\right) \tag{2.17}$$

Where C_i is the fitting parameter and must be real, σ_r is a width function set by the user and ρ is the atomic density. This formulation insures that the empirical potential varies rapidly at short r and slowly at long distances as expected from an interatomic potential. Given that equation 2.17 has an exact three dimensional Fourier transform into Q space, equation 2.16 can be expressed in Q rather than r. The Q space formulation can then be fitted to the difference between the experimental structure factor and the simulated structure factor determined from the energy minimized model. This is then done iteratively until a stable potential is reached. To control this process the user can set the amplitude of the empirical potential to determine how large an effect it can have on the total potential. If the amplitude is set too high the empirical potential may dominate the reference potential and result in semi arbitrary configurations. If it is set too low it will not have any effect. Therefore the amplitude must be gradually increased until a satisfactory fit is achieved. Once this is achieved the simulation can produce several configurations consistent with the data and the potential. These configurations are averaged to give the final result which can be extracted via separate routines.

Four main analysis routines were used in this study to extract ppdf, coordination number distributions, angular distribution and spherical density function (SDF). The first was the extraction of the ppdfs using equation 2.10 (figure 2.7).
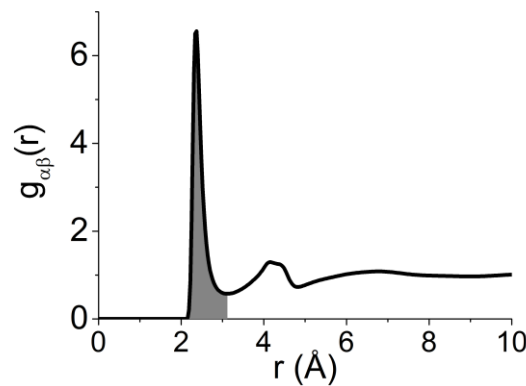

Figure 2.7: Example ppdf of calcium and oxygen (from carbonate) in ACC with the range of the first coordination sphere marked of in grey.

The ppdfs were then used to determine the ranges of interest for the e.g. mean coordination number, normally given by:

$$mean\ coordination\ number = \int_{r_{min}}^{r_{max}} 4\pi r^2 c_j \rho_0 g_{ij}(r) dr \tag{2.18}$$
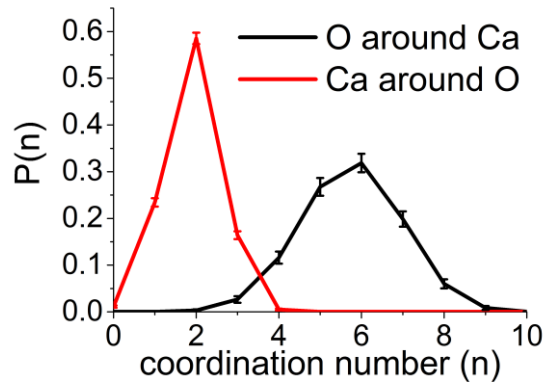
Figure 2.8: Coordination number distribution for the marked area in figure 2.7showing the number of oxygen around calcium (black) and the number of calcium around oxygen (red). Both are calculated from the grey area in figure 2.7and as is clear the mean coordination number and distributions are very different for oxygens around calcium and calcium around oxygen in the same range.

However, since the distribution of coordination numbers are of interest, a routine is set up to count the number of neighboring atoms in the range of a given coordination sphere as shown in figure 2.7 for each pair of interest, avenging over all configuration probed by the EPSR program (figure 2.8).
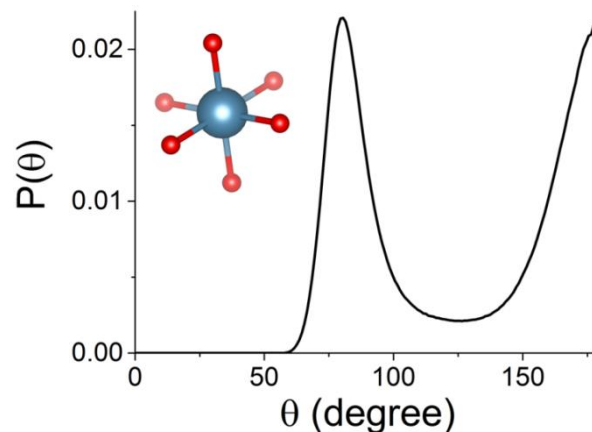
Figure 2.9: Angular distribution of oxygen from water around magnesium in AMC showing two clearly preferred angles at 90° and 180° characteristic of octahedral coordination.

The third routine extracts the angular distribution (figure 2.9), given by the angle of two atoms coordinating to a central atom within a range similar to the first coordination sphere as shown in figure 2.7. This is especially important for analyzing the coordination geometry[122] of spherical ions such as magnesium as shown in figure 2.9. The last routine involves the sdf, this routine is based on a spherical harmonic representation and involves extensive mathematical expressions, which will not be covered here but can be found in the EPSR

manual[g]. However, it is important to note that the sdf is plotted as an isosurface and will be dependent on the value set for that isosurface. In figure 2.10 the sdf of Ca around carbonate is plotted with three different values (n) for the isosurface. As see from figure 2.10 the sdf can be somewhat misleading if n is chosen at random, therefore when comparing sdfs it is important to use the same n for all sdfs.
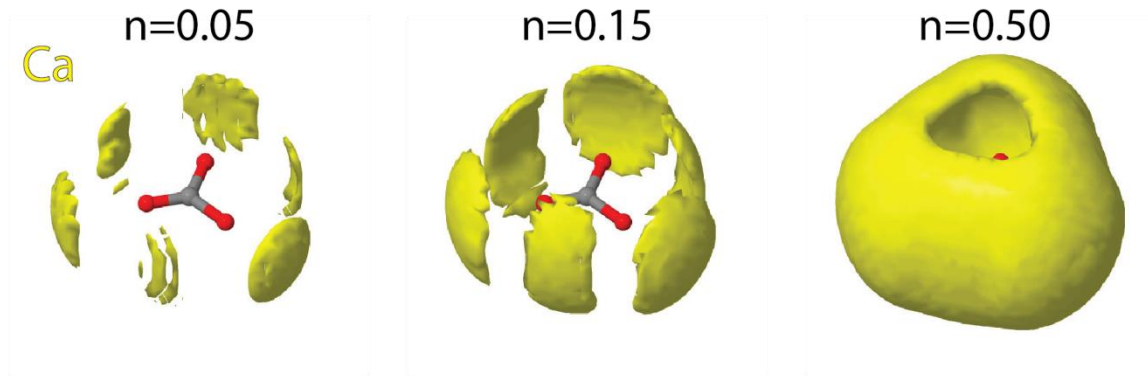
Figure 2.10: sdf of Ca coordinating to carbonate with three different isosurface values (n), taken from the EPSR model of ACC.

2.3   Neutron spectroscopy
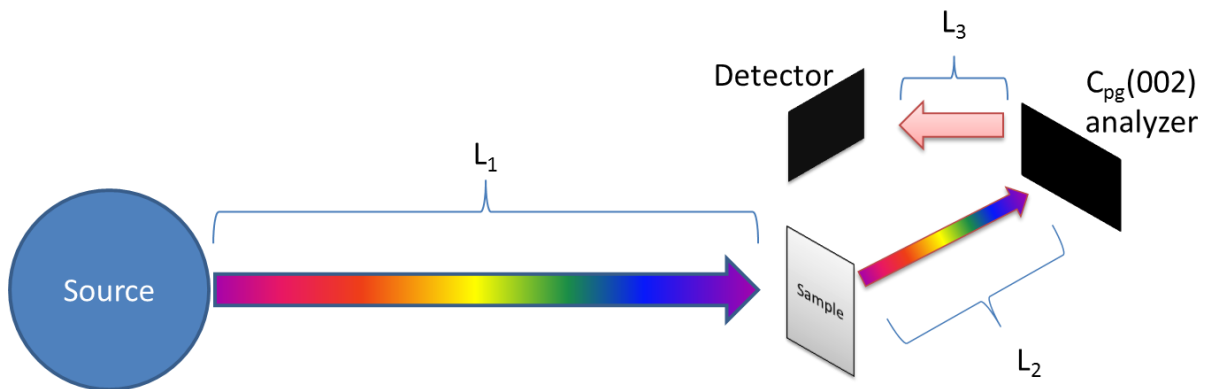
Figure 2.11: Schematic geometry for an indirect neutron spectrometer. The sample is irradiated with a white beam, the scattered beam is then monochromated by a pyrolytic graphite (PC) monochromator and the energy shift can be determined by the time of flight since L_1, L_2 and L_3 are known. Several analyzer are placed at different Q to determine the $S(Q,\omega)$ in IRIS while TOSCA measures ω at a fixed angle.

Neutron spectroscopy[123] is closely related to neutron scattering, the main difference is that the scattering is inelastic instead of elastic i.e. $\omega \neq 0$, ω being the dynamic parameter given by:

---

[g] The EPSR manual is available to anyone for free from the disordered materials group Facebook page known as delight in disorder: https://www.facebook.com/disord.matt/?ref=br_rs

$$\omega = E_i - E_f \qquad\qquad\qquad\qquad\qquad (2.19)$$

Here E_i is the energy of the incoming neutron beam and E_f is the energy of the neutron beam after hitting the sample. This technique is also relying on the incoherent scattering length instead of the coherent scattering length (see table 2.1) making it very sensitive to hydrous species. The two spectrometers used in this study are TOSCA[124](IINS) and IRIS[125](QENS) both of which are indirect geometry spectrometer as shown schematically in figure 2.11.

2.3.1 Incoherent inelastic neutron scattering (IINS)

IINS, when performed on an instrument as TOSCA, provides information analogous to infrared (FTIR) or RAMAN spectroscopy. The energy of a vibration is measured through inelastic scattering of a neutron rather than a photon as in RAMAN spectroscopy. This has several advantages and disadvantages. The disadvantages are mainly inherent to inelastic neutron experiments, large sample size (5+ grams), long measurement time (~8 hours), low resolution (1% ΔE/E) and low temperature (10 °K). However, IINS is mainly sensitive to vibrations involving hydrogen due to its large incoherent scattering length (see table 2.1) and there are no selection rules making all vibrational modes in principle measurable.
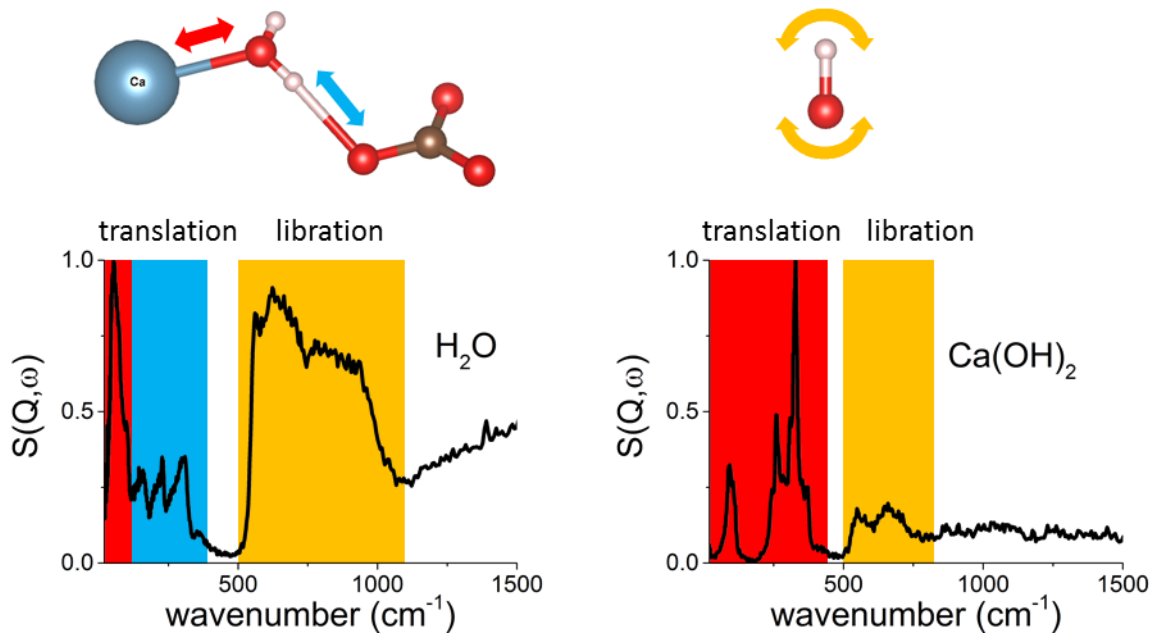
Figure 2.12: IINS spectrum of low density amorphous ice[126] and Ca(OH)₂[127] showing the X-O$_{water}$ translational vibration (red, X being any atom binding to the oxygen though its lone pair), collective vibration of a hydrogen bonded network (blue) and librational vibration (yellow). The vibrations are sketched in the top with the color of the arrows representing the band of the same color on the spectrum. The atomic structure here are represented by a hydrated calcium carbonate (i.e. monohydrocalcite[53]).

Like most vibrational spectroscopy IINS spectra are difficult to simulate and therefore the analysis was performed by comparison to reference samples. Luckily TOSCA provides an

extensive library of compounds[h] previously measured on this instrument and its predecessors TFXA. Since the hydrous species of interest here are water and hydroxide ions, plenty of reference spectra are available from the database[126-134]. In figure 2.12 two spectra are shown of low density amorphous ice[126] and $Ca(OH)_2$[127] showing the assignment of vibration in the spectrum. These vibrational modes have been extensively studied in various minerals[128-129] to assess how ion-water interaction affect the band and therefore can be used to substantiate the result available from ESPR analysis.

2.3.2 Quasi elastic neutron scattering (QENS)

The QENS measurements are very similar to that of the IINS measurement, except that the analyzer and detector (see figure 2.11) are now placed so that the beam is diffracted from the monochromator as close to 180° as possible to increase the resolution of ω. At the IRIS[125] instrument the 002 reflection of pyrolytic graphite analyzers are used, resulting in a resolution of 17.5 μeV with a analyzing energy of 1.84 meV. The resolution is given by the full width at half maximum (FWHM) of the elastic line at ω=0 (figure 2.13).
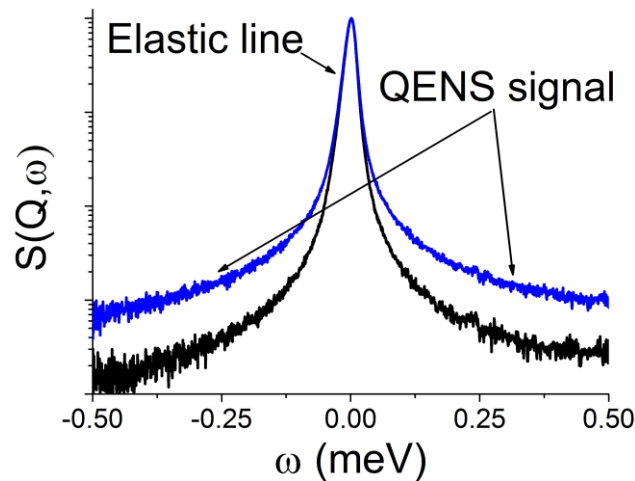
Figure 2.13: Example QENS spectrum of ACC measured on the IRIS instrument at 5 °K (black) and room temperature (blue).

The high resolution is used to measure very low energy transfer where translational and rotational motion are probed rather than the vibrational modes investigated by the TOSCA instrument. The energy transfer is then measured as the *FWHM* of a lorentzian peak convoluted with a resolution function measured at 5 °K where translational motion is negligible. ω can then be converted in to a residence time *τ* (the time between diffusive events) given as[135]:

$$\tau = \frac{2\hbar}{\Gamma} \tag{2.20}$$

Where $\hbar$ is the reduced Planck's constant and Γ the half width at half maximum *(HWHM)*. The change in ω with Q can then be used to determine the geometry of the diffusion. In this

---

study two types of diffusion were considered, confined motion and translational diffusion. For confined motion the *FWHM* is independent of Q[135] and translational diffusion has a Q dependent motion given by[136]:

$$\Gamma(Q) = \frac{DQ^2}{1+DQ^2\tau} \tag{2.21}$$

with

$$D = \frac{\langle l^2 \rangle_{av}}{6\tau} \tag{2.22}$$

Where D is the diffusion constant and l is the jump distance. As evident by equation 2.20-2.22 the residence times and jump distances measurable is hugely dependent on the Q and ω resolution and range of the instrument. Therefore, the IRIS instrument was chosen since this instrument covers the residence times reported for bulk water[136] and confined water systems[137-138], as the main question in this study was if liquid or liquid like diffusion of water was present in ACC.

3 Results and discussion

In this chapter we discuss the main experimental results that make up the bulk of this thesis. This chapter is divided into four subchapters with the first part dealing with the initial experiments and modification to the synthesis route that had to be made to facilitate the neutron diffraction experiments described in section 3.2-3.4. Here the compositional analysis of ACC is also described, and shows that the sample composition of ACC as described by Zou et al.[27] can still be reproduced when producing ACC in larger quantities. In addition, this part also covers an extensive analysis of the composition of AMC and ACMC as it was found that hydroxide ions coprecipitates with magnesium ions in the amorphous carbonate phase. Finally the initial n-pdf and IINS measurements of pure ACC and ACC with minor levels of commonly found additives are shown. These were used to design the further experiments where it was necessary to use high concentrations of additives to get a clear structural picture. In the second part, the local structure of ACC is discussed followed by a part covering the local structure of ACMC and AMC, based on pdf analysis and corroborate by vibrational spectroscopy measurements. The final part of this chapter concerns the dynamics of water in ACC/AMC as measured with quasi elastic neutron scattering. The last three parts of this chapter on ACC/AMC present a consistent description of water in the amorphous phase as structural water interacting with the ions through cation to oxygen coordination bonds and H to O hydrogen bonding. The pdf analysis of the amorphous phases also shows the material consist of a highly disordered phase with broad distribution of binding sites for all species. By studying two hydration levels for ACC/ACMC/AMC it was found shown that ACC and ACMC undergoes structural rearrangements upon dehydration which are related to a reorientation of the carbonate ions. In particular, the amount of oxygen from carbonates coordinating to each cation increases to compensate for the loss of water binding directly to the cations. In the AMC this effect was minimal and the loss of water mainly affects the amount of hydrogen bonds to the anions.

3.1 Synthesizing ACC for neutron experiments

Producing enough ACC for a neutron scattering experiment is difficult due to the large quantity of material needed and the high instability of ACC. Therefore the synthesis route used in this study was developed to maximize yield and to ensure that the composition could be reproduced consistently among different batches. The amorphous carbonate samples used in this study were produced in a modified version of the synthesis originally reported by Koga et al.[75] and later refined by Zou et al[27](reaction equation is shown below). This synthesis route has also been shown to produce samples that are structurally similar to the biogenic samples[32].

$$CaCl_2(aq) + Na_2CO_3(aq) \rightarrow CaCO_3 \cdot 1.1H_2O(s, ACC) + NaCl(aq)$$

In the original synthesis Zou et al.[27] added 2 mL 1M $CaCl_2$ to a 48 mL Na_2CO_3 solution to give a Ca/CO_3 ratio of one and an initial concentration of 40 mM for both calcium and carbonate salts after mixing. The samples were extracted by vacuum filtration followed by an

ethanol wash and dried in a desiccator. Using this method a yield of 100-200 mg of sample was obtained, requiring 25-50 batches for the 5 g of sample needed for a single neutron diffraction measurement. With 30 min per batch this would require up to 3 days of synthesis to produce. The main obstacle in producing more ACC was identified as the filtering process as the filters would get clogged if the concentration was increased. Also, if the reaction volume was increased, the sample would crystallize before it could be extracted. Therefore a larger filter was used (13 cm in diameter) with a cellulose acetate filter (0.45 μm pore size).

Figure 3.1: Left) Sample drying rack, holds six samples for drying in a desiccator. Each sample is placed on a 13 cm wide watch glass. The whole rack fits into a desiccator. Right) travel desiccator for amorphous samples, holds 10 sample vials at a time each containing ~5 grams of sample.
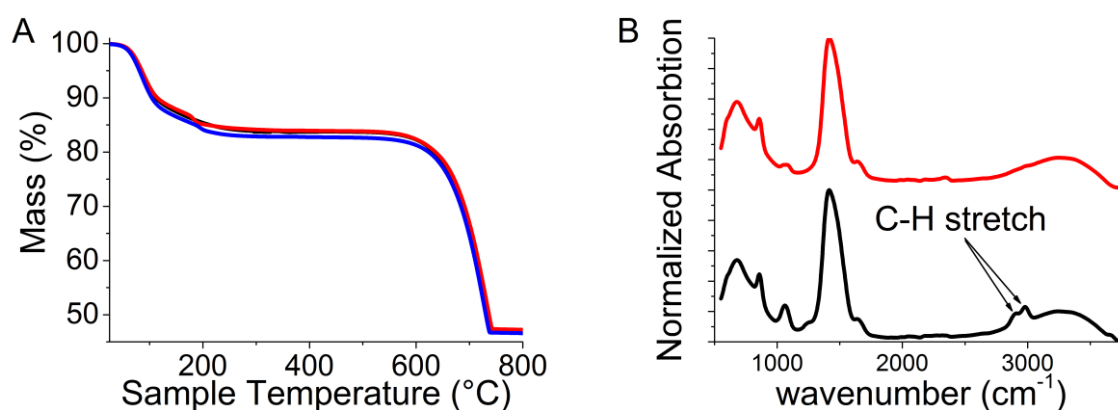
Figure 3.2: A) Three TGA measurement of ACC showing highly consistent mass loss at 100 °C and 700 °C indicating a consistent hydration level between different batches of the same synthesis. B) FTIR spectrum of ACMC after 24 hours in a desiccator (red) and a sample measured after a few hours in a desiccator (black) showing C-H stretching of the CH_3 and CH_2 groups from ethanol and a significant overlap between the symmetric stretch of the carbonate ion and the C-O stretch of ethanol at ~1075 cm^{-1}.

This allowed for the reaction volume to be increased to 0.5 L giving a yield of 2-2.5 grams of sample reducing the time to produce enough sample for 1 neutron experiment down to 1 h

plus 24 hours in the desiccator. The bottleneck now became drying the samples to remove the excess ethanol (figure 3.2B), since this takes 24 h and only one sample could be made per day per desiccator (of which we only had one). To overcome this problem, a rack was made to fit six samples in a desiccator at the same time (figure 3.1 left) resulting in a production rate of ~15 grams of sample per day or enough sample for three neutron measurements. This meant that several sample could be made in the week prior to the neutron measurements taking place, making multiple measurements possible for a single beam time facilitating limited parametric studies, such as studying the effect of dehydration and the structural change when incorporating additives (i.e. Mg^{2+}). The next challenge was transporting the ACC samples to the neutron and x-ray facilities as the ACC samples will start crystallizing if remove from the desiccator for extended periods of time (a few hours).
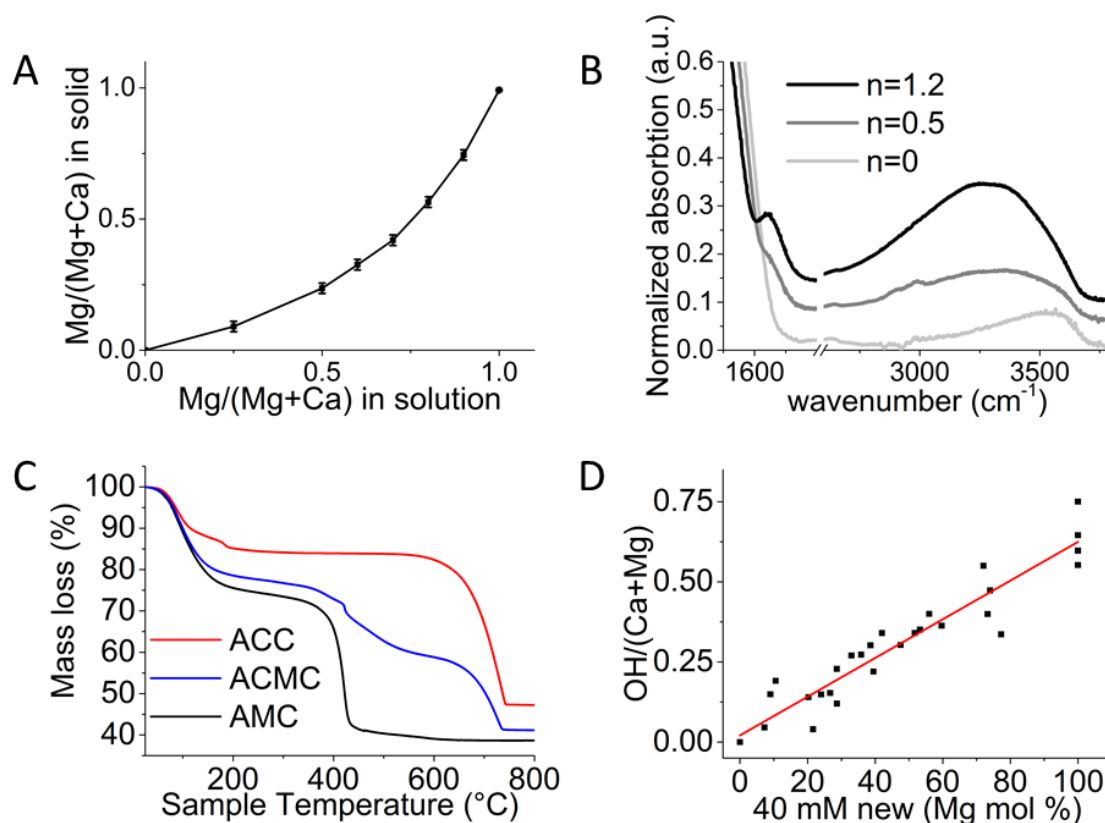
Figure 3.3: A) amount of magnesium added in solution compared to the amount incorporated into the ACMC solid. B) O-H stretch and bend regions of AMC measured by FTIR at different hydration levels obtained via thermal dehydration. A peak maximum at 3300 cm^{-1} and a bending mode at 1650 cm^{-1} at high hydration levels for H_2O can be observed. After dehydration both the stretching and bending motion of water was gone and a peak at 3600 cm^{-1} remains indicating the presence of OH^-. C) TGA measurements of ACC, AMC and ACMC with 50% Mg/(Mg+Ca). The mass loss at ~100 °C results from evaporation of water, while at 400°C the loss is due to $MgCO_3$ and $Mg(OH)_2$ decomposition. The final mass loss at 700 °C results from decomposition of $CaCO_3$. D) Hydroxide incorporation in ACMC as a function of magnesium content showing a linear incorporation of OH^- with Mg^{2+}. The OH^- content was determined from TGA measurements using equation 3.6.

For this reason, we designed and built a travel desiccator in the rather simple design of a steel box with a lid and a valve (figure 3.1 right)[i] holding up to 10 samples of 5 grams each, for extra security a vial of desiccant was often placed together with the samples to avoid high humidity which might initiate crystallization. After having addressed the transport and production issues, it was still necessary to control the composition of the samples produced, that had to be highly consistent between different batches. Since several samples had to be made for the same measurement and the sample could not be tested rigorously individually before the neutron/x-ray measurements due to time constraints, requiring the composition of the samples to be highly consistent between samples. Furthermore, to ensure a successful experiment at the neutron source the samples had to be amorphous with no crystal contaminants. In this respect, the reaction procedure mentioned above had a success rate of 95% (i.e. only 1 in 20 sample showed signs of crystallization) high enough to be considered acceptable and any crystallized samples could be measured via an express measurement as offered by the ISIS facility if beam time was available.

To test the composition of the powders, several samples were measured with TGA/DSC (figure 3.2 A) showing a highly consistent hydration level of 1.10(5) H_2O/Ca and a Ca/CO_3 ratio of one. FTIR measurements revealed that the samples contained significant amounts of ethanol directly after extraction and had to be kept in the desiccator for 24 to remove all the ethanol (figure 3.2 B). This is especially important for samples measured at the TOSCA and IRIS instruments as ethanol contains a lot of hydrogen. For this reason all the samples were measured with FTIR prior to the beam time. For ACMC and AMC (see Chapter 3.3 and 3.4 which deal with the structure and dynamic of these materials) the same synthesis procedure as that for ACC was used, but replacing the $CaCl_2$ with $MgCl_2$ while ensuring that the (Ca+Mg)/CO_3 ratio remained one to one. However, since magnesite[139]($MgCO_3$) is significantly less soluble compared to calcite[140], calcium is preferentially incorporated in to the amorphous phase as shown in figure 3.3 A. To correct for this ACMC was synthesized with an Mg/(Mg+Ca) ratio range from 0 to 1. For each Mg/(Mg+Ca) ratio the synthesis was performed three times and the magnesium content was shown to be reproducible within ~2% (figure 3.3A). Infrared analysis indicated the presence of hydroxide in AMC (figure 3.3B). This is to be expected as $Mg(OH)_2$[141] is significantly less soluble than calcite, magnesite and $Ca(OH)_2$[142]. To quantify the amount of hydroxide ion that got incorporated TGA measurements were used. However, $MgCO_3$ and $Mg(OH)_2$ decompose at the same temperature and the following derivation was made to determine the ratio of carbonate to hydroxide.

From charge neutrality, ICP and the FTIR measurements we can assume a composition of:

$$Ca_{1-x}Mg_x(CO_3)_{1-y}(OH)_{2y} \cdot nH_2O \tag{3.1}$$

where x is known from ICP measurements and the mass losses after dehydration (above 250 °C) observed in the TGA measurement originate from the following reaction occurring between 250 °C and 800 °C:

---

[i] The desiccator had to be checked in for the flight, due to the somewhat "bomb like" appearance, resulting in a rather nerve racking flight time to see if the luggage had arrived with the flight.

$$Ca_{1-x}Mg_x(CO_3)_{1-y}(OH)_{2y} \rightarrow Ca_{1-x}Mg_xO + (1-y)CO_2 + yH_2O \qquad (3.2)$$
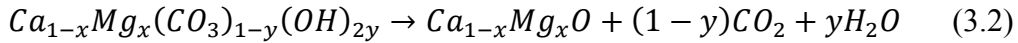
From TGA m_f and Δm can be determined as the final mass of the remaining oxide and the mass loss from 250-800 °C respectively, i.e. loss of water and carbon dioxide. Then y in equation 3.1 can be determined from the ratio between Δm and m_f assuming as follows:

$$\frac{\Delta m}{m_f} = (1-y)\frac{M_{CO_2}}{M_{ox}} + y\frac{M_{H_2O}}{M_{ox}} \qquad (3.4)$$

Here M_{CO_2} and M_{H2O} is the molar mass of CO_2 and H_2O respectively and M_{ox} is the molar mass of the calcium/magnesium oxide given by:

$$M_{ox} = (1-x)M_{Ca} + xM_{Mg} + M_O \qquad (3.5)$$

Rewriting equation 3.4 gives:

$$y = \frac{\left(\frac{\Delta m}{m_f} - \frac{M_{CO_2}}{M_{ox}}\right)}{\left(\frac{M_{H_2O}}{M_{ox}} - \frac{M_{CO_2}}{M_{ox}}\right)} \qquad (3.6)$$

Several samples with $0 \leq x \leq 1$ were measured and *2y=OH/(Ca+Mg)* was plotted as a function of *x* in figure 3.3D. A linear correlation was observed between *x* and *2y* of *2y=0.64(8)x* giving a composition of:

$$Ca_{1-x}Mg_x(CO_3)_{1-0.32(4)x}(OH)_{0.64(8)x} \cdot nH_2O \quad with \; n = 1.1 - 1.2$$
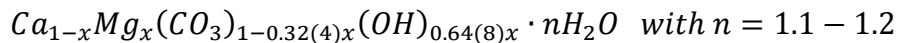
As seen from figure 3.3 D the amount of hydroxide ions incorporated varies between syntheses and despite several outliers a linear correlation is observed with a R^2=0.97. However, this variation between syntheses may result in minor errors when analyzing the ACMC and AMC samples as *n*, *x* and *y* in equation 3.1 all contribute to determining the composition of the sample which is used as an input parameter for the EPSR modelling. This is less of a problem with ACC as *n* is the only varying parameter and as seen in figure 3.2 A the hydration level is near constant in these samples.

3.1.1 Additives and the structural effect they may have on ACC

As mentioned in chapter 1.3.2 and 1.4 there are many additives that can stabilize ACC and several were measured to investigate if any of these affected the structure of ACC (figure 3.4). Focus was placed on the inorganic additives and four of the most common ones were chosen. Sodium and hydroxide ions are common impurities in synthetic ACC and are found in 0-5% compared to calcium[27, 65]. In biogenic samples magnesium and phosphate ions are the most commonly found impurities[21, 38], with Mg^{2+} generally found in the range of 0-20% Mg/(Ca+Mg), while phosphate containing samples come in both ACC[12, 32] and amorphous calcium phosphate[132] versions and compositions in between[21]. As seen from figure 3.4 A and B the n-pdf of the samples with minor concentrations of impurities (~5% impurity/Ca^{2+}) are very similar, the main difference is found in the n-pdf of phosphate stabilized ACC (figure 3.4 B) were two peaks appear at 1.6 Å and 2.4 Å. However, these two peaks originate from the P-O and O-O intra molecular distances and do not give significant information on how it affects the general structure. IINS spectra were also performed on the same samples and again no

difference was found between the samples (figure 3.4 C). The density of all samples was also measured and gave the same result within 2% of the pure ACC. Given the small difference in composition, density and pdf, it was deemed that the structural changes that may occur from small amount of additives are confined to the local environment of the additives itself and does not propagate throughout the sample. Therefore, larger concentrations were needed to understand the local environment of around these common additives. This was done for both magnesium and phosphate as additives with samples that were one-to-one mixtures of calcium/magnesium and carbonate/phosphate. However, at the time of writing only the magnesium samples have been fully analyzed (see chapter 3.3).
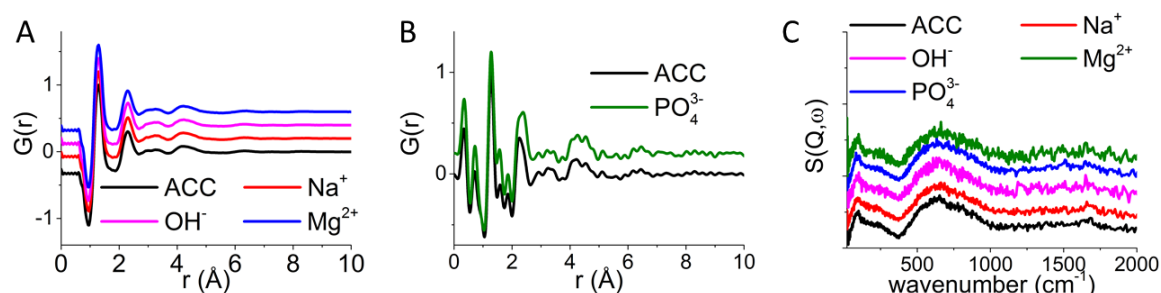
Figure 3.4: Neutron pdf measured at ISIS (A), ILL (B) and IINS spectra(C) of ACC with various additives present in small amounts (~5% relative to calcium). X-pdf of these samples was not measured as significant n-pdf and IINS beam time was available during the first year of my thesis while x-pdf did not become available until the second year. The four samples were chosen to highlight the effects of the most common additives on the structure of ACC.

3.2 Local structure in amorphous calcium carbonate and the effect of dehydration

As mentioned in chapter 1.3 there has been several structural studies on ACC reported in the literature, but so far only a handful of structural details have been elucidated, namely the Ca-O nearest neighbor distance and coordination number and the presence of multiple hydrogen binding sites. But this leaves several key structural aspects poorly understood, e.g. the distribution of hydrogen bonding as ACC contains two hydrogen bond acceptors, oxygen from carbonate and water and how the calcium and carbonate ions interact. It is also unclear how this changes with the hydration level and if the water is located in pores[63] as confined water or as structural water[143] coordinated to the ions. To answer this we present here an atomistic model of ACC derived from empirical potential structural refinement (EPSR)[61, 111, 113] based on simultaneous fitting of X-ray and neutron total scattering data. To elucidate the effect of hydration a ACC sample was thermally dehydrated at 100 °C for 90 min to give a hydration level of n=H_2O/Ca=0.50(5) giving a total of two samples; n=1.1 and n=0.5. Neutron and optical vibrational spectroscopy was used to support the findings of the EPSR model.

3.2.1 Sample characterization
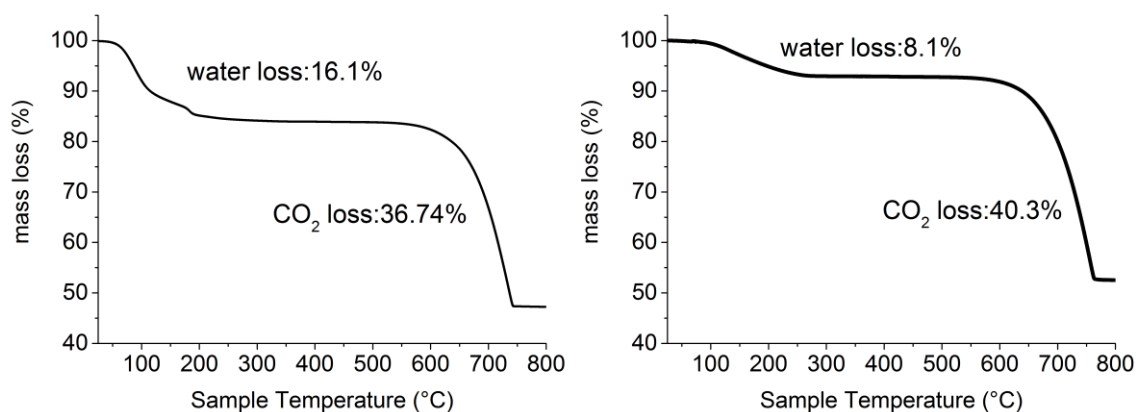
Figure 3.5: Example TGA measurements of ACC with n=1.1(left) and n=0.5 (right). Measurements were made for three samples at each hydration level and gave a hydration level of 1.1±0.05 and 0.5±0.05 and a Ca/CO_3 ratio of 0.99±0.01 for both samples.

The ACC as prepared had the composition $CaCO_3 \cdot nH_2O$ with $n = 1.1 \pm 0.05$ and a partially dehydrated sample with $n = 0.5 \pm 0.05$ was prepared by heat treatment. The composition was determined by TGA (figure 3.5). Using Ar-gas pycnometry the mass densities were determined to be 2.282(2) and 2.428(2) g/cm^3 for the samples with $n = 1.1$ and $n = 0.5$, revealing a densification during dehydration.

The neutron and X-ray structure factors and pdfs of both samples are shown in figure 3.6. In the pdfs all correlations below 2.3 Å originate from the intramolecular distances in the carbonate ions and water molecules, with the peak below 1 Å in the x-pdf originating from truncation errors in the fourier transform[62]. The first intermolecular correlation peak corresponds to the Ca-O bond at 2.4 Å (figure 3.6 B). The high intensities of the peaks at 4 Å

and 6 Å in the X-ray pdfs compared to the neutron pdfs can be attributed to the Ca-Ca correlations, to which the X-ray measurements are particularly sensitive. Given the high similarity between the pdf and structure factors of the two samples (figure 3.6) it is difficult to determine if there is a structural difference based on the pdf alone and a full deconvolution of the pdf is needed taking density and composition into account.
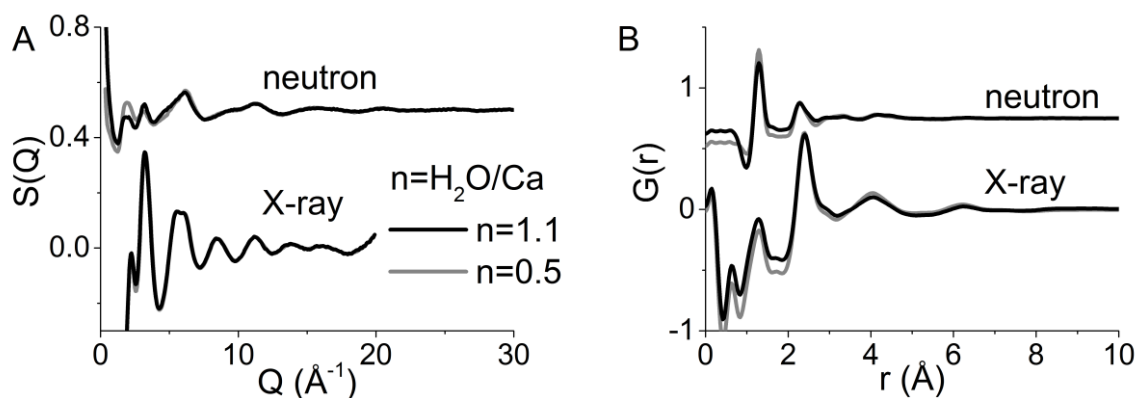
Figure 3.6: A) Structure factor of ACC measured using x-rays and neutron sources and B) the corresponding pdf.

3.2.2 EPSR fitting of amorphous calcium carbonate

For the EPSR model a cubic box was made with the following specification:

Table 3.1: model parameters for ACC modeling						
Sample	Number of Ca	Number of CO_3	Number of H_2O	Total number of atoms	box side length (nm)	Atomic density (atoms/Å^3)
n=1.1	200	200	220	1660	2.59	0.095
n=0.5	200	200	100	1300	2.46	0.087

The box size was made to ensure that it was large enough to avoid finite size effects and the model parameters (table 3.1) was chosen to reproduce the composition and density determined for the samples. To ensure the right internal structure of the carbonate and water molecules the following constraints was made:

Table 3.2: Intra-molecular constraints	
H_2O	
O-H distance:	0.976 Å
H-O-H angle:	104.5°
CO_3	
C-O distance:	1.2905 Å
O-C-O angle:	120°

These constraints defined the intra molecular potential (equation 2.11). The angles were taken from literature[50, 107] and the distances were determined from the peaks around ~1 Å (O-H distance in the water molecule) and ~1.3 Å (C-O distance in the carbonate ion) in the pdf (figure 3.6 B). The model was energy minimized via a Monte Carlo simulation using the following potentials (equation 2.13-2.15):

Table 3.3: Interatomic/molecular potentials

Atom	ε [kJ/mole]	σ [Å]	Charge [e]
Ca	0.175	3.1	1.86
O	0.1625	3.6	-1.113
C	0.5021	3.742	1.479
O$_{water}$	0.65	3.166	-0.8476
H$_{water}$	0	0	0.4238

The potentials used here are based on the work of Coung et al.[144] for the calcium and carbonate ions while the water potential is taken from the work of Imberti et al[107]. The structure factor computed from the energy minimized model was compared to the experimental data and refined via addition of empirical potentials until optimal agreement was achieved.

To gain sufficient statistics in order to accurately describe the structure of ACC, an ensemble of at least 10.000 box configurations obtained with the refined potentials was averaged. The final fit is shown in figure 3.7, where all the main features are reproduced in both the structure factors (figure 3.7 A and C) and in the pdfs (figure 3.7 B and D). A mismatch at very low Q (figure 3.7 C) is observed in the neutron structure factor and is caused by the high sensitivity to the inelastic scattering correction in this range. A slight mismatch is found in the intensity of the negative peak at ~1 Å in the neutron data suggesting that the water content might be overestimated. However, the low r region in the pdf is highly susceptible to experimental noise and if the water level was incorrect a mismatch of the high Q region in the structure factor should also be present, as this is dominated by intra-molecular distances[62]. Since the structure factor is well reproduced at high Q and the TGA analysis consistently confirmed the hydration level it is assumed that this mismatch is caused by errors in the Fourier transform and not due to errors in the assessment of the composition. It also has little effect on the fitting procedure as this is performed on the structure factor and not on the pdf. From the final model the pdf can be deconvoluted into the 15 ppdfs as shown in figure 3.8. For clarity, the different types of oxygen will be referred to as O_c, O_w and O for oxygen from carbonate, water and both respectively.
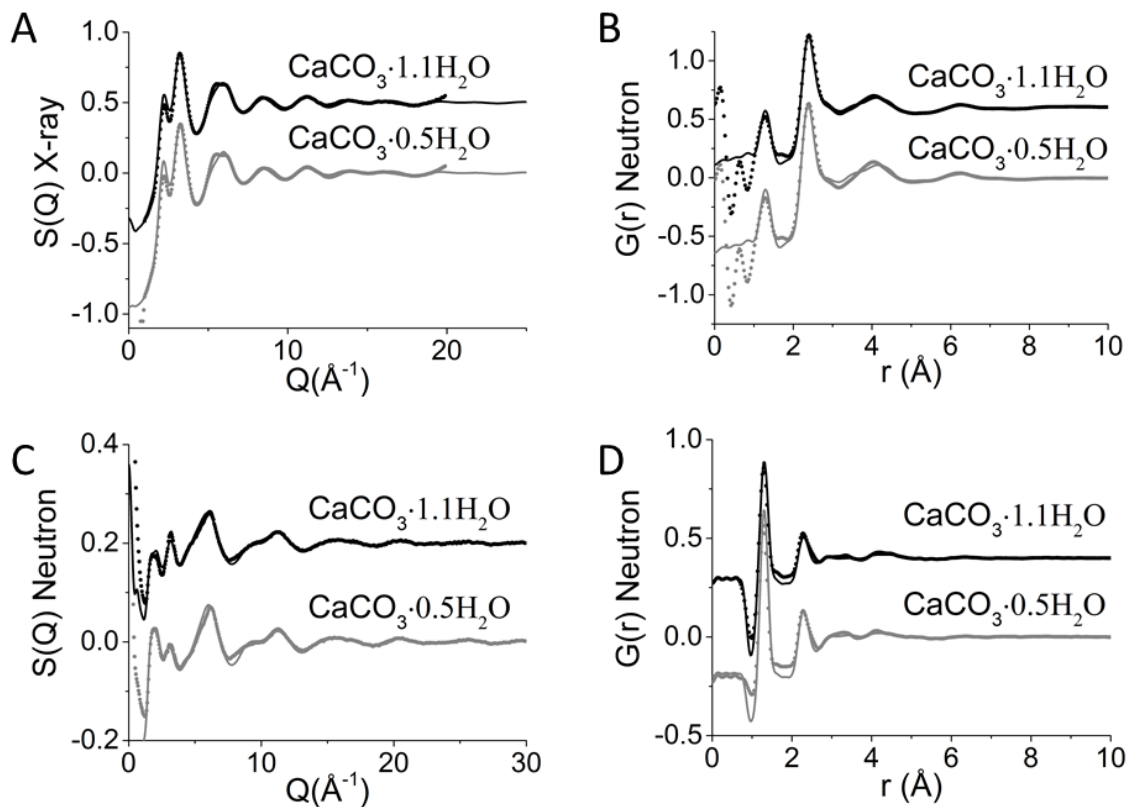
Figure 3.7: Experimental (dots) and simulated (lines) structure factor (A and C) and pdf (B and D) of ACC for both hydration levels. Data measured with X-rays (A and B) above and neutrons below (C and D).

The features in the inter-atomic/molecular ppdfs are largely confined below 5 Å and can be assigned to nearest and next nearest neighbor distances (figure 3.8). Longer distances are seen in the Ca-Ca correlation extending to 15 Å covering 4 partially overlapping coordination spheres at 4, 6, 9 and 12 Å (figure 3.8 A). The carbonate-carbonate correlations extend to 10 Å as expected given the size of the ion and that they cannot be placed direct adjacent to each other due to charge repulsion (figure 3.8 D). Calcium-carbonate and calcium-water correlations both show features in the 5-8 Å range. This suggests the presence of larger structures where three or more ions/molecules generate rigid structures (figure 3.8 B and C), e.g. a calcium ion binding to a carbonate ion which in turn binds to a water molecule.

Using the approach described in chapter 2.2 the mean coordination number was determined for several of the coordination spheres and a general increase in the mean coordination number upon dehydration was observed. Only in the coordination spheres involving O_w and H a decrease in the mean coordination number was observed (table 3.4). Despite only observing minor changes in the ppdfs (figure 3.8) the coordination numbers show that significant structural changes are introduced by dehydration. To understand how 10-30% changes in the coordination numbers (table 3.4) can occur without large effects to the pdf, we need to look into the different ion/molecules local environments in more detail.

Figure 3.8: ppdfs of the 15 atomic pair in ACC. with pairs between A) calcium and calcium, B) calcium and carbonate, C) calcium and water, D) carbonate and carbonate, E) carbonate and water and between water molecules(F).

Table 3.4: Coordination number of specific pair given as number of atom 2 around atom 1.

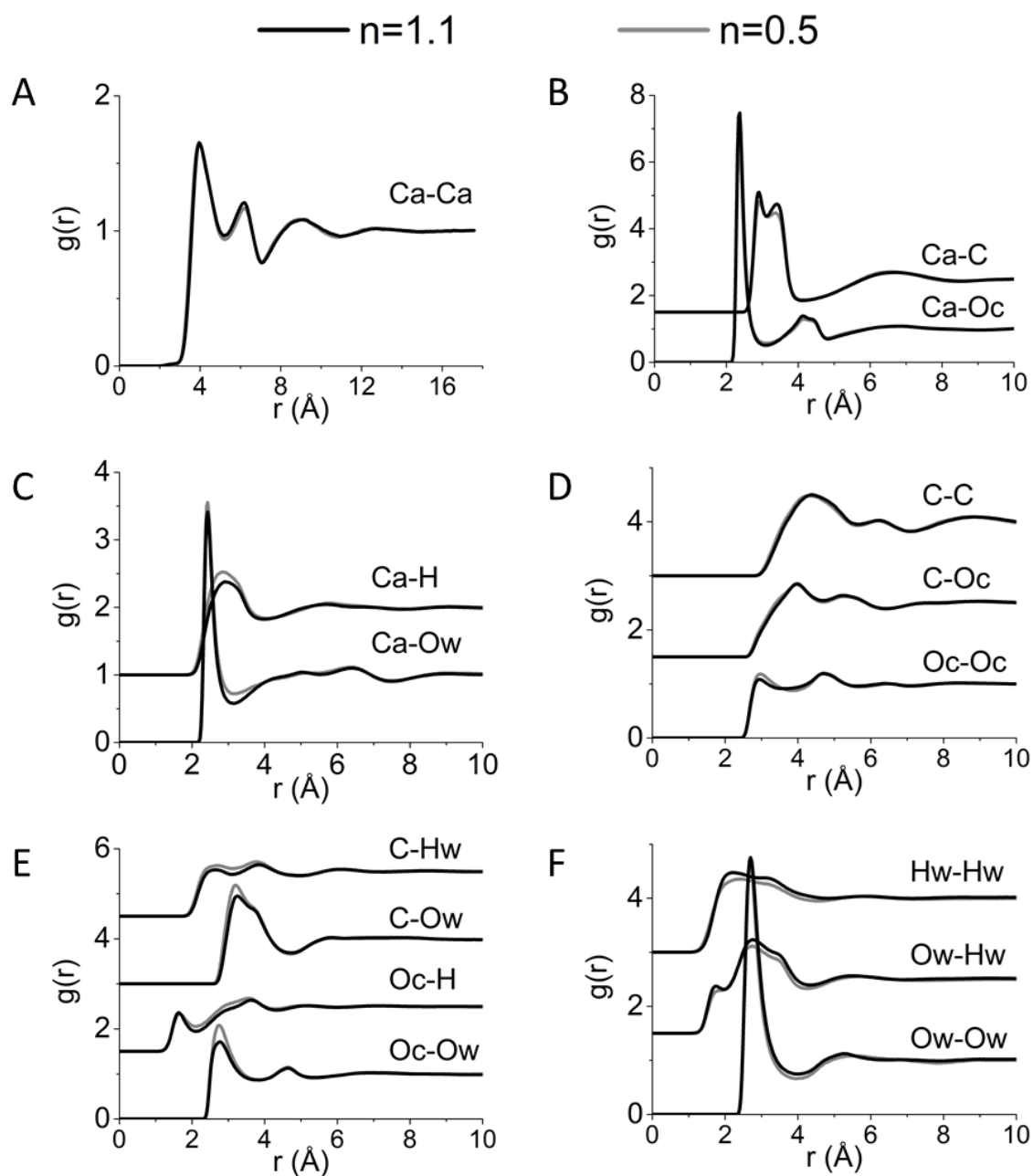| Atom 1	Atom 2	R_{min} (Å)	R_{max} (Å)	CN n=1.1	esd n=1.1	CN n=0.5	esd n=0.5	Change %
Ca	Ca	2.5	5.1	5.7	1.5	6.8	1.3	19
Ca	Ca	5.1	7.2	11.5	2.3	13.2	2.2	15
Ca	O_c	2.0	3.1	5.8	1.2	6.3	1.1	10
O_c	Ca	2.0	3.1	1.9	0.7	2.1	0.7	10
Ca	C	2.0	3.0	1.1	0.9	1.2	0.9	8
C	Ca	2.0	3.0	1.1	0.8	1.2	0.8	8
Ca	C	3.0	4.1	3.7	1.3	4.1	1.4	12
C	Ca	3.0	4.1	3.7	1.2	4.1	1.2	12
Ca	O_w	2.0	3.2	1.4	1.1	0.9	0.9	-40
O_w	Ca	2.0	3.2	1.3	0.7	1.7	0.7	32
Ca	H	2.0	3.8	5.1	3.0	3.0	2.2	-41
H	Ca	2.0	3.8	2.3	1.0	3.0	0.9	29
O_c	O_w	2.0	3.9	2.7	1.7	1.5	1.2	-41
O_w	O_c	2.0	3.9	7.3	2.1	9.3	1.8	28
O_c	H	1.2	2.2	0.5	0.7	0.3	0.5	-41
H	O_c	1.2	2.2	0.7	0.6	0.9	0.5	29
O_w	O_w	2.0	3.9	4.1	2.0	2.0	1.5	-51
O_w	H	1.2	2	0.4	0.6	0.2	0.5	-51
H	O_w	1.2	2	0.2	0.4	0.1	0.3	-51

3.2.2.1 Calcium and carbonate environment

The local environment of calcium is shown in figure 3.8 A-C. Figure 3.8 A shows the Ca-Ca ppdf, where four coordination spheres are observed with almost no difference between the two samples. However, when the mean coordination number is calculated for the first two coordination sphere at 4 and 6 Å and increase of 19% and 15% in the number of calcium around calcium is observed respectively for the first and the second sphere (Table 3.4). As shown in Figure 3.9 A, the distribution of coordination numbers in these coordination spheres are characterized by a broad distribution for both spheres. In the dehydrated sample (n=0.5) the distribution is shifted to higher numbers, as expected, but the width of the distribution remain nearly the same, indicating that there is no increased order in the system. The Ca-O correlation are shown in figure 3.8 B and C, in both the Ca-O_c and Ca-O_w ppdf a sharp peak is seen at ~2.4 Å assigned to direct bonding between calcium and oxygen. By analyzing the

coordination numbers it can be observed that all calcium ions are bonded to carbonate ions and vice versa, as expected. However, only 77% of the calcium ions bind to water molecules and they drop to 59% after dehydration. Similarly, 10% of the water is not binding directly to any calcium ions dropping to 3% after dehydration. In both samples a mean coordination number of oxygen around calcium is 7.2. For n=1.1 there are 5.8 oxygens from O_c and 1.4 from O_w while for n=0.5 there are 6.3 oxygens from O_c and 0.9 from O_w. As seen in figure 3.9 B this comes from a shift in the distribution of coordination numbers to lower numbers for O_w while the distribution for O_c goes to higher numbers, suggesting that the binding site left behind by O_w is taken over by O_c.

As mentioned in chapter 2.2 the angle between ligands binding to the same cation is very sensitive to the local geometry and in figure 3.9 C and D the angular distributions for O_c and O_w around calcium are shown. In the angular distribution of O_c (figure 3.9 C) two preferred angles are observed at ~50° and 70°. Comparing with the structure of monohydrocalcite[53] these can be assigned to oxygens from the same carbonate ion binding to the same calcium ion (i.e. bidentate binding) and oxygens from adjacent carbonate ions binding to the same calcium (i.e. monodentate binding) respectively.
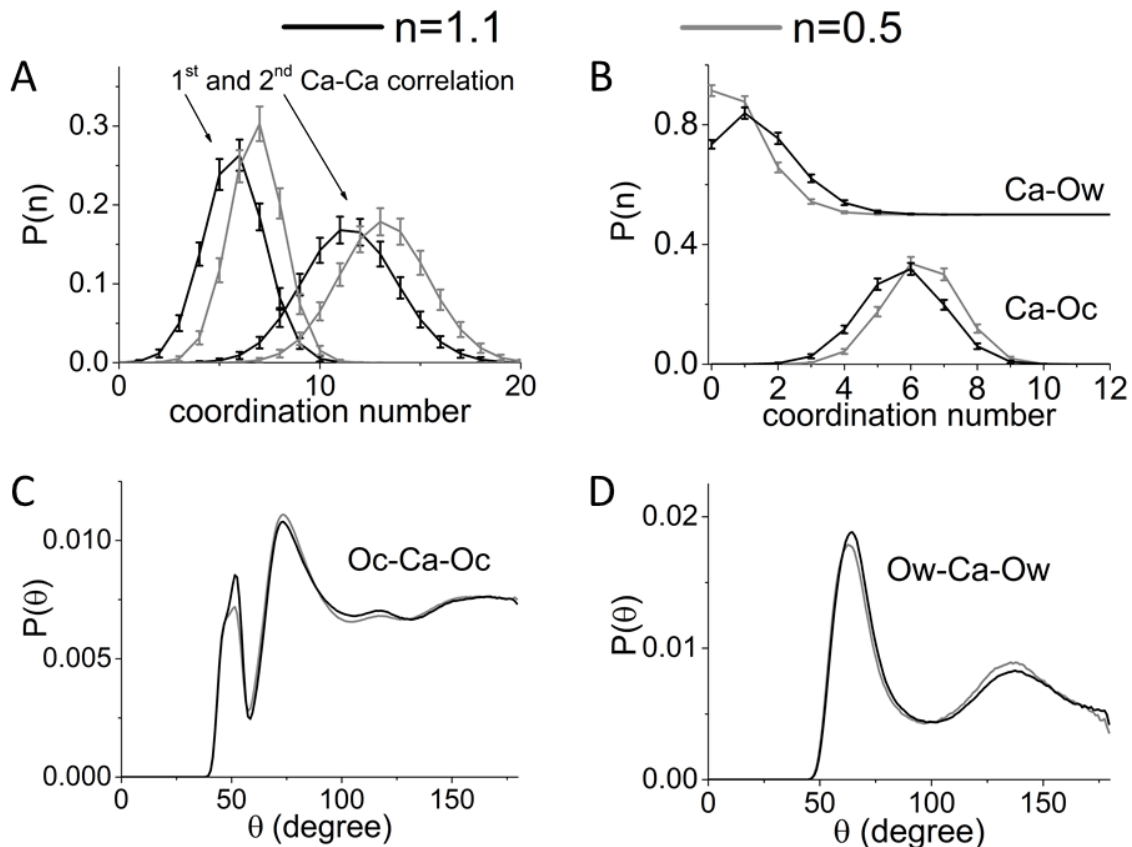

Figure 3.9: A) distribution of coordination numbers for the first two Ca-Ca coordination spheres at 4 and 6 Å (figure 3.8 A). B) Distribution of coordination number for the first coordination sphere of O_w and O_c around Ca at 2.4 Å (figure 3.8B and C). Angular distribution showing the angle between oxygens binding to the same calcium ion for O_w (C) and O_c (D).

The lack of any peak above 100° reflects the broad distribution of coordination number (figure 3.9 B) since averaging all the different types of coordination spheres smears out any correlations at higher angles. For the angular distribution of O_w (figure 3.9 D) two preferred angles are also present at ~70° and ~140° from adjacent and next nearest neighbor water molecules binding to the same calcium ion. Comparing this with the local structure of calcium ions in solution the two angles are characteristic of an 8-fold square antiprism coordination[145], suggesting a correlation between the structure in the amorphous phase and the hydration of the ion in solution. However, this angular distribution can only be calculated for calcium ions with two or more water molecules binding to Ca^{2+} directly, 43% and 21% of the calcium centers for n=1.1 and n=0.5 respectively. The peak between 2.5 and 5 Å in the ppdf relating to calcium and carbonate (figure 3.8 B) reveals how the carbonate is binding to the calcium. The split peak in the Ca-C ~3 Å can be assigned to bidentate (2.9 Å) and monodentate(3.6 Å) binding in a ratio of roughly 20% bi- and 80% mono-dentate (table 3.4). This is also present in the shape of second peak of the Ca-O_c ppdf although to a lesser extent. In the Ca-H ppdf (figure 3.8 C) one broad peak is shown with a significant overlap with the first peak in the Ca-O_w ppdf, showing that while the H generally points away from the cation it is free to coordinate oxygen in any direction away from the calcium ion. To view this in 3D the sdf is plotted for calcium binding to carbonate and water in figure 3.10.

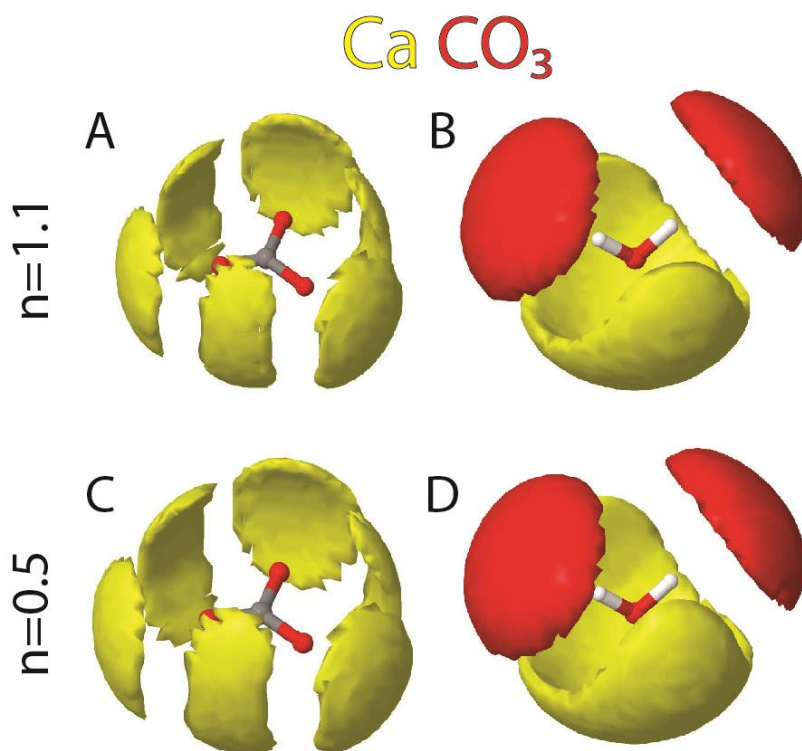*Figure 3.10: SDF of the Ca (yellow) coordinating to the carbonate ion (A and C) and the water molecule (B and D) for both n=1.1(A and B) and n=0.5 (C and D). In B and D the SDF of carbonate (red) is also shown for clarity. The Surface is plotted here in the range 2-5 Å away from the C and O atom in carbonate and water respectively using an isosurface value of 0.15.*

The sdf of the carbonate ion shows that there are two distinct binding site bidentate and monodentate as seen in the ppdfs as well (figure 3.8 B), it also shows that the site are anisotropic in shape (figure 3.10 A and C). The sdf is spread out towards the normal to the molecular plane suggesting that there is some freedom to bind to the carbonate at different angles in this direction. In the plane of the carbonate ion there is little spread in the sdf suggesting that the Ca has to bind in either bidentate or monodentate positions with some spread in the monodentate binding site which is expected as this site is more open. For calcium binding to water only one site is observed. This site is located on the side where the oxygen is exposed, as expected. The sdf is anisotropic with some spread towards the lone pair positions on the O_w (figure 3.10 B and D). In both cases the dehydration only has a small effect leading to a minor increase in the anisotropy of the sdf.

3.2.2.2 Hydrogen-bonding in amorphous calcium carbonate
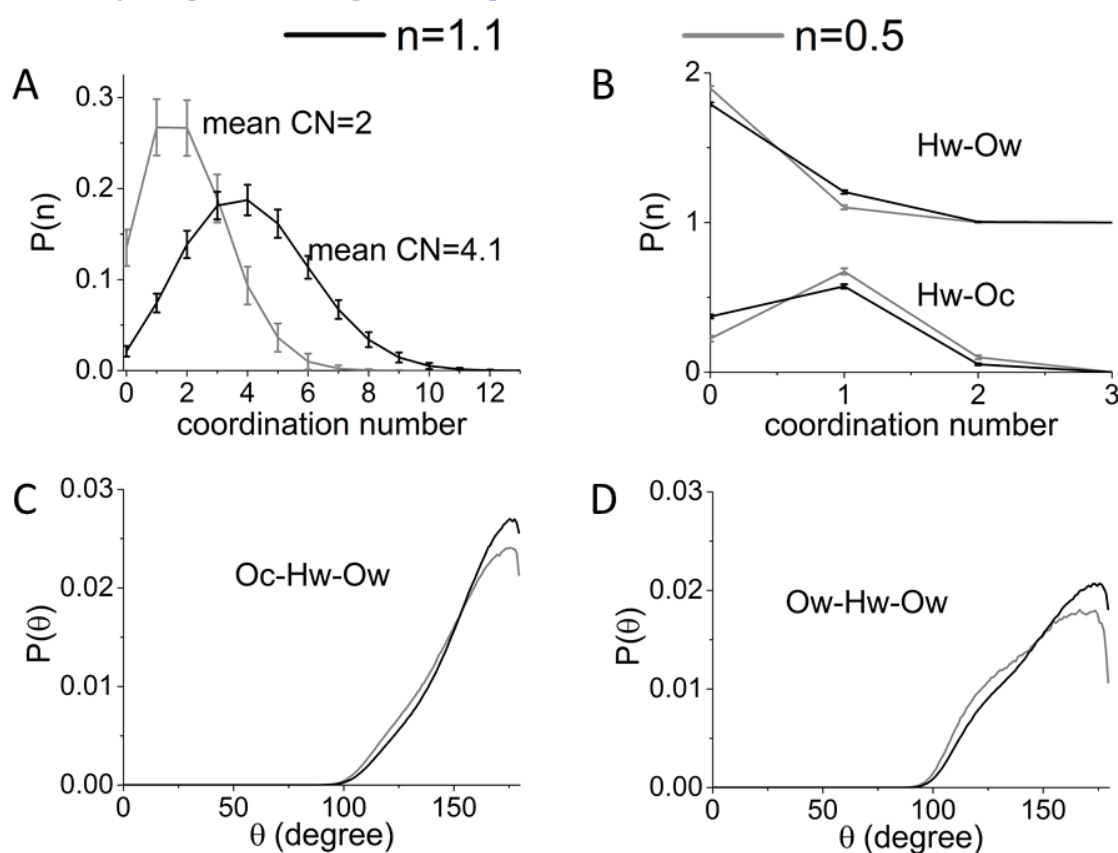
Figure 3.11: A) distribution of coordination numbers for the first O_w-O_w coordination sphere at 2.7 Å (figure 3.8 F). B) Distribution of coordination number for the two hydrogen bonding peaks at 1.8 Å in the O-H ppdf (figure 3.8 E and F). Angular distribution showing the angle of the hydrogen bond between water and carbonate ions(C) and between water molecules (D).

Hydrogen bonding between water and carbonate/water is the second attractive interaction in ACC, the other and stronger one being the calcium to oxygen bonding. The ppdf related to hydrogen bond are shown in figure 3.8 E and F. The hydrogen bond is evident by the peak at 1.8 Å in the O-H ppdfs and the peak at 2.7 Å in the O-O ppdfs. Although the O-O distance of 2.7 Å is not unique to oxygens in close proximity due to hydrogen bonding. Analyzing the coordination numbers of the 1.8 Å peak in the O-H ppdfs showed that only 10% of the water

molecules are hydrogen bonded with other water molecules, while all water molecules are hydrogen bonded to a carbonate ion via at least one hydrogen bond. The coordination number for O_w around O_w for n=1.1 is 4.1 consistent with the tetrahedral coordination found in liquid water[108] (table 3.4). However, when looking at the distribution of coordination numbers, the coordination number ranges from 0 to 10 (figure 3.11 A) and while 10 is a high number is it similar to what is found for ikaite[52] for the same O_w-O_w distances (table 3.4). The mean coordination number of O_w binding to H (i.e. hydrogen not on the same water molecule) is 0.2 suggesting that while water molecules are in close proximity to each other there are little direct interactions between them. Also, this can be inferred from the distribution of coordination numbers for O_w around H, where 80% (n=1.1) to 90% (n=0.5) of the hydrogen are not forming hydrogen bonds to any O_w (figure 3.11 B). The 1.8 Å peak in the O_c-H ppdf is more prominent compared to the one in the O_w-H ppdf (figure 3.8 E and F), indicating a preferred hydrogen bond between water and carbonate compared to hydrogen bonds between water molecules. This is also seen in the distribution of coordination number for O_c binding to H (figure 3.11B) where 63% (n=1.1) and 78% (n=0.5) of the hydrogens are hydrogen bonded to O_c. In figure 3.11 C and D the angle of the hydrogen bond are shown. The water-carbonate hydrogen bond is highly linear similar to what is found in ikaite and monohydrocalcite[52-53] (figure 3.11 C). The water-water hydrogen bonds although also mostly linear, exhibits a shoulder on the angular distribution at 120° (figure 3.11 D), suggesting a weaker hydrogen bond.
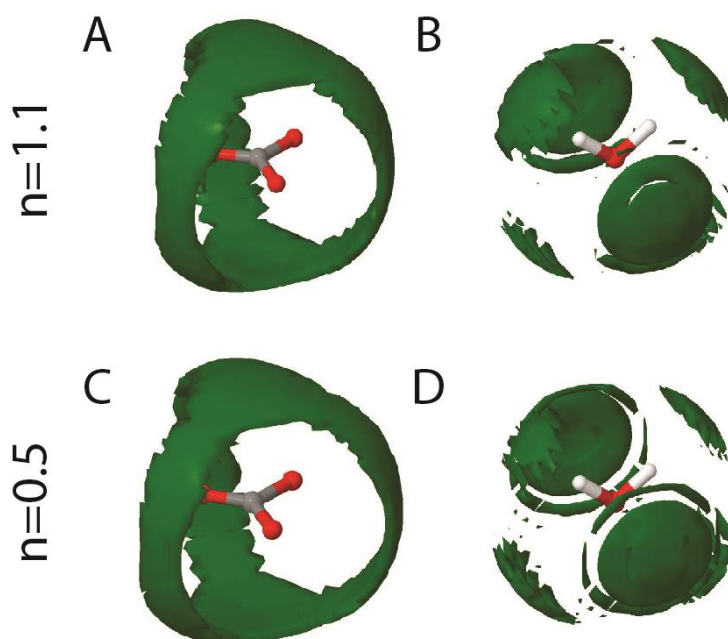
Figure 3.12: SDF of the water (dark green) coordinating to the carbonate ion (A and C) and the water molecule (B and D) for both n=1.1(A and B) and n=0.5 (C and D). The isosurface is plotted here in the range 2-5 Å away from the C and O atom in carbonate and water respectively using an isosurface value of 0.15 for the carbonate sdfs and 0.05 for the water sdfs. The isosurface value for the water-water sdf was lowered as the correlations between water molecules are weak and was not distinguishable at higher values.

In figure 3.12 the sdf of water around carbonate and water are shown. The sdf of water around carbonate (figure 3.12 A and C) show that water preferentially binds between the O_c (bidentate bonding). However, as evident from the double peak in the ppdf (figure 3.8 E), part of the water will also bind on the outside of the carbonate molecule. The bidentate binding is unexpected as this binding site is absent in both hydrated calcium carbonate minerals[52-53]. The sdfs of hydrogen bonding to water (figure 3.9 B, D and figure 3.12 B, D) show that the O_c are placed in a narrow binding site directly on top of the H (figure 3.9 B and D). In contrast to this the water-water sdf does not show a clear binding site given the weak correlation between the water molecules, although there is a correlation on top of the H from the limited hydrogen bonding between water molecules present in the structure (figure 3.12 B and D).

3.2.2.3 Large scale structure in amorphous calcium carbonate
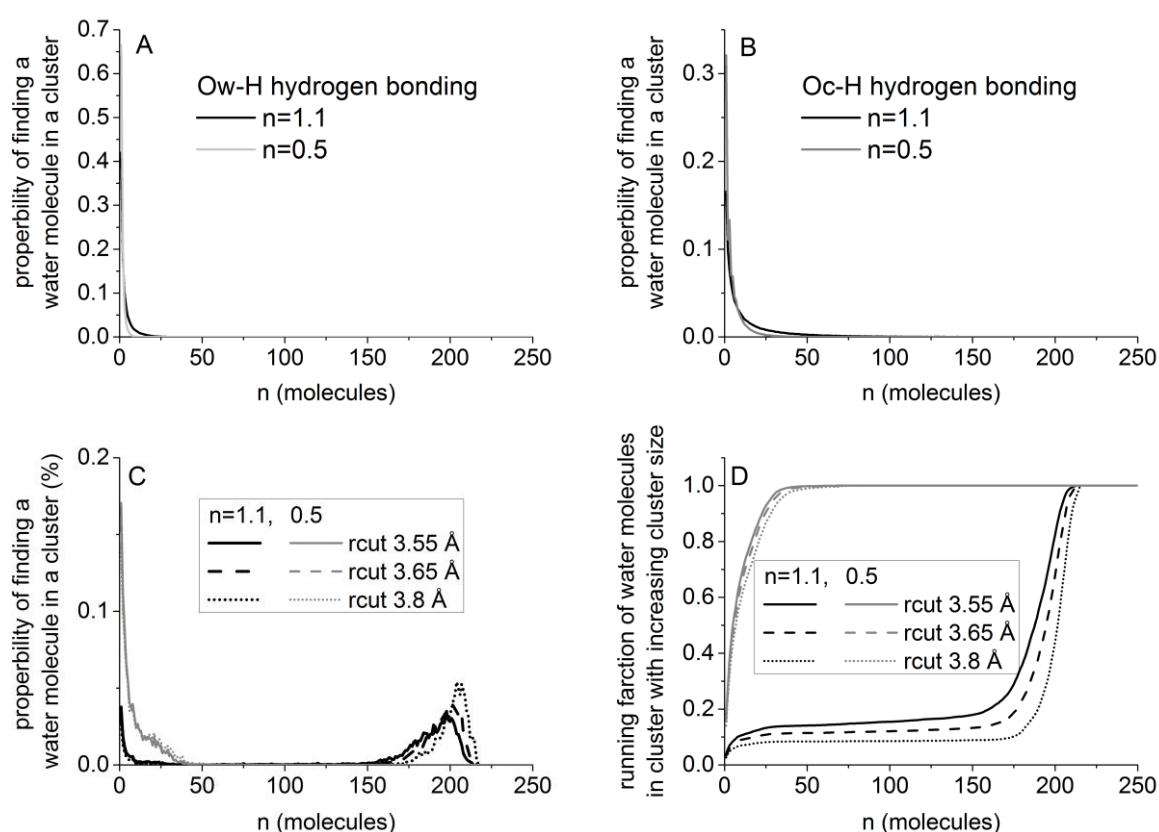
Figure 3.13: Cluster size distribution for the two ACC sample with n=1.1 and n=0.5 with water molecules considered to be in the same cluster if: A) water molecules share a hydrogen bond. B) Water molecule shares a hydrogen bond with a carbonate C) O_w-O_w distances are within r_{cut} as given by Bushuev et al. The large population of clusters at ~200 reflects that the box contains 220 water molecules and these clusters are in principle infinite, due to the periodic boundary conditions. D: cumulative sum of water molecules in a cluster as a function of the cluster size distribution shown in C.

Given the extensive attention to large scale structure involving water pores or water percolation, the EPSR model was used to analyze the presence of confined water pockets and inter connected water pockets[43, 63, 69]. To scrutinize the presence of water percolation, water molecules were counted as being in the same cluster if the O_w-O_w distance is smaller than r_{cut}

(figure 3.12 C and D, r_{cut}=3.55-3.8 Å as defined by Bushuev et al.[69]). A second definition of percolation was also used to determine not just if the water molecules are in close proximity but also if they are linked together by hydrogen bonding, allowing only hydrogen bonds to connect water molecule (figure 3.13 A) and allowing water molecules to be connected via hydrogen bonding to same carbonate ion (figure 3.13 B). With this definition, percolation would result in clusters containing ≈220 or ≈100 water molecules for n = 1.1 and n = 0.5, respectively (*i.e.* almost all of the water molecules in the box). Based on the r_{cut} values percolations were found in the sample with n = 1.1, where approximately 80 – 90 % of the water molecules (≈ 220) are found in clusters, while no clusters with more than 40 molecules are found for the sample with n = 0.5 as expected from the work of Bushuev et al.[69] (figure 3.13 C and D). However, if the water cluster is defined by hydrogen bonding between water molecules, no clusters with more than 25 molecules are found (figure 3.13 A). For hydrogen bonding between water and carbonate ions no clusters with more than 50 molecules are found (figure 3.13 B). This reveals that no long-range hydrogen bonded networks are present in either sample (figure 3.13 A and B). The identification of a water percolated structure, then, critically depends on the definition: samples with n = 1.1 resides above the percolation if defined by Bushuev et al.[69], but water molecules inside these clusters are only infrequently linked by hydrogen bonds between each other and, in this sense; we find no confined "liquid" water structures in any of the samples.

3.2.3 Vibrational spectroscopy of amorphous calcium carbonate

To substantiate the findings of the x-ray and neutron total scattering measurements analyzed through the EPSR model, vibrational spectroscopy was used. Particular focus was put on the change in the carbonate environment using FTIR and the interactions between water and the ions using FTIR and IINS. To emphasis the shift in the vibrational band a third hydration level was added with an n=H_2O/Ca ratio of 0.2 (only measured with FTIR). The vibrational modes of the carbonate and their changes with hydration were investigated with infrared (FTIR) and Raman spectroscopy (figure 3.14). The v_1 (symmetric stretch) and v_3 (asymmetric stretch) bands shift to higher frequencies upon dehydration (figure 3.14 B and F, very small shift for the v_1 band) and the intensity of the v_2 (out-of-plane bending) band increases relative to the v_3 band (figure 3.14 D), confirming a change in the local environment of the carbonate ions. On the v_1 band, a shoulder at 1050 cm^{-1} decreasing with dehydration is observed (figure 3.14 E) while the splitting of the v_3 band increases at lower hydration levels (figure 3.14 F). This band is sensitive to carbonate-related hydrogen bonding and an increase in the splitting indicates a decrease in hydrogen bonding[146], in agreement with the X-ray and neutron scattering results. The vibrational modes of water were compared to liquid water and to a saturated solution of Na_2CO_3. The broad O-H stretching band at 3300 cm^{-1} of H_2O in ACC samples and in the Na_2CO_3 solution show a longer tail towards the low frequency side compared to pure water, suggesting strong hydrogen bonding between carbonate ions and water molecules[147]. This is confirmed by a shift in the bending mode at 1650 cm^{-1} found in both the ACC and carbonate solution spectrum (figure 3.15).
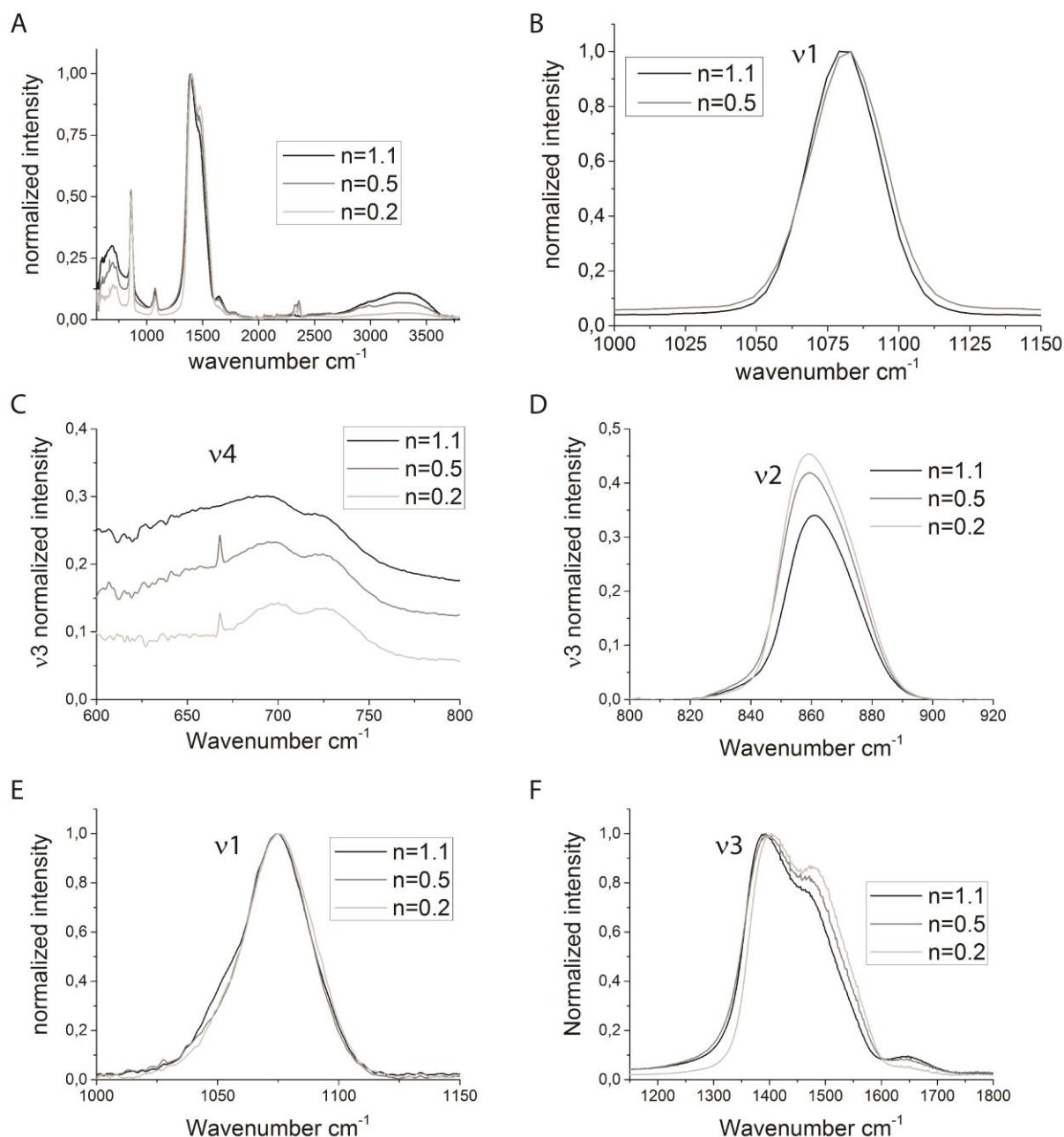
Figure 3.14: A) Full FTIR spectra showing the four carbonate vibrational modes: v_4 in-plane bending at ~700 cm^{-1}, v_2 out-of-plane bending at ~860 cm^{-1}, v_1 symmetrical stretch at ~1050 cm^{-1} and v_3 asymmetrical stretch at ~1400 cm^{-1}. The peaks at ~3300 cm^{-1} and 1650 cm^{-1} correspond to the water stretching and bending modes. The librational mode of water is also seen below 800 cm^{-1}. The various vibrational modes of the carbonate are highlighted. v1 measured with Raman (B) and FTIR (E), v2 normalized to the height of the v3 peak (D), v4 normalized to the height of the v3 peak (C) and the v3 peak (F).
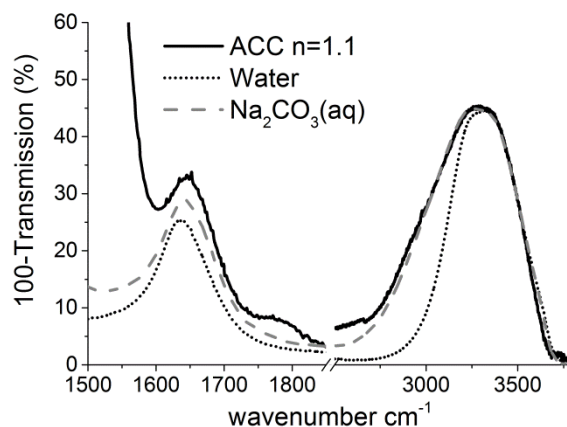
Figure 3.15: FTIR spectra of ACC, H₂O and a saturated Na₂CO₃ solution. Showing the water bending mode at ~1650 cm⁻¹ and the O-H stretch mode at ~3250 cm⁻¹. The spectra have been rescaled to obtain comparative intensities in the O-H stretch bands.

The vibrational modes at very low frequencies, measured by IINS (figure 3.16 A), are assigned to vibrations of inter molecular bonds involving H, in this case between water and the ions. The ACC spectra were compared to the spectra of several compounds available from the online TOSCA database. The spectra show two regions of interest; the translational region (20-400 cm⁻¹) and the librational region (400-1000 cm⁻¹). The low frequency edge of the librational bands is at 400 cm⁻¹ typical of water binding to a single cation[128], as expected from the total scattering analysis where ~40% of the water molecules coordinate to one Ca. The translational band shows a sharp Ca-OH₂ stretch band at 85 cm⁻¹, indicating that the Ca-OH₂ bond is weaker in ACC than in MHC where the Ca-OH₂ stretch is located at 157 cm⁻¹ (figure 3.16 B).
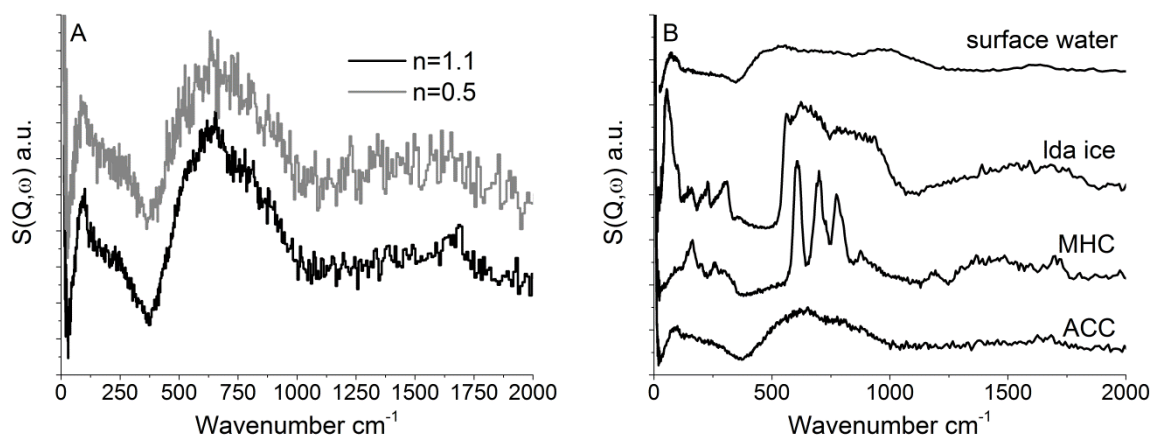
Figure 3.16: IINS spectra of ACC with n=1.1 and n=0.5 performed at <30 °K (A) and comparison of ACC (n=1.1), monohydrocalcite (MHC), low density amorphous ice (LDA ice) and water on a PdO catalyst (B). The band seen at 20-400 cm⁻¹ originate from the translational modes and the bands at 400-1000 cm⁻¹ originate from librational modes of the water molecules as explained in chapter 2.3.1[128].

The absence of a peak in the 200-400 region rules out any large scale hydrogen bond network as found in both amorphous (*e.g.* low density amorphous ice[126]) or crystalline (e.g. MHC) compounds containing hydrogen bonded networks (figure 3.16 B). The IINS spectra show considerable similarity to that of disordered water bound to the surface of a PdO catalyst[133] and to that of water in amorphous calcium phosphate, in which local hydrogen bonding interactions exist but there is no extended hydrogen bonded network[132].

3.2.4 Discussion

The EPSR model was compared to the previously published structural analysis of ACC and it was found that the Ca-O distances of ~2.4 Å similar to that found by previous EXAFS[6, 29, 33, 45-46, 48-49, 55, 148], NMR spectroscopy[64] and diffraction studies[43, 63]. The mean coordination number of oxygen binding to calcium reported in literature for both biogenic and synthetic ACC ranges from 4 to 8, with most studies reporting values around 6-7, with values for synthetic ACC[29, 43, 70] close to the coordination number of 7.2 found in this study. The broad distribution in coordination numbers (figure 3.9 B) is similar to what was reported by Goodwin et al.[63] (figure 1.2 B). The percolation analysis showed that water percolation may exist similar to what was described by Bushuev et al[69], but that water in these percolation are only infrequently hydrogen bonded together. Unlike the previous studies that have used EPSR[43] and RMC[63] we found no unphysical bond distance in our model, nor were there any charge separation present. All the direct bond distances found in the model, i.e. calcium to oxygen bond and hydrogen to oxygen bonds were very similar to what has been reported for the crystalline phases[50-54]. We also found that the nearest neighbor coordination numbers were within the range reported for the crystalline calcium carbonates[50-54]. The comparison with the previously published experimental data and with the known crystalline phases show that the model may indeed be accurate as nothing was found to contradict the model.

The deconvolution of the pdf into the various ppdfs showed correlation up to 5 Å for most of the pairs originating from direct interactions between ion/molecules (figure 3.8). The pairs that showed longer correlation lengths (up to 15 Å) were the pairs related to the carbonate molecules or the highly charged Ca ion, indicating that order beyond the first coordination sphere is introduced by the strong repulsion between highly charged atoms or via sterical constrains generated by rigid molecular structure. This correlation can reach long distances when these are combined as seen in the carbon-carbon ppdf related to adjacent carbonate ions that reaches >10 Å, since this correlation is caused by multiple carbonate ions sharing the same calcium ions to form a rigid structure. The coordination number distributions were calculated for all coordination spheres mentioned in table 3.4 but only shown for a few coordination spheres (figure 3.9 A, B and 3.11 A, B). These showed a broad distribution for all coordination spheres, except the ones where sterical constrains limited the coordination number as seen in the first coordination sphere of O around H (figure 3.11 B). This reflects that there is a wide diversity of binding site in ACC caused not only by the amorphous nature of ACC but also by the numerous combinations of O_w and O_c making up the local environment of the calcium ions. The diversity in binding site for the various ion/molecules making up ACC placed a huge requirement for any structural analysis of ACC as simplistic models[149-150] such as the small box models mentioned in chapter 1.5 cannot fully describe this disorder.

The dehydration process resulted in a general increase in the mean coordination number (table 3.4). This is likely caused by the removal of water molecules from the calcium ions, generating oxygen "vacancies" on the calcium ion (figure 3.9 B) evident from the shift of the distribution of coordination numbers for oxygen from water around calcium to lower numbers. This in turn induced a reorientation of the carbonate molecule to remove the vacancy and maintain the same mean coordination number of oxygen around calcium causing an increased mean number of calcium ions binding to each carbonate ion and vice versa (figure 3.9 B and table 3.4). Consistent with the increase mass density of the dehydrated sample (n=0.5) compared to the as prepared sample (n=1.1).

The angular distribution of oxygen from carbonate around calcium only showed preferred angles below 100° indicating that the angle between adjacent carbonates (O_c) in most the calcium sites are close to 70° (figure 3.9 C). The lack of preferred angle above 100° reflects that these angles are strongly dependent on the coordination number[50-54] and is averaged out by the wide distribution of coordination numbers (figure 3.9 B). The two preferred angles (figure 3.9 D) of 65° and 140° between oxygens from water binding to Ca are reminiscent of the values observed for the square antiprism coordination of the Ca ion in solution[145], but the combination of angles is not present in any of the known hydrated minerals nor do they show the squared antiprism coodination[52-53], suggesting that the hydration shell of the ion may be partially preserved during the precipitation event. This is further corroborated by the high similarity of the O-H stretch bands in the FTIR spectra of the ACC sample and that of the saturated Na_2CO_3 solution. Our model indicates that water is highly important to the structure of ACC as it adopts conformations that are comparable to the average structure of water interacting with ions in solution. Although the water in ACC are likely to be highly static, while water bound to ions in solution is highly labile[151]. No evidence was found for conformations close to those found in any of the crystalline compounds. This is in good agreement with ACC forming via spinodal decomposition[152-154], where precipitation occurs instantly by instability of the solution and where dissolution/reprecipitation of ions is very limited causing the hydration water associated with the ions to get trapped during the precipitation event.

Several binding sites for water were found in ACC, with hydrogen bonding occurring mainly between water and carbonate and less frequently water hydrogen bonded to other water molecules. However, all the water molecules were found to bind to the carbonate molecule through at least one hydrogen bond. The water was also found to coordinate calcium for over 90% of the water molecules. Since all the water molecules were found to have water-anion bonds and most binding to both calcium and carbonate ions, the water can best be described as structural rather than a mixture of structural, mobile and liquid like as have been suggested by previous studies[56, 59]. The different hydrogen bonding environments could explain the fact that NMR studies[57-59] report multiple mobility's for hydrogen. However, the model presented here is purely structural, making dynamical considerations only possible at a speculative level. Moreover, our results suggest that the observation of different dehydration rates in ACC, as measured by TGA, is related to a gradual change in local structure upon dehydration rather than originating from an initial state with distinct water species[59]. This also implies that

molecular rearrangement, at least to some extent, takes place at much lower temperature than the crystallization temperature.

The addition of vibrational spectroscopy corroborated the findings in the EPSR model. The FTIR analysis showed that hydrogen bonding to the carbonate ion was lowered during dehydration as evident by a splitting of the asymmetric stretch of the carbonate ion (figure 3.14 F) as suggested by the EPSR model (table 3.4). The change in the intensity of the in-plane bending compared to the asymmetrical stretch band (figure 3.14 D) also show a change in the local environment of the carbonate ion[155], likely caused by a change in the number of calcium ions coordinating to the carbonate ion (table 3.4). The IINS spectrum (figure 3.16) showed that the water molecule was bound to calcium by the position of the translational mode, consistent with the EPSR where 90% of the water molecules are bound to calcium. Consistent with the EPSR analysis of the hydrogen bonding in ACC, the lack of a peak in the 200-400 cm^{-1} range further indicated that no extended hydrogen bonded network was present[128, 132] as one would expect from any liquid-like water present in the sample[130]. Finally the low energy of the libration band suggested that the water molecules mainly bind to a single calcium ion, again supporting the EPSR model that suggested that 40% of the water molecules bind to a single calcium ion.

3.2.5 Conclusion

We produced an atomistic model of ACC based on X-ray and neutron scattering data analyzed by the EPSR program. This model is in excellent agreement with analyses of vibrational spectroscopy data and in good agreement with the previous reported structural information on ACC. Furthermore no unphysical structural motifs were found in the model as have plagued previous attempts to model the structure of ACC[43, 63]. Herein, we described several structural features beyond that of the Ca-O distance and average coordination number that have so far not been available from literature. E.g. the ratio between bidentate($\sim$20%) and monodentate(80%) binding, fraction of hydrogens participation in hydrogen bonding with water($\sim$10 %) and carbonate ($\sim$70%), amount of water molecules interacting with carbonates(100%) and Ca ions($\sim$90%). We found that the dehydration of ACC by heating results in a densification of the material and in a change of its local structure. This change is mainly associated to a rearrangement of the carbonate ions induced by the removal of water. Analysis of large scale structure in the model reveal that water percolation may exist, but there is no evidence for long-range hydrogen bonded networks (i.e. water pores but without any hydrogen bonding between water molecules in the pore). We also find that the local structure of ACC studied here is related to the structure of the ions in solution prior to precipitation, which seems to support recent observations suggesting that ACC forms by rapid precipitation in unstable solutions. Although, to better understand the formation of ACC, a more detailed structural understanding of the ions in solution is likely needed, our results provide detailed insight into the structure of ACC and how dehydration leads to reorientation of the ions far below the crystallization temperature.

Furthermore the deconvolution of the pdf into the ppdfs showed correlation up to 15 Å with the four calcium-calcium coordination spheres originally reported by Michel et al[36]. This could essentially be used to assess changes to the local structure of ACC in future studies

given that the pdf of a purely amorphous sample can be measured and the ppdf of interest has a high enough intensity in the data. However it should be noted that the correlations in the pdf above 8 Å are very small and may not be experimentally accessible unless a full deconvolution is performed.

3.2.6 Materials and methods

Synthesis: ACC samples was made by a modified version of the procedure reported by Zou et al[27]. 20 mL of 1 M $CaCl_2$ solution (>99% $CaCl_2.2H_2O$ Sigma Aldrich) was added to 480 mL Na_2CO_3 solution (99.999% $Na_2CO_3.10H_2O$ Sigma Aldrich) to a final concentration of 40 mM. The suspension was filtered through cellulose acetate filters with 0.45 μm pore size. The samples were washed with cold ethanol and dried in a desiccator under vacuum. Each batch yielded 2-2.5 grams of sample. To make the dehydrated sample, ACC was placed on a watch glass and heated in a muffle oven at 100 °C for 90 min. The samples were transported in a desiccator for both x-ray and neutron pdf measurements.

ICP-OES: Sodium impurity levels was checked by ICP-OES (optima 8000 ICP-OES spectrometer, PerkinElmer, Waltham, MA)

TGA/DSC: hydration levels were determined by TGA/DSC (SENSYS evo TGA-DSC, SETARAM instrumentation, Caluire, France). The samples (>10 mg) were heated in alumina crucibles to 800 °C at 2 °C/min under argon gas flow.

Pdf measurements: x-ray pdf was measured at ID11 at the ESRF (Grenoble, France) using a 0.14088 Å beam and a Frelon2K detector. Neutron PDF was measured at the SANDALS Instrument[120] at ISIS (STFC Rutherford Appleton Laboratory, Didcot, UK). ~5 g of sample was placed in a 12 mm thick sample can with vanadium windows. The thick sample can was chosen due to the low sample packing fraction of ~ 10%. Each sample was measured for ~ 8 hours. Data reduction for both x-ray and neutron measurement was performed in Gudrun[117].

Incoherent inelastic neutron scattering(IINS): IINS was performed at the TOSCA instrument at ISIS (STFC Rutherford Appleton Laboratory, Didcot, UK). Samples were mounted in aluminum envelopes and placed in 6 x 6 cm aluminium cans of 5-10 mm thickness and sealed with indium wire. Samples were cooled to <30 °K before measuring and kept at ~10 °K during the measurement. Spectra were measured in energy loss mode from -20 cm^{-1} to 4000 cm^{-1}. The spectra are only displayed to 2000 cm^{-1} due to high peak overlap at high energy transfer, as is common for spectrometers of this design.

Pycnometry: Pycnometer measurement was performed on a Ultrapycnometer 1200e MUPY-31-T (Quantachrome Instruments, Boynton Beach, Florida, US). ~ 1 g was place in a ~4 mL sample holder and measured using Ar gas. 18 measurements were performed of which the last 5 were averaged for the final measurement.
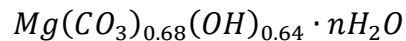
FTIR: FTIR-ATR was performed on a Nicolet IS5 (Thermo Fisher scientific, Waltham, MA, US) with an ID5 ATR module. Spectra was measured from 550 to 4000 cm^{-1} and averaged over 64 spectra.

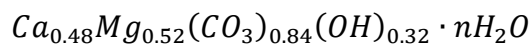## 3.3   The effect of Mg as an additives on the structure of ACC

As mentioned in chapter 1.4 Mg^{2+} is one of the most common additives found in biogenic ACC[21] acting as a kinetic stabilizer. However, it is unclear what the local structure around magnesium is in the amorphous phase and how it affects the local environment of the other ions, especially when mixed with calcium in ACMC. The only extensive structural model of AMC available is of $MgCO_3 \cdot 3H_2O$[84]. However, this compound contains three times the water compared to biogenic ACC and a structural model of comparable hydration level is required. Moreover the coprecipitation of hydroxide with magnesium in both ACMC and AMC (see chapter 3.1) makes it important to take hydroxides into account as this ion by itself is also known to stabilize the ACC phase. Here we present a atomistic model of ACMC and AMC based on combined x-ray and neutron total scattering analyzed using empirical potential structural refinement (EPSR)[110-111], substantiated with vibrational spectroscopy. This has revealed that magnesium places significant constraints on its local environment by adopting near octahedral coordination in the first coordination sphere. During dehydration the local environment of calcium in ACMC showed significant more change then the one of magnesium, whereas almost no change is observed in the local environment of magnesium in AMC. Finally the incorporation of hydroxide ions significantly change the hydrogen bonding from primarily occurring between water and carbonate in ACC (see chapter 3.2) and ACMC to a mix of hydrogen bonding occurring between water, hydroxide and carbonate in AMC.

3.3.1   Sample characterization

Samples were made with two Mg/(Ca+Mg) ratios of 100% and 52%. Given a composition for AMC of (see chapter 3.1):

$$Mg(CO_3)_{0.68}(OH)_{0.64} \cdot nH_2O$$

And for ACMC:

$$Ca_{0.48}Mg_{0.52}(CO_3)_{0.84}(OH)_{0.32} \cdot nH_2O$$

Partially dehydrated samples were prepared for both AMC and ACMC. TGA measurements showed a water content of n=1.1 and 0.5 for ACMC and 1.2 and 0.7 for AMC. Fully dehydrated samples were also prepared for FTIR analysis. He gas pycnometric measurements showed that the density of AMC was 1.924(4) and 1.933(4) g/cm^3 for n=1.2 and n=0.7 and for ACMC the density was determined to be 2.032(3) and 2.158(2) g/cm^3 for n=1.1 and n=0.5 respectively. The structure factors and pdfs of AMC and ACC are shown in figure 3.17. Given the low scattering power of the magnesium samples, the x-ray measurement are inherently noisy and for the ACMC measured at I15 the background measurement contributed with ~90%[j] of the total signal, making background subtraction difficult for these samples

---

[j] We were advised to used fused silica capillaries with a wall thickness of ~1mm at the I15 which turned out to scatter x-rays 10 times more than the sample, while the samples measured at the ESRF were mounted in kapton capillaries with <0.1 mm wall thickness where capillary scattering was less of a problem.

(explained in chapter 2.1.1). The intra molecular distances for all samples are found at 1Å (negative peak only observed in n-pdf), 1.3Å and 2.2Å from O-H, C-O and O-O intramolecular distances in water/hydroxides and carbonates (figure 3.17 B and C). In the pdf from the AMC samples (figure 3.17 B) interatomic/molecular peaks are seen at 2.2, 3, 4, 5, 6 and 7 Å in the n-pdf and at 2.2, 3 and 4 Å with several overlapping minor peaks in the range between 5 and 8 Å for the x-pdf. The first peak at 2.2 Å originate from the Mg-O distance as expected when compared with magnesite[50]. The correlation at 3 Å is more difficult to assess as this distance is characteristic of O-O[91, 93], Mg-Mg[156], Mg-C[50] and O-H[91] distances. The correlation from 4 Å to 8 Å become more obscure and given the similar scattering lengths of the elements in both x-rays and neutrons it is nearly impossible to assign pairs to each of these correlations without using computer modeling.
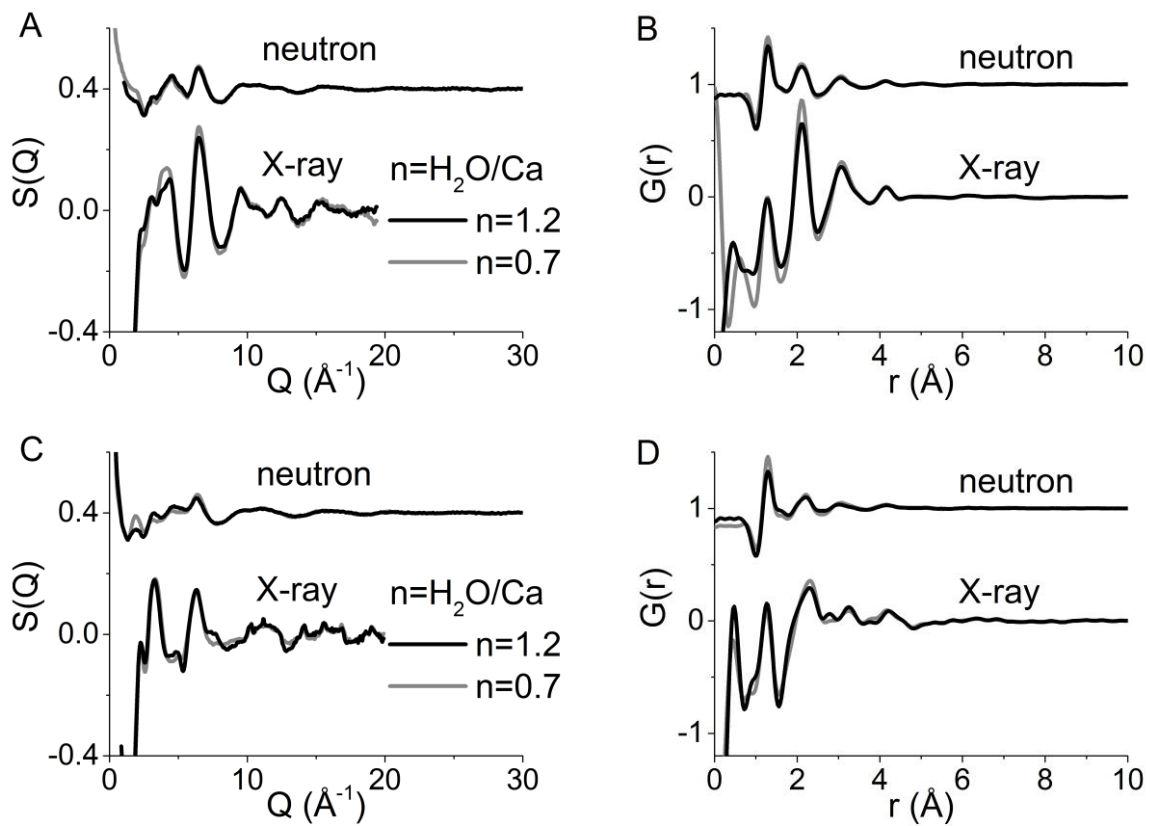
Figure 3.17: Structure factor of AMC (A) and ACMC (C) measured using x-rays and neutron sources and the corresponding pdf (B and D). The minor peaks in the X-ray pdf of ACMC are caused by the high background of the measurements taken at I15.

For the ACMC samples (figure 3.18 D) a broad peak is present between 2.2 and 2.4 Å originating from the Mg-O and Ca-O nearest neighbors distances and the O-O intramolecular distance in the carbonate ion. In the x-pdf most of the peaks from 5-8 Å are overlapping with truncation ripples and cannot be discerned although a weak broad peak may be present at 6 Å. The shorter distances at 3 and 4 Å are present as expected since these are also present in AMC and ACC. In the n-pdf the peaks at 3 and 4 Å are also present but again the peaks at larger distances are missing. The loss of peaks at larger distances is expected as the number of ppdf increases as mentioned in equation 1.1 giving 28 ppdfs for AMC and 36 ppdfs for ACMC,

with so many ppdf it is likely that several of the long range correlations are hidden in the pdf. However, given the right density, molecular structure and potentials they can be estimated using the EPSR method[61, 112].

3.3.2 EPSR fitting of amorphous magnesium and calcium/magnesium carbonate

For the ESPR model cubic boxes were made with the following specifications:

Sample	Number of Mg	Number of Ca	Number of CO_3	Number of OH	Number of H_2O	Total number of atoms	box side length (nm)	Atomic density (atoms/$Å^3$)
Table 3.5: model parameters for AMC and ACMC modeling								
AMC								
n=1.2	4000	0	2800	2400	4800	34.400	6.97	0.102
n=0.7	4000	0	2800	2400	2800	28.400	6.74	0.0927
ACMC								
n=1.1	104	96	168	64	220	1660	2.57	0.098
n=0.5	104	96	168	64	100	1300	2.44	0.089

The very large box size for the AMC samples were chosen as there was a suspicion of finite size effects coming from the box size, fortunately no box size effect was found when comparing the larger (4000 formula units) and smaller box (200 formula units). However, the larger box had accumulated significantly more statistics on the structure and was therefore used for the analysis. The same intra molecular constraints were used here as for the ACC samples (table 3.2) with the added constrain of a 0.976 Å O-H distance for the hydroxide ion. The intermolecular potentials from the ACC model was again used for the calcium, carbonate and water ion/molecule (table 3.3) and for the magnesium[145] and hydroxide[107] ions the following potentials were added.

Table 3.6: Interatomic/molecular potentials

Atom	E [kJ/mole]	σ [Å]	Charge [e]
Mg	0.175	2.3	1.86
O_{hydroxide}	0.251	3.5	-1.3538
H_{hydroxide}	0	0	0.4238

Given the high number of partial pairs, the minimum number of configuration for the final fit was increased to 50.000^k to ensure a minimum level of noise in the ppdf. Especially the ppdfs related to hydroxides suffered from low statistics as this is the component with the lowest concentration. The fit to the AMC samples are shown in figure 3.18. The x-ray structure factor (figure 3.18 A) for both samples is reproduced fairly well by the model except the region around 5 $Å^{-1}$ with a corresponding region around 3 Å in the x-pdf (figure 3.18 B) where the largest difference between the calculated and experimental measurements are seen. The fit to the neutron pdfs (figure 3.18 D) and structure factors (figure 3.18 C) also show a difference at ~3 Å and ~5 $Å^{-1}$ suggesting that this is a real correlation present in the system that is not described well by the model. However, the difference is minor and could be caused by error in the compositional analysis, inherent when so many molecule/atom are present in the same sample. The poorly fitted area below 2 $Å^{-1}$ (figure 3.18 C) is caused by the correction for the incoherent scattering that is an inherent problem with samples with high hydrogen content.

Figure 3.18: Experimental (dots) and simulated (lines) structure factor (A and C) and pdf (B and D) of AMC for both hydration levels. Data measured with X-rays (A and B) above and neutrons below (C and D).

The fit to the ACMC sample is shown in figure 3.19. The poor background subtraction for the x-ray structure factor makes it difficult to determine if the model reproduces the fine details of the x-ray pdf. However, the major components of the pdf is clearly reproduced well by the model (figure 3.19 A). Fortunately the formulation of the empirical potential (equation 2.16)

---

^{k} Configurations were accumulated for 5+ days per sample on a desktop computer.

does not allow the program to fit the sharp peaks at high Q present in the x-pdf (figure 3.19 A). The x-pdf shows that the peaks are at 1.3, 2.3, 3 and 4 are all described by the model, since the peaks at longer distances are not present in the pdf, deconvoluting them will depend mainly on the potentials and the constrains placed on the model by the shorter distance correlations. The fit to the neutron structure factor show that the model describes the data well with only minor differences, mainly present in the low Q due to the correction for the inelastic scattering (figure 3.19 C). However, this was less of a problem in these samples compared to the AMC samples (figure 3.18 C). The n-pdfs also show a good fit to the experimental data with the four main peaks described well. From the final model the pdf was deconvolute into the 28 and 36 ppdfs from AMC and ACMC respectively as shown in figure 3.20 and 3.25. For clarity the three types of oxygen will be referred to as O_c, O_h, O_w and O for oxygen from carbonate, hydroxide, water and all respectively and the two types of hydrogen will be referred to as H_w, H_h and H for hydrogen from hydroxide ions, water molecules and both respectively.
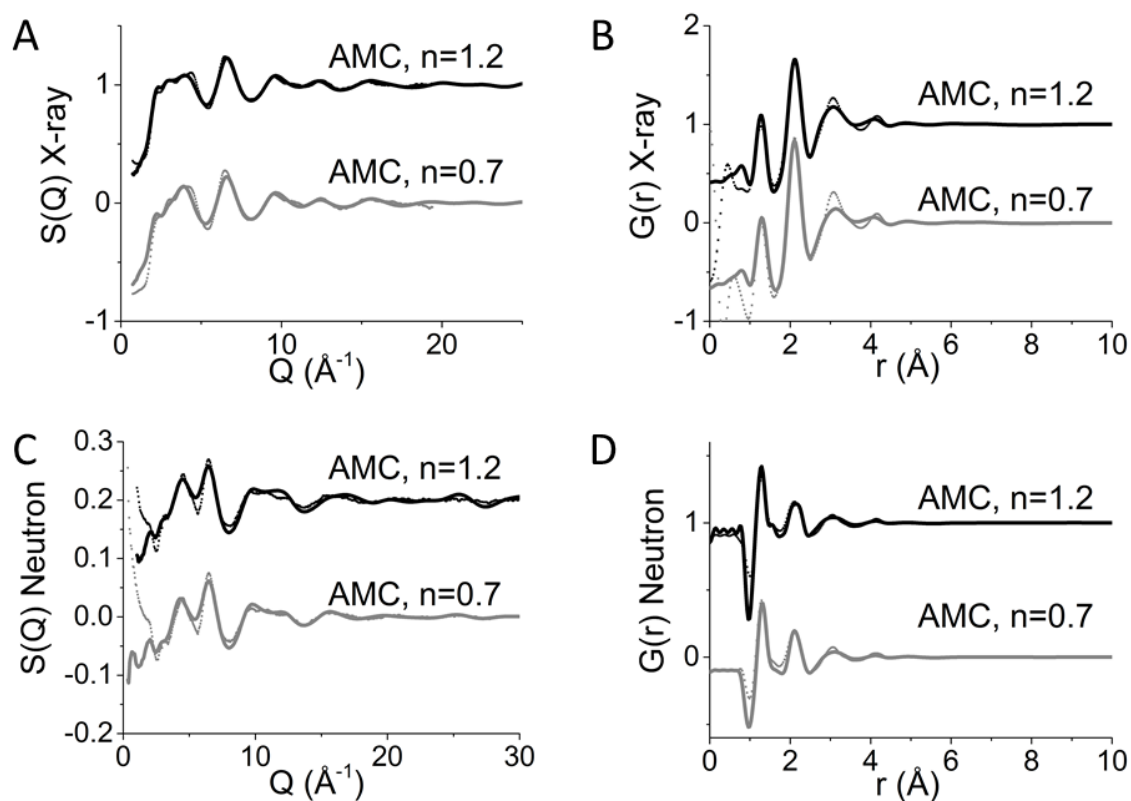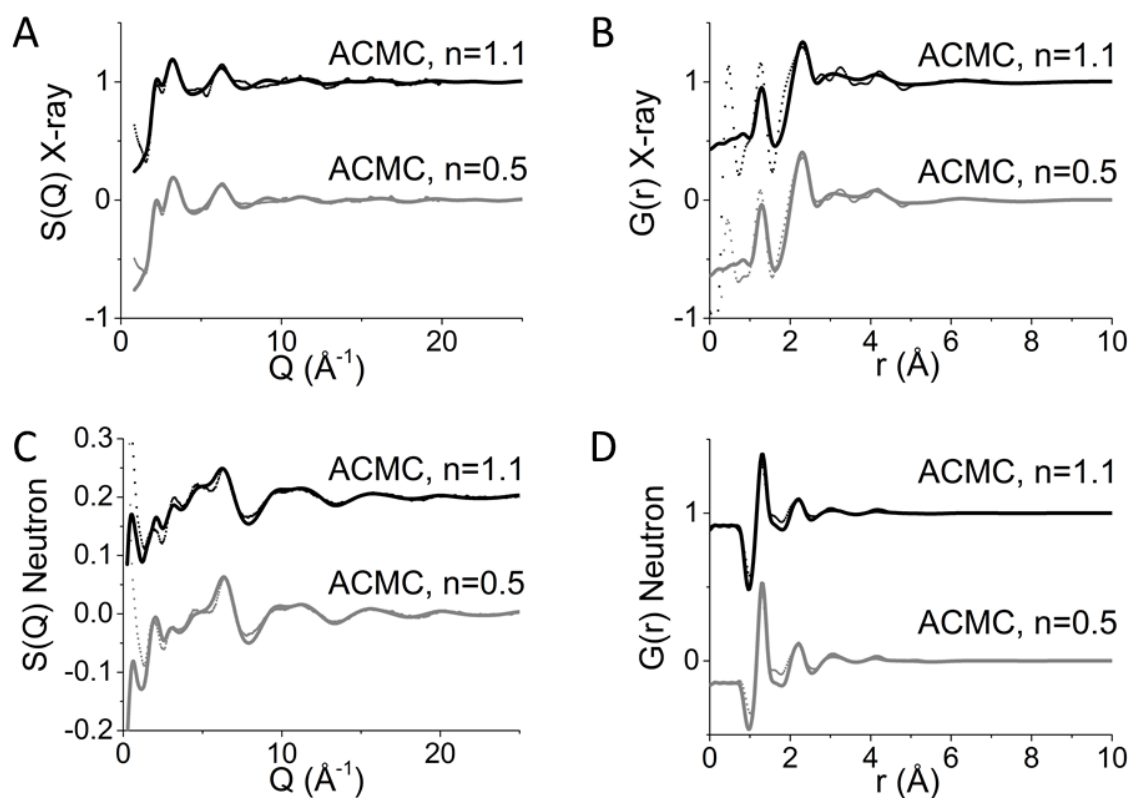

Figure 3.19: Experimental (dots) and simulated (lines) structure factor (A and C) and pdf (B and D) of AMC for both hydration levels. Data measured with X-rays (A and B) above and neutrons below (C and D). The x-ray data was weighted less than the neutron data in these samples due to the high noise and poor background subtraction.

3.3.2.1 Ppdf and coordination number of AMC

Similar to the ACC most of the features in the ppdf (figure 3.20) are confined to the region below ~5 Å and can be assigned to nearest and next nearest neighbor distances. However, several of the ppdf show broad peaks above 5 Å indicating a broad diffuse third coordination sphere. The Mg-Mg ppdf (figure 3.20 A) shows three coordination spheres at 3.6, 5.7 and 8.3

Å with a splitting of the 3.6 Å peak and no correlations above 10 Å. The split peak at 3.6 Å can be assigned to an Mg-O_h-Mg motif with an expected distance of 3.2 Å[91] and an Mg-$O_{c/w}$-Mg motif with a distance of 3.6 Å[91]. Only three correlation spheres are seen compared to the four observed in the Ca-Ca ppdf in ACC (figure 3.8 A). The intense peak at 2.2 Å in the Mg-O ppdfs show that carbonate, hydroxides and water ion/molecules all bind directly to the magnesium ion (figure 3.20 B-D). In the Mg-O_w ppdf (figure 3.20 D) a second and third coordination sphere is observed, this is also observed in the Mg-O_h ppdf (figure 3.20 C) where a fourth coordination sphere is also present.
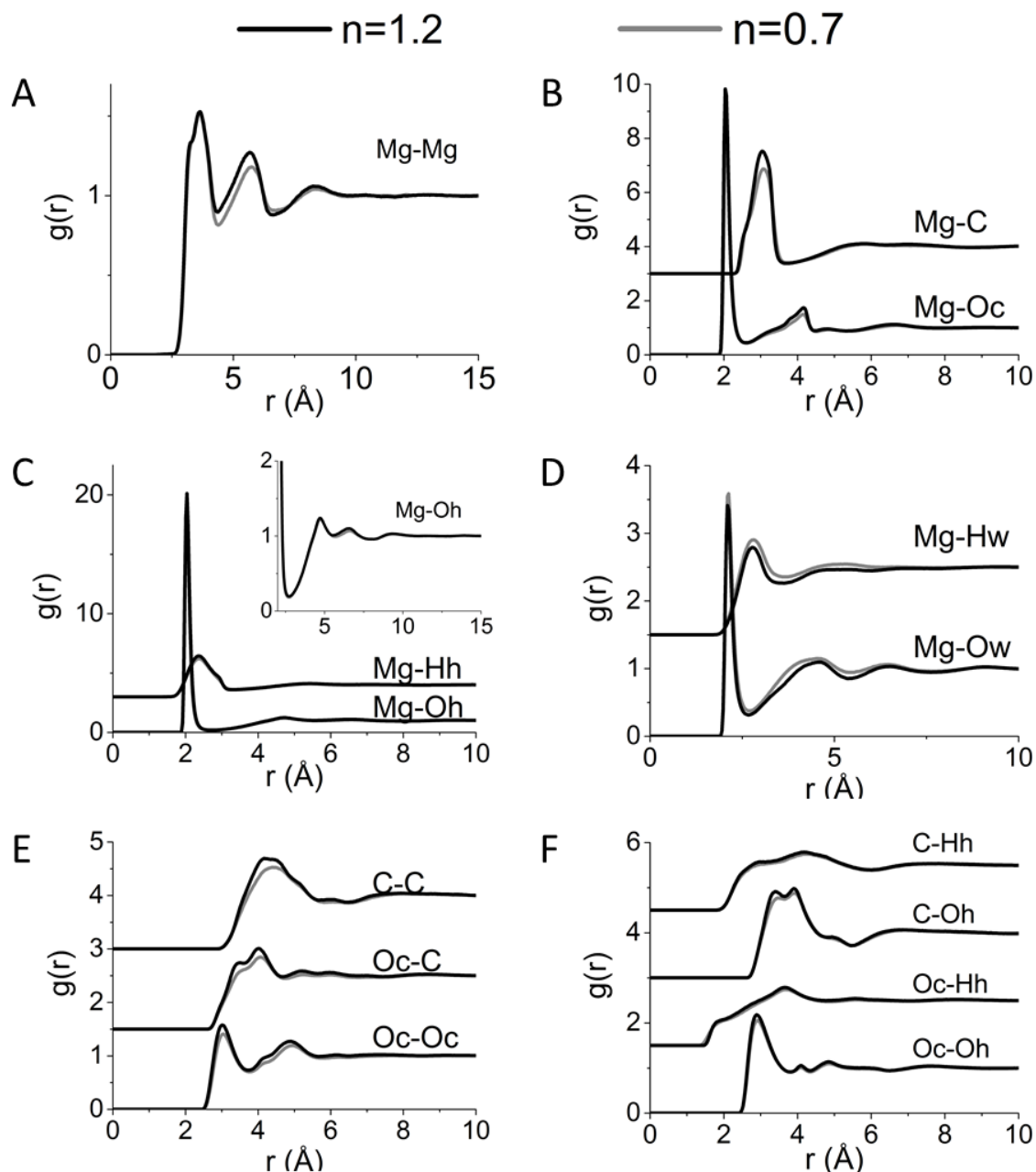
Figure 3.20: Intermolecular ppdfs of the 28 atomic pair in ACC. with pairs between A) magnesium and magnesium, B) magnesium and carbonate, C) magnesium and hydroxide, D) magnesium and water, E) carbonate and carbonate and between carbonate and hydroxide ion(F). The figure is continued on the next page.
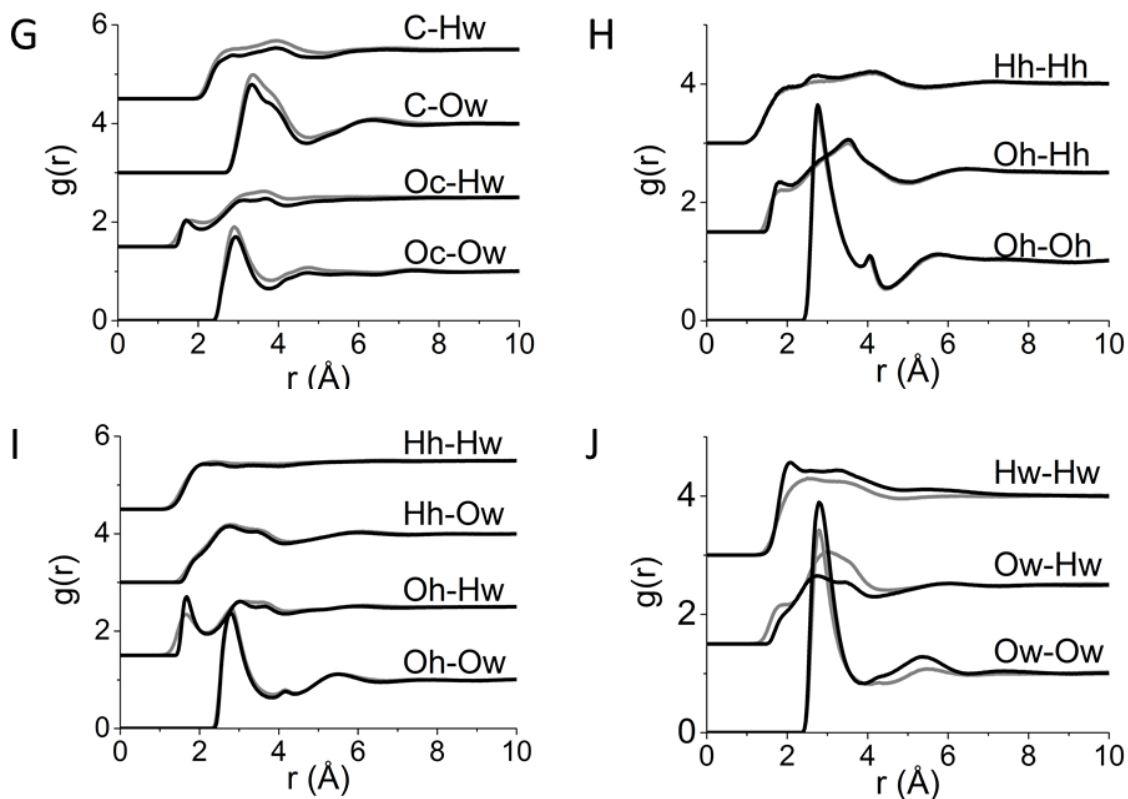
Figure 3.20 continued: Intermolecular ppdfs of the 28 atomic pair in ACC. with pairs between G) carbonate and water, H) hydroxide and hydroxide, I) hydroxide and water and between water molecules (F).

For the $Mg-O_c$ ppdf (figure 3.20 B) no sharp third peak is observed, but the second peak is significantly different in shape then what was observed for $Ca-O_c$ ppdf in ACC (figure 3.8 B). Combining this with the single peak in the Mg-C ppdf (figure 3.20 B) at 3.6 Å suggests that magnesium prefers monodentate binding to the carbonate more so than calcium. In all the O-O ppdfs, (figure 3.20 F-J) peaks are seen at ~4.2 Å this would correspond to a linear O-Mg-O motif[50] suggesting a well-defined first coordination sphere.

Hydrogen bonding can be assessed from the 1.8 Å peak in the O-H ppdfs (figure 3.20 F-J). Comparing the $O-H_w$ and the $O-H_h$ ppdfs it is clear that the peaks in $O-H_w$ ppdfs at 1.8 Å are more pronounced, suggesting that H_w is the main hydrogen bond donor with hydrogen bonding between H_w and O_h being the most favored hydrogen bond (figure 3.20 I). Similar comparison can be made between O_c-H, O_h-H and O_w-H ppdfs and here it is clear that the 1.8 Å peak in the O_h-H ppdfs are more pronounced (figure 3.20 F-J), suggesting that O_h is the main hydrogen bond acceptor followed by O_c and O_w being the least favored. Mean coordination numbers were calculated for 83 coordination spheres from the ppdfs shown in figure 3.20, some selected mean coordination numbers are shown in table 3.7. Most coordination spheres showed an increased mean coordination number with an average increase of 25 %(median 8%) and the coordination spheres related to water molecules generally showed a decreased mean coordination number with an average of -30%(median -32%). The coordination number of O around Mg was determined to be 5.0 for both samples with minor increases in the number of O_h and O_c around magnesium with dehydration (table

3.7) similar to what was seen for ACC (table 3.4). Analysis of the $Mg-O_w$ direct binding peak at 2.2 Å (figure 3.20 D) showed that 66% and 77% of the water molecules bind directly to the magnesium ion for n=1.2 and 0.7 respectively. Since there is no clear minimum between the monodentate and bidentate peak in the Mg-C ppdf the ratio could not be directly estimated and the number of carbonates (i.e. number of C around Mg) coordination to Mg of 2.9 (table 3.7) includes both binding types. However, using Mg-C distances taken from the nesquehonite[92] ($MgCO_3 \cdot 3H_2O$) and magnesite[50] the ratio of monodentate/bidentate binding was roughly estimated to be 10% bidentate binding and 90% monodentate binding for both samples. However, this is highly sensitive to the distances chosen. The relative change to number of magnesium around magnesium in AMC is roughly one third of what was seen for the first two coordination spheres in the Ca-Ca ppdf (table 3.4), indicating that there is less structural change, relating to the ions, occurring in AMC compared to the ACC during dehydration. However, some of this is also attributed to the smaller change in hydration level between the two AMC samples compared to the two ACC samples. Analysis of the H_w-O binding peaks at 1.8 Å (figure G, J and I) shows that nearly all the water molecules are interacting with either hydroxide or carbonate through hydrogen bonding and 21% of the water is hydrogen bonded together for n=1.2.

Table 3.7: Mean coordination number from AMC of specific pair given as number of atom 2 around atom 1.

Atom 1	Atom 2	R_{min} (Å)	R_{max} (Å)	CN n=1.1	esd n=1.1	CN n=0.5	esd n=0.5	Change %
Mg	Mg	1	4.3	3.4	1.4	3.6	1.3	7.6
Mg	Mg	4.3	6.55	10.8	2.5	11.3	2.4	4.2
Mg	O_c	1	2.65	2.9	1.2	3	1.2	3
O_c	Mg	1	2.65	1.4	0.6	1.4	0.6	3
Mg	C	1	3.75	2.9	1	2.9	1	1
C	Mg	1	3.75	4.1	0.9	4.2	0.8	1
Mg	O_h	1	2.75	1.3	1	1.4	1	4
O_h	Mg	1	2.75	2.2	0.6	2.3	0.6	4
Mg	O_w	1	2.75	0.8	0.8	0.6	0.7	-30
O_w	Mg	1	2.75	0.7	0.6	0.8	0.5	19
H_h	O_c	1	2.2	0.4	0.5	0.4	0.6	6
H_w	O_c	1	2.2	0.3	0.5	0.4	0.5	39
H_h	O_h	1	2.2	0.2	0.4	0.6	0.6	312
H_w	O_h	1	2.2	0.2	0.4	0.2	0.4	8
H_h	O_w	1	2.2	0.1	0.3	0.1	0.3	22
H_w	O_w	1	2.2	0.2	0.4	0.5	0.6	157

After dehydration around half of the water is hydrogen bonded together, but nearly all the water molecules still show hydrogen bonding to the anions.

3.3.2.2 Magnesium and carbonate environment in AMC

In figure 3.21 (A and B) the distribution of coordination numbers for the most relevant pairs around magnesium is shown. The distributions of number of nearest and next nearest neighbor magnesium around magnesium in the first two coordination spheres (figure 3.20 A) are both broad distributions, comparable to what was shown for calcium pairs in ACC (figure 3.9 A). Similar to ACC a shift is observed to higher coordination numbers (figure 3.21 A). However, the shift is significantly smaller compared to that of ACC indicating that the overall structural changes related to the ions in the system are minor.

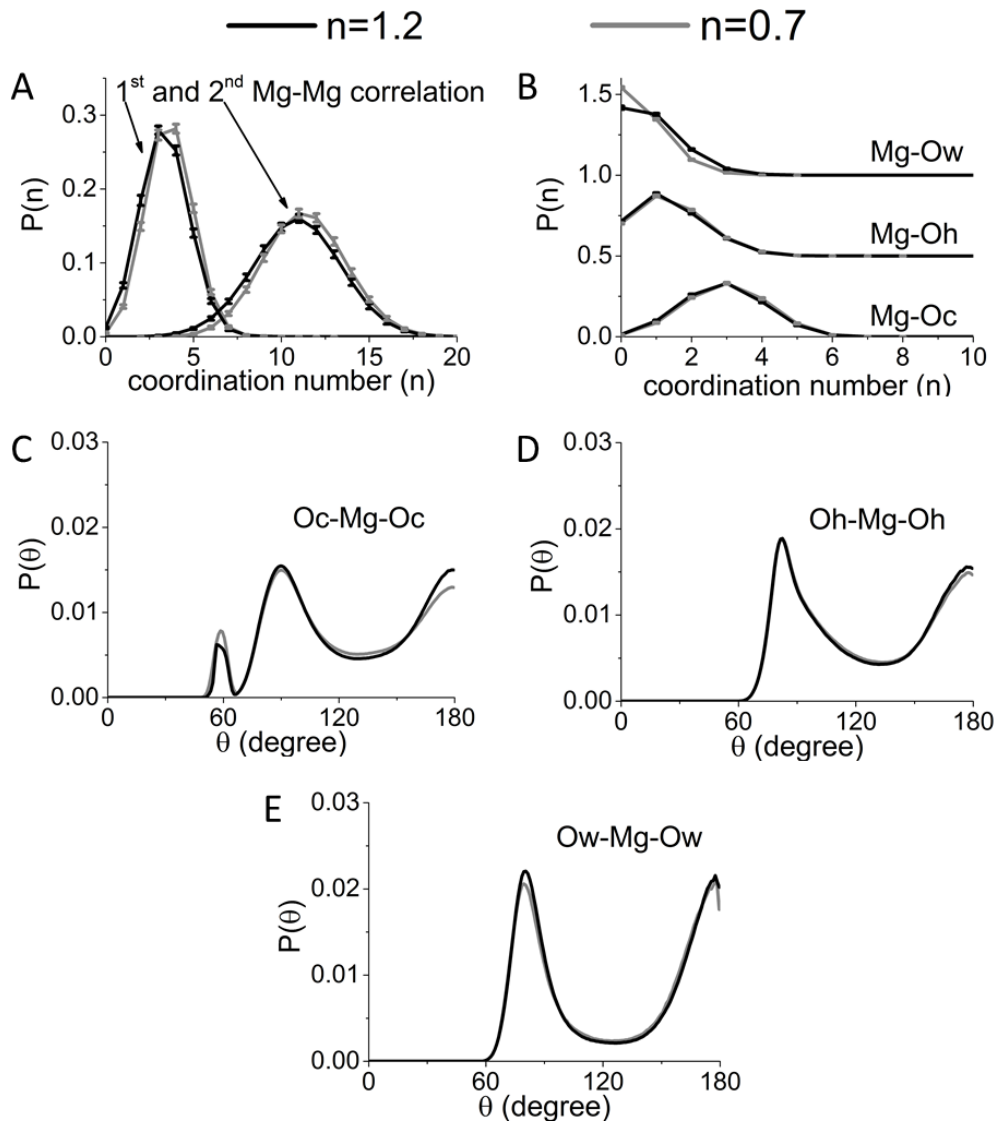Figure 3.21: A) distribution of coordination numbers for the first two Mg-Mg coordination spheres at 3.6 and 5.7 Å (figure 3.20 A). B) Distribution of coordination number for the first coordination sphere of O_c, O_h and O_w around Mg at 2.2 Å (figure 3.20 B-D). Angular distribution showing the angle between oxygens binding to the same magnesium ion for O_c (C), O_h (D) and O_w (E).

The distribution of coordination numbers of oxygen around magnesium shows that O_c is the main ligand to magnesium followed by O_h and O_w (figure 3.21 B), but all showing very broad distributions. Again almost no change is observed upon dehydration. The number of O_w coordination to magnesium goes down as expected and is mainly compensated for by an increased number of O_c binding to magnesium. The coordination geometry of the magnesium ions are shown in the angular distributions of oxygen binding to magnesium (figure 3.21 C-E). The angular distribution of O_c around magnesium shows three peaks at 60°, 90° and 180°, the first two peak are characteristic of adjacent oxygen from bidentate and monodentate binding respectively. The peak 180° is characteristic of octahedral geometry as expected for magnesium as this is the only geometry reported in several magnesium minerals of oxides[157], carbonates[50, 92, 94], basic carbonates[91, 93] and hydroxides[156] as well as magnesium ions in solution[145]. The angular distributions of O_h and O_w around magnesium both show two peaks with the 90° and 180° angles expected from the octahedral coordination, which is strongly preferred. For all the angular distribution shown in figure 3.21 (C-E) angles between 90° and 180° are also present caused by the disordered octahedral coordination and non-octahedral coordination related to 4 and 5 fold coordination which are also present in the structure.
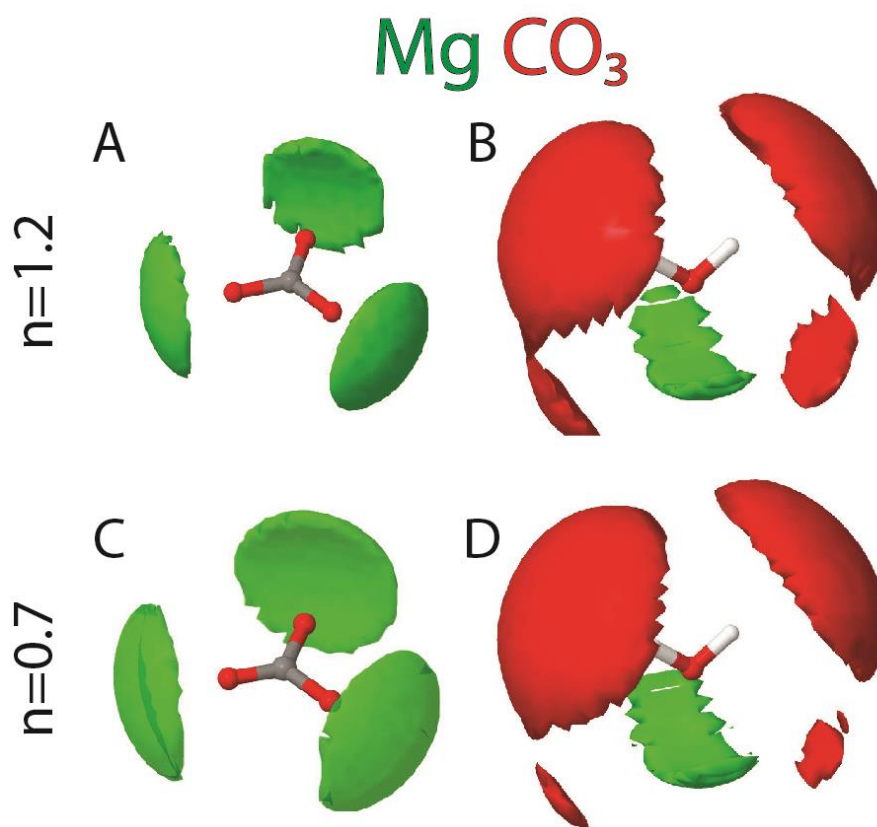
Figure 3.22: SDF of the Mg (green) coordinating to the carbonate ion (A and C) and the water molecule (B and D) for both n=1.2(A and B) and n=0.7 (C and D). In B and D the SDF of carbonate (red) is also shown for clarity. The Surface is plotted here in the range 2-5 Å away from the C and O atom in carbonate and water respectively using an isosurface value of 0.15. In the sdf of O_c around the water (red) molecule a minor population is seen adjacent to the magnesium population (green) originating from O_c-Mg-O_w motif with a 90° angle and is not caused by direct interaction between the carbonate ions and water molecules.

The sdf of magnesium coordination to carbonate (figure 3.22 A and C) shows the monodentate binding between the carbonate and magnesium ions. Given the low population of bidentate binding this coordination is not visible in the sdf for this isosurface value. For both samples the sdf shows three isotropic binding sites directly on top of the O_c, unlike calcium which showed anisotropy towards the normal to the molecular plane of the carbonate ion (figure 3.10). The water/magnesium sdf (figure 3.22 B and D) show a very confined binding site of magnesium on the oxygen side of the water molecules with an anisotropy spread towards the lone pairs of the oxygen. The narrow binding site of the magnesium ion around both the carbonate ion and the water molecule compared with the sdf related to calcium in ACC (figure 3.10) indicate that the magnesium environment is better defined and hence more constrained. The preferred octahedral coordination geometry of the magnesium ion is also seen in the carbonate/water sdf where there is a second small binding site on the oxygen side, in addition to the hydrogen bond population, this is caused by a O_w-Mg-O_c motif with a 90° angle between the two bonds (figure 3.22 B and D).

3.3.2.3 Hydrogen-bonding in AMC

Hydrogen bonding in AMC is more complex compared to ACC given that there are three hydrogen bond acceptors (O_c, O_h and O_w) and two donors (H_h and H_w). The peaks related to hydrogen bonding at 1.8Å in the O-H ppdfs are analyzed in this section (figure 3.20). The coordination number distribution of oxygen hydrogen bonded to H_h is shown in figure 3.23 A. There is no clear preference observed in contrast to what was seen for the hydrogen bonding in ACC, although there is some preference for hydrogen bonding of the hydroxide with the anions.

Figure 3.23: A) distribution of coordination numbers for the first H_h-O coordination sphere at 1.8 Å related to hydrogen bonding from the H_h (figure 3.20 F, H and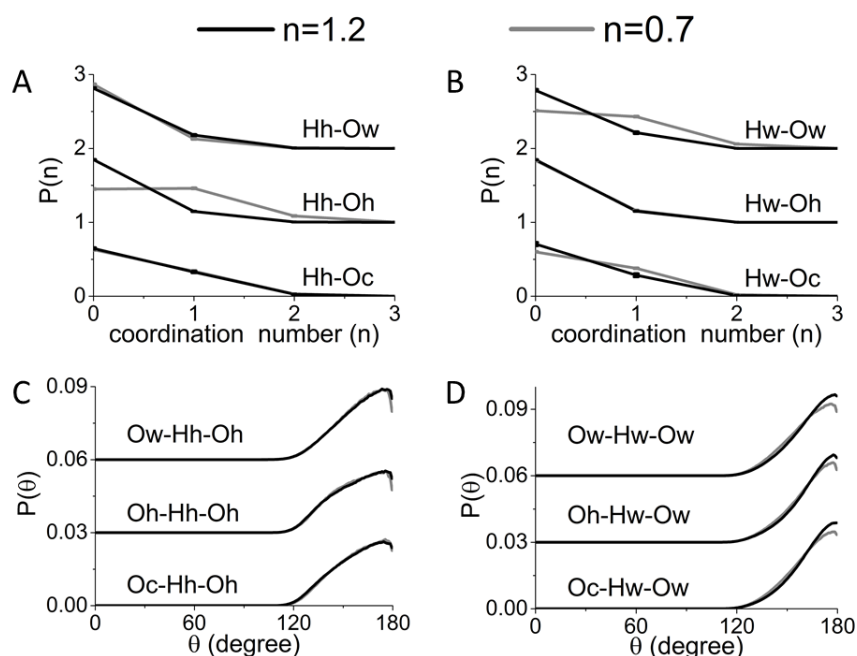 I). B) Distribution of coordination numbers for first the H_w-O coordination sphere at 1.8 Å related to hydrogen bonding from the H_w (figure 3.8 F, I and J). Angular distribution showing the angle of the hydrogen bond related to hydroxide hydrogen (C) and water hydrogen (D).

A large change is observed in the hydrogen bonding between hydroxides upon dehydration (figure 3.23 A), it is unclear if this is an artifact in the model or an accurate description given the relative low concentration of the hydroxide ion and hence the relative low signal in the data (figure 3.19). The hydrogen bonding related to H_w show a similar mix of hydrogen bonding between H_w and the various oxygens with a slight preference towards the anion oxygens. Despite the hydroxides only making up 25% of the anion oxygens present in the system, they make up 40% of the anion oxygens hydrogen bonded to the water molecule (table 3.7), which is likely the cause of the mixed hydrogen bonding observed in this system. The hydrogen bonds in AMC tend to be linear with the H_w-O hydrogen bonds being highly linear and the H_h-O bonds showing a shoulder in the angular distribution at 140° suggesting a weaker hydrogen bond. The sdfs of water and hydroxide around carbonate and water is shown in figure 3.24 and the sdf of hydrogen bonding between carbonate and water is shown in figure 3.22. The water molecules and hydroxide ions tend to coordination carbonate above and below the molecular plane of the carbonate and in between the O_c. The hydroxide/carbonate sdf shows a second binding site directly in front of the O_c and a smaller population above and below the molecular plane compared to water. The two populations for the hydroxide are similar to the monodentate/bidentate binding seen for the cations binding to carbonate.
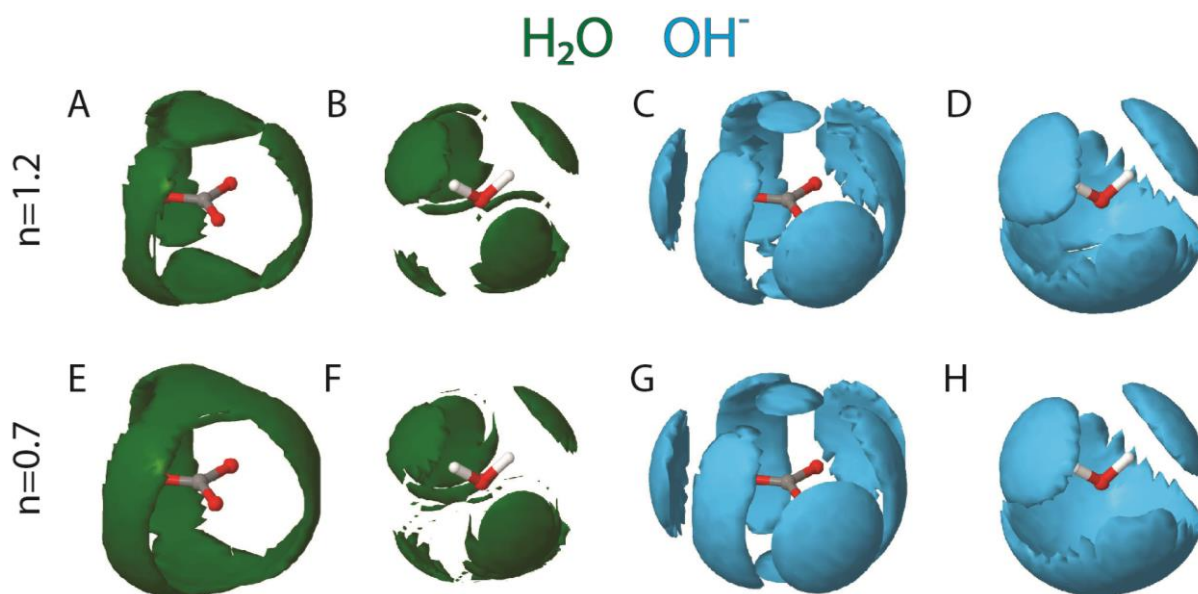
Figure 3.24: SDF of the water (dark green) coordinating to the carbonate ion (A and E) and the water molecule (B and F) for both n=1.2(A and B) and n=0.7 (D and E). SDFs of the hydroxide ion coordinating to water (D and H) and carbonate (C and G). The Surface is plotted here in the range 2-5 Å away from the C and O atom in carbonate and water respectively using an isosurface value of 0.15 for the water/carbonate and hydroxide/water sdfs and 0.05 for the water sdfs. The isosurface value for the water-water sdf was lowered as the correlations between water molecules are weak and was not distinguishable at higher values.

Comparison of the O_h-C and O_w-C ppdfs (figure 3.20 F and G) with the H-C ppdfs (figure 3.20 F and G) indicate that these two sites are related to the oxygens in water and hydroxides

by the split peak in the O-C ppdfs at ~3.8 Å that is not seen to the same extent in the H-C ppdfs, suggesting that the oxygens preferentially occupy one of these two sites while the hydrogen can orientate to optimize the hydrogen bonding. The sdf of water coordination to water (figure 3.24 B and F) shows several populations similar to that of water/water sdf of ACC (figure 3.10 B and D), despite the higher frequency of water-water interaction in the AMC model compared to ACC the water/water correlation related to hydrogen bonding is still very weak in AMC compared to O_w-O_w correlation between water molecules not hydrogen bonded together. The hydroxide/water sdf shows three populations; two are placed directly in front of the H_w and correlate to H_w-O_h hydrogen bonding and the third population is placed on the oxygen side of the water molecule originating from H_h hydrogen bonding to the oxygen lone pairs. In all of the sdfs there are only minor changes observed upon dehydration, suggesting that the structural change is mainly quantitative (i.e. change in the coordination number), while the geometric correlation between the components remain more or less the same.

3.3.2.4 Ppdf and coordination number of ACMC
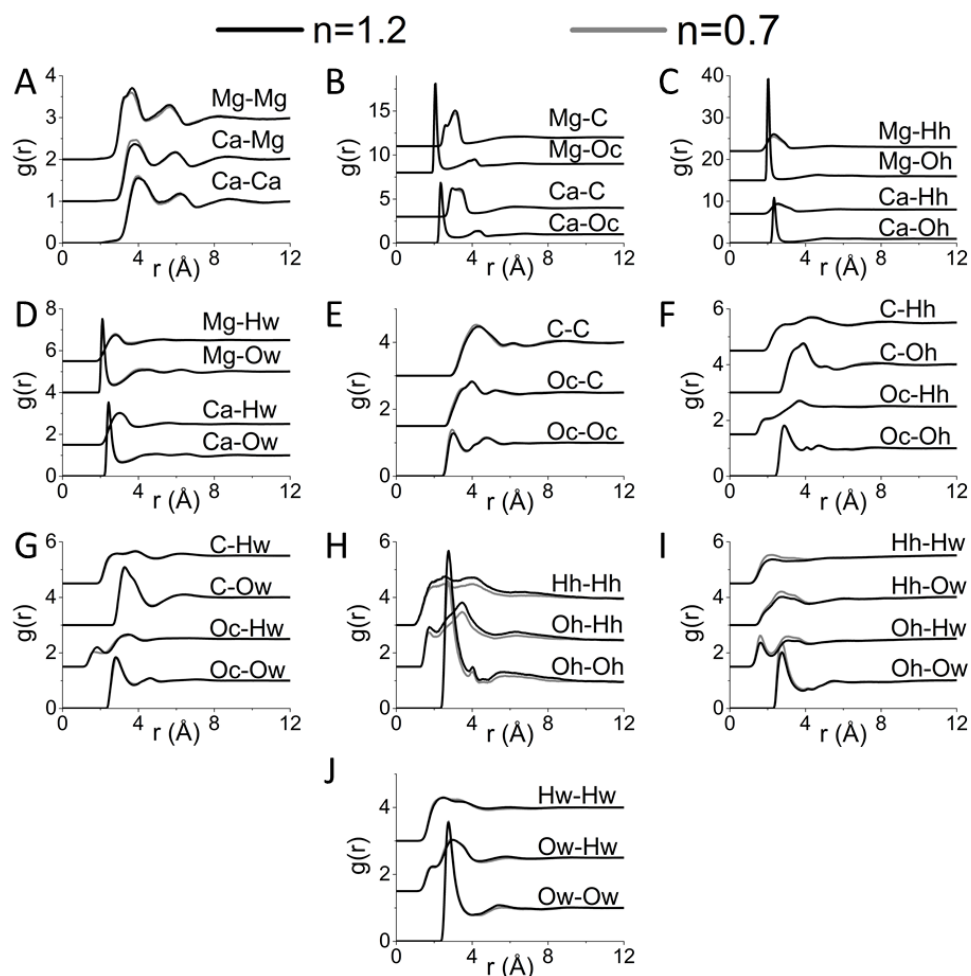
Figure 3.25: ppdfs of the 36 atomic pairs in ACC. with pairs between A) magnesium/calcium and magnesium/calcium, B) magnesium/calcium and carbonate, C) magnesium/calcium and hydroxide, D) magnesium/calcium and water, E) carbonate and carbonate, F) carbonate and hydroxide, G) carbonate and water, H) hydroxide and hydroxide, I) hydroxide and water and between water molecules (J).

We now move on to the EPSR model derived for the ACMC samples. From the fits shown in figure 3.19 the pdfs of the ACMC samples were deconvoluted into the 36 ppdfs related to ACMC (figure 3.25). Most of the ppdf are very similar to the corresponding ppdfs described for ACC (figure 3.8) and AMC (figure 3.20) below 8 Å with most of the longer range correlation missing. As the interatomic pairs of these ppdfs have already been assigned in the previous section they will not be discussed further here.

Table 3.8: Mean coordination number from ACMC of specific pair given as number of atom 2 around atom 1.

Atom 1	Atom 2	R_{min} (Å)	R_{max} (Å)	CN n=1.1	esd n=1.1	CN n=0.5	esd n=0.5	Change %
Ca	Ca	1	5.1	2.9	1.5	3.4	1.5	17
Ca	Ca	5.1	7.2	5.9	2.1	6.7	2.2	14
Ca	Mg	1	4.8	2.3	1.4	2.8	1.4	23
Mg	Ca	1	4.8	2.1	1.3	2.6	1.4	23
Ca	Mg	4.8	6.8	5.3	2.1	6.1	2.2	15
Mg	Ca	4.8	6.8	4.9	1.9	5.7	2	15
Ca	O_c	1	3.3	5.2	1.5	5.9	1.5	13
Ca	C	2	3	0.8	0.8	0.9	0.9	20
Ca	C	3	4.1	3.2	1.3	3.5	1.3	10
Ca	O_h	1	3.3	0.7	0.9	0.8	0.9	12
Ca	O_w	1	3.2	1.5	1.1	0.8	0.9	-46
Mg	Mg	1	4.5	2.2	1.5	2.5	1.4	12
Mg	Mg	4.5	6.5	5.2	2	5.8	2.1	13
Mg	O_c	1	2.75	3.7	1.3	4.1	1.2	11
Mg	C	1	3.75	3.3	1	3.7	1	12
Mg	O_h	1	2.75	0.9	1	0.9	1	-2
Mg	O_w	1	2.72	0.8	0.8	0.4	0.6	-49
H_h	O_c	1	2.2	0.5	0.6	0.5	0.6	14
H_w	O_c	1	2.2	0.6	0.6	0.6	0.6	-1
H_h	O_h	1	2.2	0.2	0.4	0.2	0.4	-10
H_w	O_h	1	2.2	0.1	0.3	0.1	0.3	47
H_h	O_w	1	2.2	0.2	0.4	0.1	0.3	18
H_w	O_w	1	2.2	0.3	0.5	0.2	0.4	-45

The ppdfs with no equivalent in ACC and AMC are the Ca-Mg, Ca-O_h and Ca-H_h ppdfs (figure 3.25 A and C). The Ca-Mg ppdf shows three coordination spheres similar to the Ca-Ca and Mg-Mg ppdfs but at 3.8, 6 and 8.7Å. The Ca-O_h and Ca-H_h show that the hydroxides are binding directly to calcium via the oxygen as expected. The O-H ppdfs show a similar hydrogen bonding as in AMC with H_w being the preferred hydrogen bond donor and O_h the preferred acceptor (figure 3.25 F-J). The various peaks in the ppdfs were analyzed for their coordination number (84 peaks in total, table 3.8) and an increase was found for most of the pairs related to the ions (average increase 18%, median 17%), while the ones related to water showed a decrease (average decrease -31%, median -40%). The change in the coordination number of the Ca-Ca first coordination sphere is very similar to what was seen in ACC (17% in ACMC and 19% in ACC) while the Mg-Mg coordination number for the first coordination sphere is almost twice of what was observed in AMC (12% in ACMC and 7.6% in ACC). The number of O_c around the cations in the first coordination sphere increased by ~10% similar to what was observed for ACC and three times what was observed in AMC. Almost no change is observed for the coordination number of O_h coordinating to magnesium and a minor change is observed for O_h coordinating to Ca from 0.7 to 0.8. The overall coordination of oxygen around Ca and magnesium was determined to be 7.4 and 5.4 for Ca and Mg respectively for both hydration levels, similar to the coordination number determined for the cations in AMC and ACC. The hydroxide ions seem to preferentially bind to magnesium as O_h constitute 10% and 16% of the total number of oxygens around the calcium and magnesium respectively. The coordination number of oxygen around hydrogen show that the majority hydrogen bonds are formed between H and O_c despite the O_c-H 1.8 Å peaks in the ppdfs are less pronounced then the O_h-H peaks (figure 3.25 F-I), indicating that the O_h are the preferred hydrogen bond acceptor but the sheer number of O_c present in the system makes it the most common hydrogen bond acceptor.

3.3.2.5 Calcium, magnesium and carbonate environment in ACMC

The mean coordination number of nearest and next nearest neighboring cations showed that dehydration induces a larger change in the local environment of the ions ACMC compared to AMC (table 3.8) and the shift of the coordination number distributions show a similar trend (figure 3.26 A-D). The four cation-cation pairs all show a shift to higher coordination numbers, with a slightly larger shift in the number of cations around calcium compared to cation around magnesium. There also seems to be no preference for the type of neighboring cations around calcium/magnesium, although there are calcium and magnesium ions that only have nearest neighbor cations of the same type, as seen by the non-zero population of calcium ions with 0 magnesium ions in the first coordination sphere (figure 3.26 C) and similar for magnesium (figure 3.26 D). However, there are also calcium ions that only have magnesium ions in the first coordination sphere as seen by the non-zero population of calcium ions having 0 calcium ions in the first cation coordination sphere (figure 3.26 A) and again similar for Mg (figure 3.26 B). All four coordination number distributions peak around 2-3 neighboring cations (figure 3.26 A-D) indicating a well-mixed[l] amorphous phase given that the expected

---

[l] But given the very broad distribution a very heterogeneous phase

coordination number of nearest neighboring cation around calcium and magnesium is expected to be 6 (table 3.4) and 4 (table 3.7) respectively. The distribution of coordination numbers of oxygen around calcium and magnesium are shown in figure 3.26 E and F.
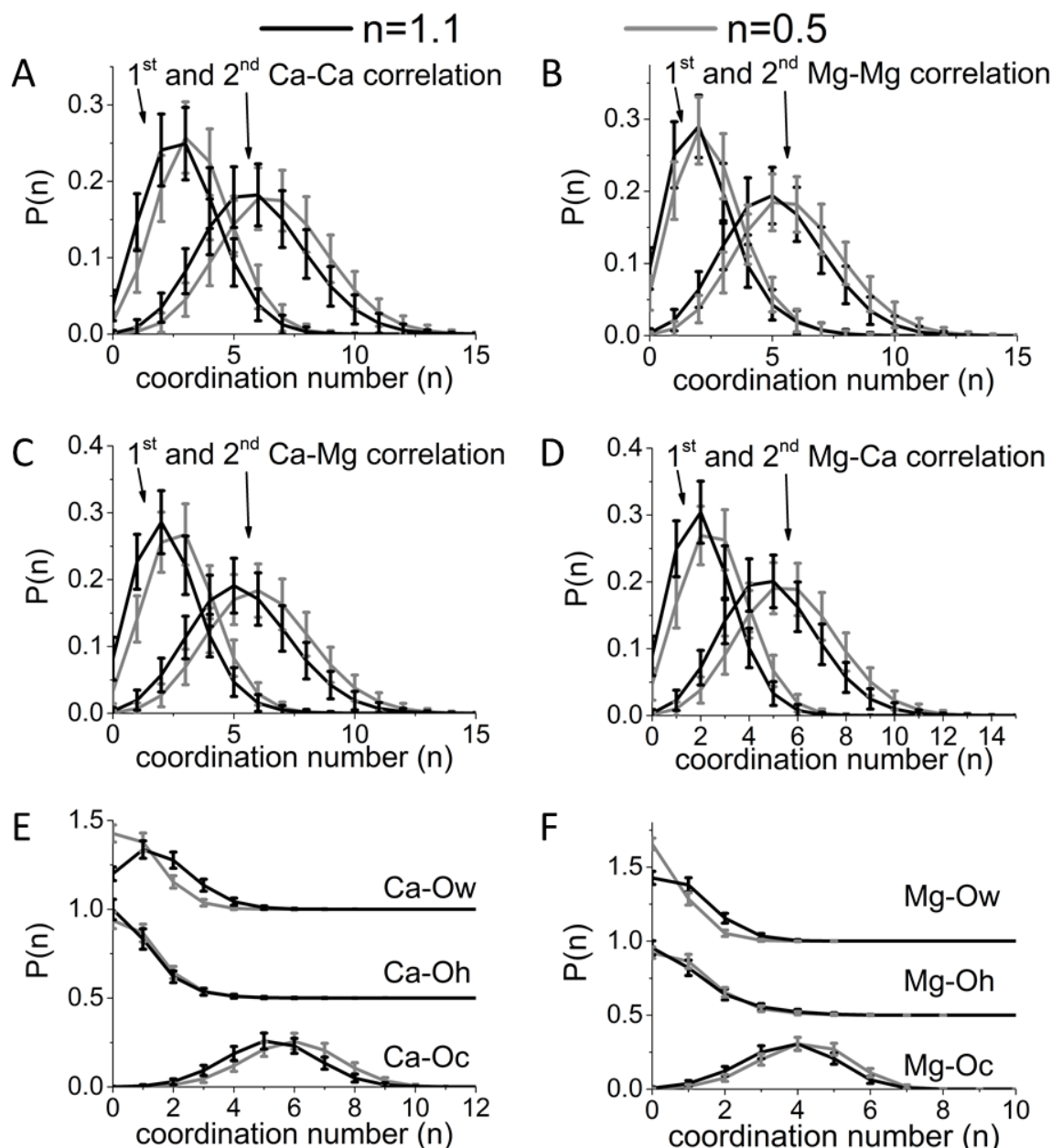
Figure 3.26: A) distribution of coordination numbers for the first two Ca-Ca coordination spheres at 4 and 6.2 Å, the first two Mg-Mg coordination spheres at 3.6 and 5.7 Å and distribution of coordination number of magnesium around calcium (C) and calcium around magnesium (D) in the first two Ca-Mg coordination spheres at 3.8 and 5.9 Å. In E and F the distribution of coordination number of oxygen binding to calcium (E) and magnesium (F) is shown.

As expected from the ppdfs (figure 3.25) both calcium and magnesium show a mix of the three types of oxygen in the first coordination sphere. For calcium the first coordination sphere is mainly composed of O_c, with O_w being the second most common and O_h being the

least favored as expected since this is the oxygen with the lowest concentration in the system. A similar trend is seen for magnesium in the dehydrated sample with O_h being the second most favored and O_w the least, but in the fully hydrated sample the distributions for O_h and O_w around magnesium are very similar. This is quite unexpected given the low concentration of O_h in the system, but shows a clear preference for Mg-OH binding. Analysis of the number of magnesium ions around O_h also showed that all O_h are coordinating directly to at least one magnesium ion with the majority coordinating two, consistent with the magnesium ion being responsible for the hydroxide ion incorporation. For both cations a shift to higher coordination number for the anion oxygen are seen similar to what was shown for ACC.

Figure 3.27: Angular distribution showing the angle between oxygens binding to the same calcium ion for O_c (A), O_h (C) and O_w (E) and for oxygen binding to the same magnesium ion for O_c (B), O_h (D) and O_w (F). Notice the strong preference for 90° and 180° in the angular distributions related to magnesium indicating a preference for octahedral coordination of the magnesium ion.
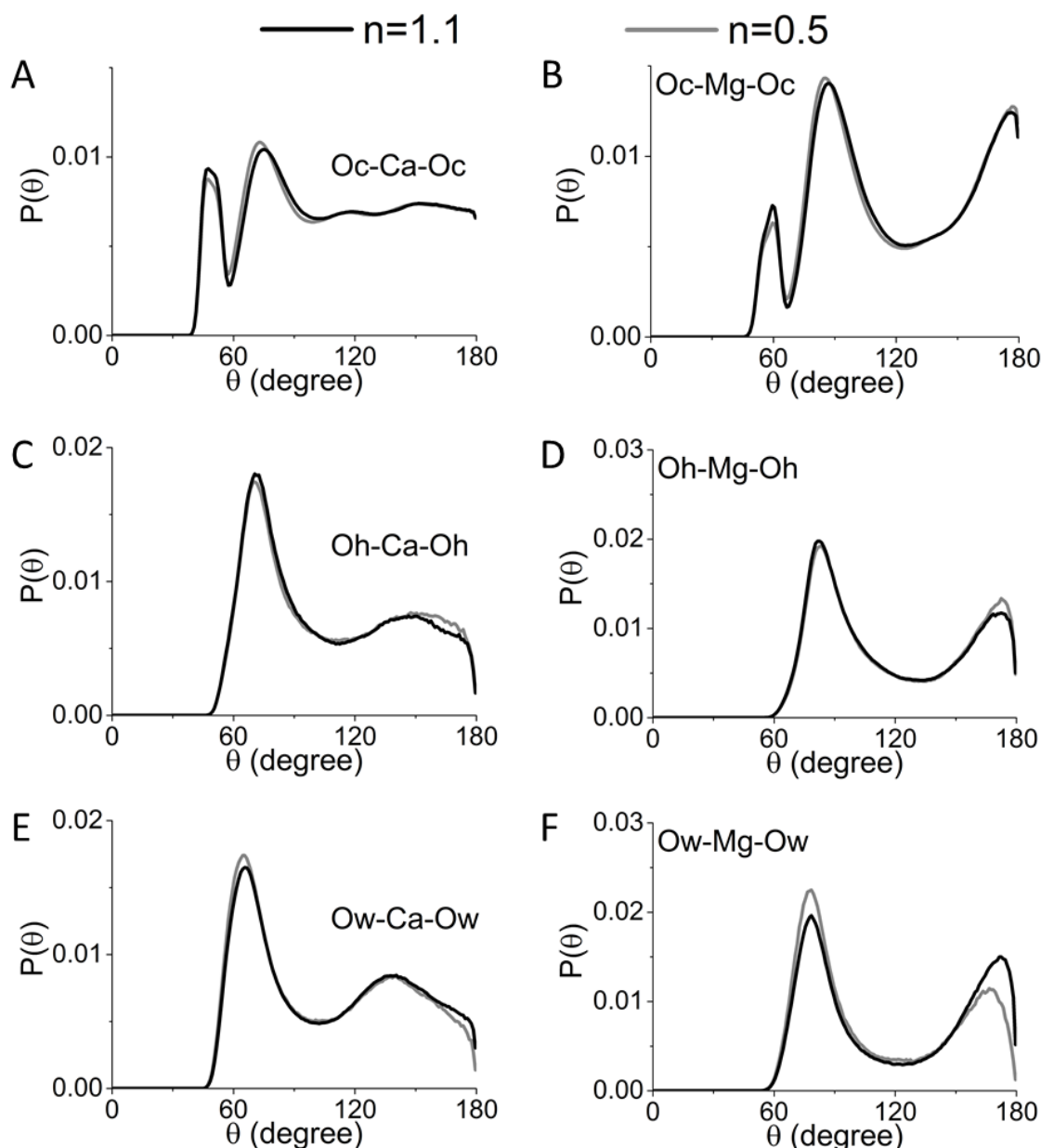
However, the shift to higher coordination numbers is mainly seen for O_c with the accompanying shift in the O_w distribution to lower coordination number, showing that the dehydration process removes a significant part of the cation coordinating O_w accompanied with a reorientation of the anions, mainly the carbonate ion. The local environment of the calcium ions is very similar to what is found in ACC (figure 3.9 A) with an angular distribution for O_c (figure 3.27 A) around calcium with two low angle peaks at 50° and 75° between adjacent O_c from bidentate and monodentate binding respectively and no peaks at higher angles. The distribution for O_h (figure 3.27 C) shows a peak at 75° from adjacent O_h and a minor peak at 150°. The O_w distribution (figure 3.27 E) show two peaks at 75° and 140° comparable to what has been found for calcium ion in solution[145]. The angular distribution of oxygen around magnesium (figure 3.27 B, D and F) all show two peaks at 90° and 180° characteristic of octahedral coordination with an additional peak at 60° in the O_c angular distribution (figure 2.27 B) between adjacent O_c from carbonate with bidentate binding to magnesium.

The angular distribution from AMC all showed a similar probability of the 90° and 180° peaks (figure 3.21 C-E), while the angular distribution related to magnesium in ACMC (figure 3.27) show a higher probability for the 90° peak over the 180° peak indicating that the local environment of magnesium in ACMC is slightly more disordered compared to AMC.
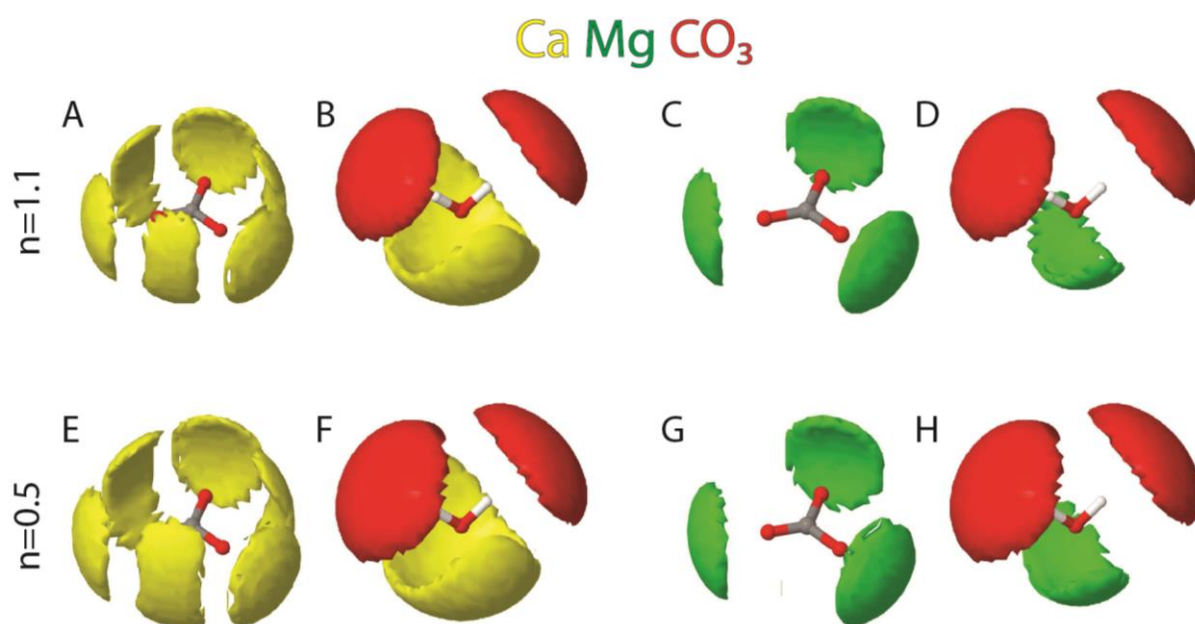
Figure 3.28: SDF of the Ca (yellow) coordinating to the carbonate ion (A and E) and the water molecule (B and F) for both n=1.1(A and B) and n=0.5 (E and F). SDF of the Mg (green) coordinating to the carbonate ion (C and G) and the water molecule (D and H) for both n=1.1(C and D) and n=0.5 (G and H). In B, D, F and H the SDF of carbonate (red) is also shown for clarity. The Surface is plotted here in the range 2-5 Å away from the C and O atom in carbonate and water respectively using an isosurface value of 0.15.

The sdfs of calcium and magnesium around carbonate and water (figure 3.28) in ACMC are again very similar to what has been shown for ACC (figure 3.10) and AMC (figure 3.22). For the sdfs related to calcium (figure 3.28 A, B, E, F) virtually no difference is seen compared to

the sdf from ACC and will not be discussed further here as they have already been described in chapter 3.2.2.1. The sdfs related to magnesium shows minor differences compared to what was shown for AMC (figure 3.22). The monodentate binding site of magnesium on carbonate shows a very slight anisotropy towards the normal to the molecular plane of the carbonate for both samples. The magnesium binding site to O_w is broadened compared to AMC, resembling more the shape of calcium coordinating to O_w, but still strongly confined behind the O_w compared to calcium. The second coordination site (figure 3.22 B and D) of the carbonate coordinating to the O_w is not present in the ACMC (figure 3.28 D and H) consistent with a more disordered local geometry of the magnesium compared to AMC and since a smaller fraction of the water molecules bind to magnesium in ACMC compared to AMC since there is less magnesium in ACMC and the water is shared between both calcium and magnesium ions.

3.3.2.6 Hydrogen-bonding in ACMC

The hydrogen bonding in ACMC resembles that of AMC when comparing the O-H ppdfs of ACMC (figure 3.25) with those determined for ACC (figure 3.8) and AMC (figure 3.20), showing that the strength of the hydrogen bond acceptors are in the order of $O_h > O_c > O_w$ and the hydrogen bond donor are in the order of $H_w > H_h$ in both samples.

Figure 3.29: A) distribution of coordination numbers for the first H_h-O coordination sphere at 1.8 Å related to hydrogen bonding from the H_h (figure 3.20 F, H and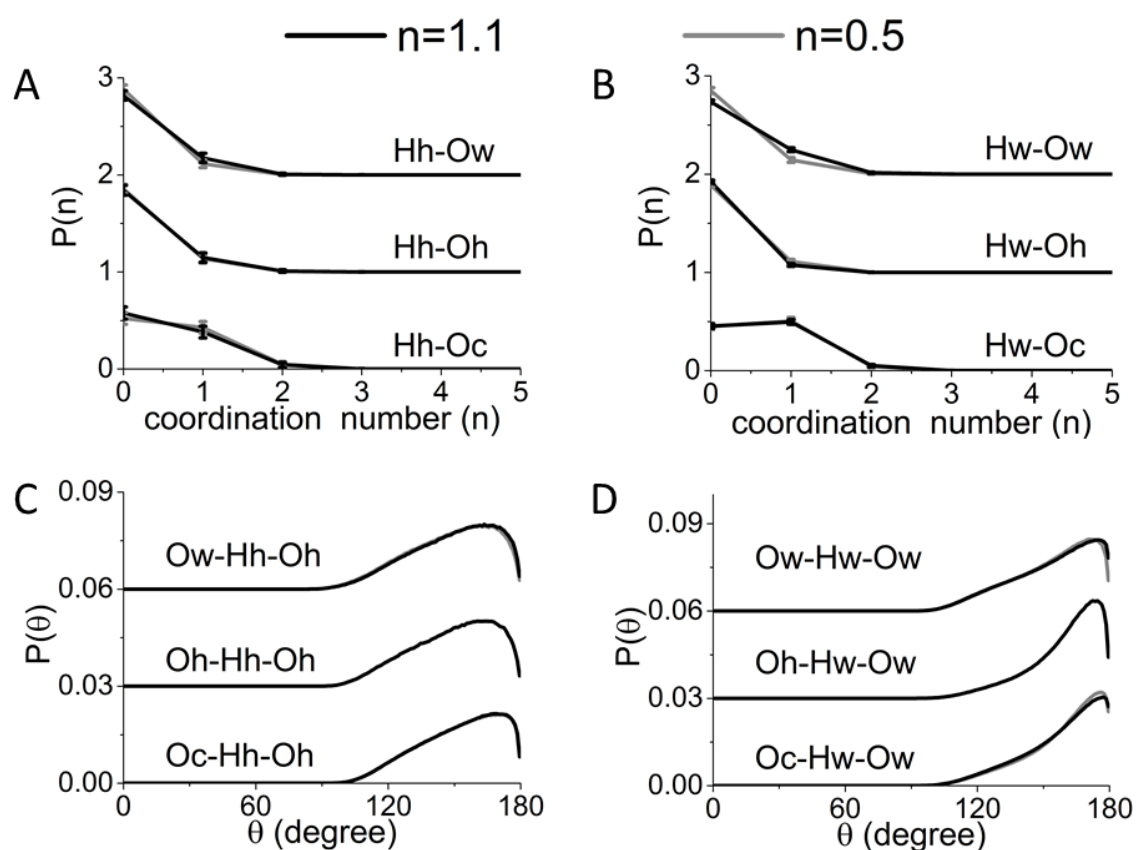 I). B) Distribution of coordination numbers for first the H_w-O coordination sphere at 1.8 Å related to hydrogen bonding from the H_w (figure 3.8 F, I and J). Angular distribution showing the angle of the hydrogen bond related to hydroxide hydrogen (C) and water hydrogen (D).

Comparing the coordination numbers gives a different pictures here it is clear that the most common hydrogen bonding are between hydrogen and O_c followed by O_w and O_h(figure 3.29 A and B) similar to the situation in ACC. While this may seem contradictive it is caused by the normalization of the ppdf by the fraction of the species in question (equation 2.10). Meaning that the ppdf will indicate what pairs are preferred relative to the fraction of the molecules in question present in the system, while the mean coordination number (table 3.8) will show what type of hydrogen bonding is most common in the system regardless of how many oxygen atoms are present from the molecule/ion of interest. From the coordination number distribution of oxygen around hydrogen it is clear that nearly half of the hydrogens are binding to O_c. The low amount of hydrogen bonding to O_h (figure 3.29 A and B) is caused by the low concentration of hydroxides in the system and analysis of the number of hydrogen around O_h show that 40% of the hydroxides are coordinating to H_w and 15% to H_h, both of which compete with the magnesium ion for space on the oxygen exposed side of the hydroxide ion. Almost no change is seen upon dehydration indicating that the hydrogens can reorientate with the ions upon dehydration to optimize the hydrogen bonds and that this is determined by the amount of available oxygen in the local vicinity. The angular distribution (figure 3.29 C and D) show a similar pictures of what was seen in AMC with highly linear hydrogen bonds for H_w-O hydrogen bonding and slightly bended hydrogen bonded H_h-O bond with an angle of 160°, indicating a weaker hydrogen bond between oxygens and H_h compared to H_w.
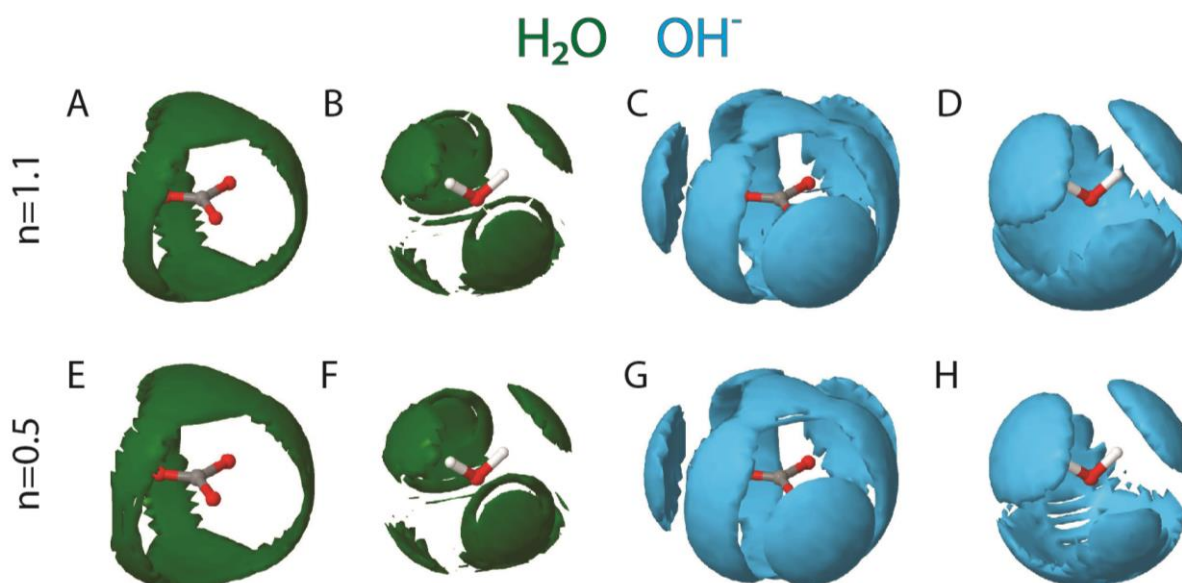
Figure 3.30: SDF of the water (dark green) coordinating to the carbonate ion (A and E) and the water molecule (B and F) for both n=1.1(A and B) and n=0.5 (D and E). SDFs of the hydroxide ion coordinating to water (D and H) and carbonate (C and G). The Surface is plotted here in the range 2-5 Å away from the C and O atom in carbonate and water respectively using an isosurface value of 0.15 for the water/carbonate and hydroxide/water sdfs and 0.05 for the water sdfs. The isosurface value for the water-water sdf was lowered as the correlations between water molecules are weak and was not distinguishable at higher values.

The sdf of water around water and carbonate (figure 3.30) again looks very similar to the sdf determined for both ACC and AMC, indicating that the cations do not influence how the water molecules interact with the carbonate and water molecules. The sdf related to the hydroxide ions are qualitatively very similar to those of AMC (figure 3.24). The main difference is found in the population of hydroxide (figure 3.30 C and G) above and below the carbonate molecular plane; these are likely caused by indirect correlations (e.g. a carbonate coordinating to a cation that is also coordinating to a hydroxide) rather than direct correlation as the hydroxides cannot form hydrogen bonding from this position. The increased presence of this population may simply arise from the lowered fraction of hydroxide ions in these models compared to the models of AMC.

3.3.3 Vibrational spectroscopy of amorphous calcium carbonate

Similar to the approach used for ACC (chapter 3.2.3) FTIR and neutron vibrational spectroscopy was used to corroborate the finding of the EPSR model. Due to the limited beam time at the TOSCA instrument it was not possible to measure the IINS spectra of ACMC and it was decided that second TOSCA beam time would not be applied for given the high similarity between the AMC (figure 3.32 F) and ACC (figure 3.16) IINS spectra and that of ACMC with low Mg concentrations (figure 3.4 C). For the FTIR spectra a fully dehydrated sample could be made for both AMC and ACMC as these samples do not crystallize during heat treatment[m]. The full FTIR spectra of AMC and ACMC are shown in figure 3.31. The spectra shown all four expected vibrational band from carbonate: in-plane bending vibration mode at ~700 cm^{-1}, out-of-plane bending at ~860 cm^{-1}, symmetrical stretch at ~1050 cm^{-1} and asymmetrical stretch at ~1400 cm^{-1}, with the in-plane bending mode overlapping with the librational mode of water/hydroxides. The bending mode of water is present at ~1650 cm^{-1} for the hydrated samples and the O-H stretching band is present in all the samples at ~3400 cm^{-1}, the last mode is the librational mode ~600 cm^{-1} related to both hydroxide and water molecules and is significantly larger in AMC compared to the ACC and ACMC samples.
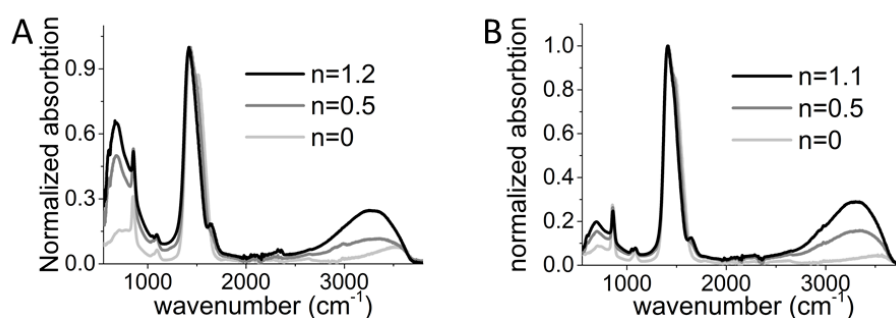
Figure 3.31:FTIR spectra of AMC (A) and ACMC (B)showing the in-plane bending vibration mode at ~700 cm^{-1}, out-of-plane bending at ~860 cm^{-1}, symmetrical stretch at ~1050 cm^{-1} and asymmetrical stretch at ~1400 cm^{-1} from the carbonate ion. The peaks at ~3300 cm^{-1} and 1650 cm^{-1} correspond to the water stretching and bending modes. After full dehydration a mode is present at 3600 cm^{-1}characteristic of hydroxide O-H stretching vibration. The asymmetrical stretching mode from carbonate and the O-H stretching mode from water/hydroxide are shown in more detail in figure 3.32.

---

[m] Crystallization occurs after simultaneous decomposition of carbonate and hydroxide to MgO at 400 °C

Close up of the asymmetrical stretch of the carbonate ion and O-H stretch from water/hydroxide are shown in figure 2.32, these band were chosen to analysis as they proved the most informative from the analysis of ACC in chapter 3.2. For both AMC (figure 3.3A) and ACMC (figure 3.32 D) a splitting of the asymmetric stretch band of the carbonate ion is observed. This increased splitting with increasing dehydration indicates a change in the local environment of carbonate similar to what was observed for ACC (chapter 3.2.3). This splitting is also related to hydrogen bonding to the carbonate ion[146] and indicates that the water molecules that are being removed have been hydrogen bonded to the carbonate ion as described by the EPSR model. The O-H stretch band of water and hydroxides in the AMC (figure 3.32 B) and ACMC samples (figure 3.32 E) show no sign of a hydroxide band at high hydration level due to the overlapping of the water and hydroxide stretching band at ~3300 and ~3600 cm^{-1}. However, after dehydration the broad peak at 3600 cm^{-1} characteristic of hydroxides becomes visible. The broadening of this peak also indicates that the hydroxides are acting as a hydrogen bond donors as expected from the pdf analysis.
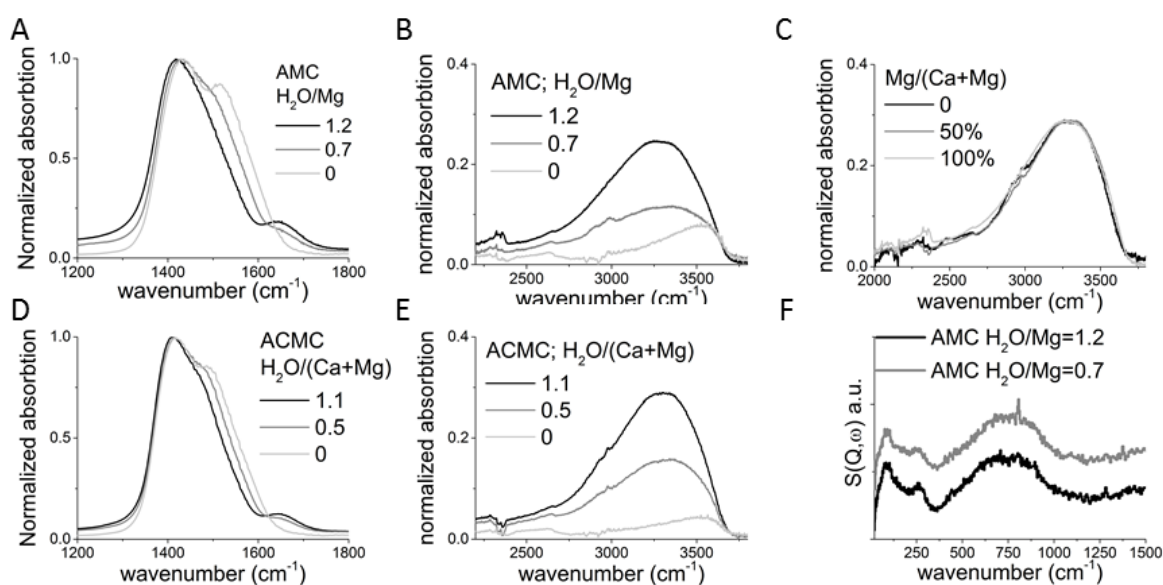
Figure 3.32: FTIR spectrum of AMC (A,B) and ACMC (D,E) from figure 3.31 showing splitting with increasing dehydration of the asymmetric stretching mode from the carbonate ion(A,D) and the O-H stretching mode of water/hydroxide where the hydroxide band is clear seen in the fully dehydrated samples (B,E). C) Comparison of the O-H stretching mode ACC, AMC and ACMC showing a very similar band in all samples, indicating strong water-carbonate/hydroxide hydrogen bonding as shown in figure 3.15. F) IINS of AMC at both hydration levels showing two band in the translational region at 90 and 260 cm^{-1} and a broad librational band from 350 cm^{-1} to 1000 cm^{-1}. The ACMC sample was not measured during the initial beam time at the TOSCA instrument and a second beam time was not available for measuring these samples.

Comparison of the low frequency tail of the O-H stretch band show a high similarity between ACC, ACMC and AMC indicating that hydrogen bonding mainly occur between water and carbonate/hydroxides as shown for ACC (figure 3.15). The low frequency part of the vibrational spectrum was measured using IINS (figure 3.32 F) showing three features, a broad

librational band from 350-1000 cm^{-1} indicating that the water is mainly binding to a single Mg[128]. Two translational bands at 90 cm^{-1} and 265 cm^{-1} are observed, with the former being consistent with Mg-OH$_2$ stretching mode. The 265 cm^{-1} could indicate an extended H-bonded network[128, 130, 132] or a translational vibration of the hydroxide ion[127]. Since no fast translational diffusion of water was determined from the QENS analysis (chapter 3.4), the hydroxide translational mode seems more likely. RAMAN Spectroscopy was used to determine the frequency of the symmetrical stretch of the carbonate (figure 3.33) as this is much more sensitive to this band than FTIR. As evident from figure 3.33 A this band shifts to higher frequency with increasing Mg content and a linear correlation was determined between the magnesium/cation ratio and the frequency of this vibrational mode (figure 3.33 B). The linear correlation matches that determined by Wang et al.[158] for Mg/(Mg+Ca) ratio from 0 to 50%. This indicates that the ACMC is indeed a mixed amorphous phase without Ca and Mg rich domains, as suggested from the ESPR model (figure 3.26).
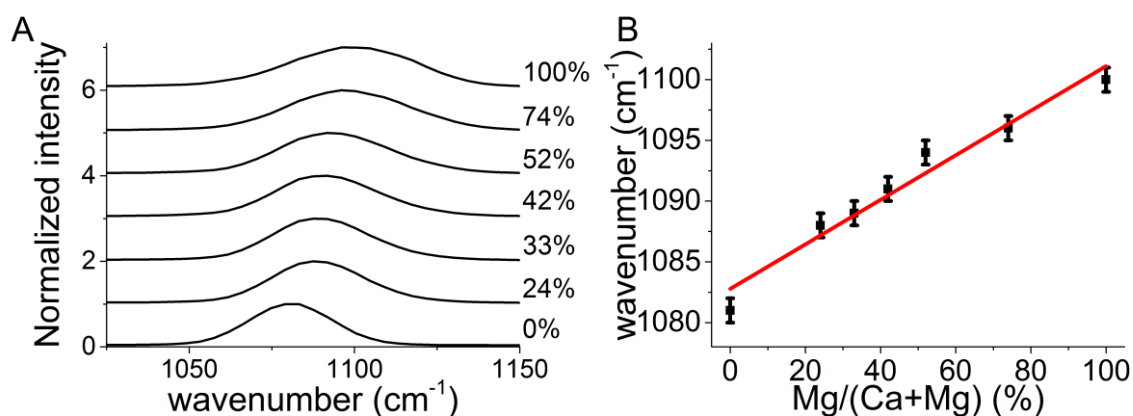
Figure 3.33: A) RAMAN spectrum of ACMC samples with varying magnesium content from 0% (ACC) to 100% (ACMC) showing the symmetrical stretching vibration of the carbonate ion. B) Frequency of the symmetrical stretching motion of the carbonate ion from the spectrum shown in A, a linear fit was made with a R^2 value of 0.9.

3.3.4 Discussion

To validate the structure of the AMC and ACMC phases, the EPSR model was compared to the limited structural details available on AMC and ACMC from literature[38, 47, 84] and the local environment of calcium in ACMC was compared to that of the ACC model described in chapter 3.2. The Mg-O distance of ~2.2 Å found for AMC and ACMC are similar to what has been determined previously from pdf analysis[38, 84] and EXAFS spectroscopy[47]. The coordination number of 5 and 5.4 is somewhat lower then what has been reported for Mg in synthetic ACC[47], but quite similar to what has been reported for Mg in biogenic ACC samples[47]. It is also quite similar to what was reported for a more hydrated AMC sample(n=3) based on pdf analysis[84]. This is also consistent with the fact that Mg is always octahedrally coordinated in the known crystalline carbonate[50, 92, 94] and mixed hydroxide/carbonate[91, 93] phases. The Ca-O distance of ~2.4 Å and coordination number of 7.4 oxygens around calcium found in ACMC is very similar to that found for ACC (chapter 3.2). The broad distribution of nearest cation-cation neighbors (figure 3.21 and 3.26) indicate that the AMC and ACMC phases consists of a mixture of highly inhomogeneous cation centers. However, it does not

suggest that ACMC is a micro separated compound with adjacent magnesium and calcium rich domains, as previous suggested[34].

The coordination numbers of oxygen around the cation are near constant for all the samples before and after heating. This suggests that the anions have to reorientate to compensate for the loss of water, similar to what was found for ACC (chapter 3.2). This effect is quite clear for Ca in both ACC (chapter 3.2) and ACMC and less so for Mg in ACMC (figure 3.26). However, there is almost no change around magnesium in AMC (figure 3.21). It is also clear in ACMC that the carbonate molecule compensates for the loss of water, whereas the hydroxides show little to no change in the coordination number distributions. The small change in the $Mg-O_w$ coordination number in AMC is caused by the large amount of water not interacting with magnesium (33% of the total water). This contradicts the notion that magnesium stabilizes ACC by the strong interaction with water, since the lower coordination number of magnesium (compared to calcium) leaves a larger portion of the water that is bound only by hydrogen bonds[47, 89]. However, the strong interaction between magnesium and water may still have an effect at lower hydration levels.

The smaller radii of the magnesium ion put significant constraints on the local environment. This is seen in the sdf of magnesium around carbonate (figure 3.22 And 3.28) where magnesium has a strong preference for monodentate binding with the carbonate ion and a very confined binding site to O_w. It is also seen in the angular distributions (figure 3.21 and 3.27) that magnesium adopts an octahedral coordination sphere, whereas calcium seems to adopt a wider range of coordination geometries as seen by the lack of high angle peaks in the angular distribution (figure 3.27). This all indicates that magnesium may provide a stabilizing effect by acting as points of order in an otherwise disordered material. Another stabilizing effect from magnesium may arise from the coprecipitation of hydroxides with magnesium. The lack of a change in the coordination number distribution(figure 3.21 and 3.26) involving O_h indicate that hydroxide ions are less flexible then carbonate ions, making remodeling more difficult leading to a stabilizing effect as have also been reported for hydroxides in ACC[39, 75]. This also indicates that large scale phase separation has to take place prior to any crystallization as the composition of AMC and ACMC does not match any of the known crystalline phases. However, it is not clear if the basic magnesium carbonates hydromagnesite[91] $[Mg_5(CO_3)_4(OH)_2 \cdot 4H_2O]$ and artinite[93] $[Mg_2(CO_3)(OH)_2 \cdot 3H_2O]$ can incorporate calcium or form directly from amorphous materials that do not have the same hydration level or the same carbonate to hydroxide ratio.

The pdf analysis, FTIR spectra and IINS all indicate that the water in all the samples is of a structural nature. The pdf analysis shows that the majority of the water is interacting with both the cation and anions, with a smaller population of the water interacting only with anions through hydrogen bonding. The ratio between these two populations seems to be linked to the ratio of Mg/Ca with an increased amount of cation free water environments with decreasing calcium content. The splitting of the asymmetric stretch band of the carbonate ion (figure 3.32) is related to hydrogen bonds involving carbonate and indicates a loss of carbonate-water/hydroxide hydrogen bonds[146]. This is substantiated by the low frequency tail of the O-H stretch of the amorphous phases (figure 3.32) compared to liquid water (3.15). The IINS

spectrum furthermore showed that the water is directly binding to magnesium by the 90 cm^{-1} band observed in the IINS spectrum and the presence of hydroxides by the translational vibration band of the Mg-OH bond at 265 cm^{-1}.

3.3.5 Conclusion

Through our analysis we have shown that magnesium places significant constraint on its local environment compared to calcium. This is seen in the form of an increase ratio of monodentate/bidentate binding for carbonate to magnesium (roughly 90%/10% respectively). Mg also strongly favors octahedral coordination whereas calcium shown no clear preferred coordination geometry. The main stabilizing effect of magnesium seems not to come from the cation itself but from coprecipitation of hydroxides with magnesium that greatly reduces the molecular reorientation during dehydration. Analysis of the cation-cation nearest and next nearest neighbors also showed that the ACMC phase is highly inhomogeneous but did not show any evidence for a phase separated system

Analysis of the hydrogen bonding in AMC and ACMC suggests that hydroxide is the strongest hydrogen bond acceptor in the system. However, most hydrogen bonding occurs between carbonate and water molecules due to the sheer number of oxygen from carbonate ions. Pdf analysis and vibrational spectroscopy both suggests that the water in the samples is of a structural nature, but distributed between many different binding site, i.g. bonding to cation and anions, only binding to anions split between hydrogen bonded to carbonate and hydroxide and bonded to water and ions at the same time. But no evidence was found for water molecules only binding to other water molecules.

3.3.6 Materials and methods

Sample were made by rapid mixing of 20 mL 1 M (Ca/Mg)Cl$_2$ (CaCl$_2$·2H$_2$O ≥99%, MgCl$_2$·6H$_2$O 99-102%, Sigma Aldrich) solution with 480 mL Na$_2$CO$_3$ (Na$_2$CO$_3$·10H$_2$O 99.999%, Sigma Aldrich) to get an initial concentration of 40 mM of both the carbonate and Ca/Mg ion. The solution was filtered, after which the solid was washed with cold ethanol (99.8%, Sigma Aldrich) and dried in a vacuum desiccator for a minimum of 24 hours to remove all ethanol.

IINS: IINS was performed at the TOSCA[124] instrument at ISIS (STFC Rutherford Appleton Laboratory, Didcot, UK). Samples were mounted in aluminium cans and sealed with indium wire. Samples were cooled to <30 °K before measuring and kept at ~10 °K during the measurement.

FTIR: FTIR-ATR was performed on a Nicolet IS5 (Thermo Fisher scientific, Waltham, MA, US) with an ID5 ATR module. Spectra was measured from 550 to 4000 cm^{-1} and averaged over 64 spectra.

Pdf measurement and analysis: x-ray pdf was measured at ID11 at the ESRF (Grenoble, France) using a 0.14088 Å beam and a Frelon2K detector and at I15 at the diamond light source (Didcot, UK) using a 0.16 Å beam and a Perkin Elmer detector. Neutron PDF was measured at the SANDALS Instrument[120] at ISIS (STFC Rutherford Appleton Laboratory, Didcot, UK). 5-6 g of sample was placed in a 12 mm thick sample can with vanadium windows. The thick sample can was chosen due to the low

sample packing fraction of ~10%. Each sample was measured for ~8 hours. Data reduction for both x-ray and neutron measurement was performed in Gudrun[117].

He-Pycnometry: Pycnometer measurement was performed on a Ultrapycnometer 1200e MUPY-31-T (Quantachrome Instruments, Boynton Beach, Florida, US). ~ 1 g was place in a ~4 mL sample holder and measured using He gas. Five measurements were averaged for the final result

ICP-OES: Sodium impurity levels was checked by ICP-OES (optima 8000 ICP-OES spectrometer, PerkinElmer, Waltham, MA)

TGA/DSC: hydration levels were determined by TGA/DSC (SENSYS evo TGA-DSC, SETARAM instrumentation, Caluire, France). The samples (>10 mg) were heated in alumina crucibles to 800 °C at 2 °C/min under argon gas flow.

3.4 Dynamics of hydrous species in ACC and AMC

In the previous two sections we have discussed the structure of amorphous calcium and magnesium carbonates using pdf analysis and while this techniques is excellent for structural investigation it is only sensitive to the time averaged structure, meaning that it cannot look into the fast dynamics occurring in the system. For this the dynamic structure factor $S(Q,\omega)$ is needed. Much like the Q range in a diffraction experiment determines what length scales a measurement can probe; the dynamic range (ω) determines what time scale can be probed from the dynamic structure factor. This has already been seen in the IINS spectrums shown for ACC and AMC in the previous sections were the time characteristic of inter-molecular vibrations were probed on the femtosecond time scale (figure 3.16 and 3.32). Using QENS we look into atomic/molecular motion on the picosecond time scale. Similarly to the IINS measurement this technique is 100 times more sensitive to motion related to hydrous species over any other species. From the dynamic structure factor confined motion and the possibility of diffusional motion of hydrous species in ACC and AMC on the picosecond time scale can be investigated (specifically <75 ps, determined by the resolution of instrument). This approach was chosen given the multiple studies suggesting mobile or liquid like water[56, 59] and the presence of water confined in pores present in ACC[63, 69], which contradict the description of structural water we have just made based on the pdf analysis and the vibrational spectroscopy analysis.

The IRIS[125] instrument was chosen given its wide dynamic range, where translation diffusion is found for bulk and confined water in many hydrated mineral systems[136-138, 159]. This range also covers the time scales for confined motion (i.e. non-translational motion) of the hydrogen as found in both clays and zeolites[135, 159]. The samples studied here range from ACC to AMC with a composition of $Ca_{1-x}Mg_x(CO_3)_{1-0.32x}(OH)_{x0.64}*nH_2O$. Five Samples were chosen for analysis with x=0, 0.22, 0.52, 0.73 and 1, with n=1.1-1.2.

3.4.1 Results

Two types of measurements were performed at the IRIS instrument: A fixed elastic window scan (FEWS) and a quasi-elastic neutron scattering (QENS) measurements. The FEWS measurement can reveal phase (freezing of water) transitions typically found for liquid or confined water and the short exposure time (20 min) allows the measurement to be conducted over a wide temperature range with decent resolution (5-300 °K with 5 °K resolution in this case). The QENS measurement takes significantly longer (6 hours) but allows for the Q resolved dynamic structure to be measured, from which the geometry of the motion can be determined.

3.4.1.1 Fixed elastic window scan

Figure 3.34 A shows the QENS measurement after 20 min exposure with the elastic line marked in gray. The elastic line is determined by the resolution of the instrument, 17.5 μeV (FWHM of the elastic line for a static sample, i.e. vanadium at 5 °K). This line can be integrated and plotted against the temperature to determine changes in dynamics in the system (figure 3.34 B). Since any diffusion occurring faster than the

resolution limit of the instrument results in a decrease of the intensity of the elastic line, by following the variation of this intensity phase transition can be determined. Such as the melting of any bulk or confined water[138]. For ACC a steady decrease in the intensity is observed from 5 °K to 300 °K with no apparent phase transition. For AMC the same steady decrease is observed from 5 °K to ~240 °K after which a drop in intensity is observed indicating a change in dynamics. However, the drop here is significantly smaller and at higher temperatures compared to what has been reported for freezing transition of water confined in pores as small as 1.5 nm[138].
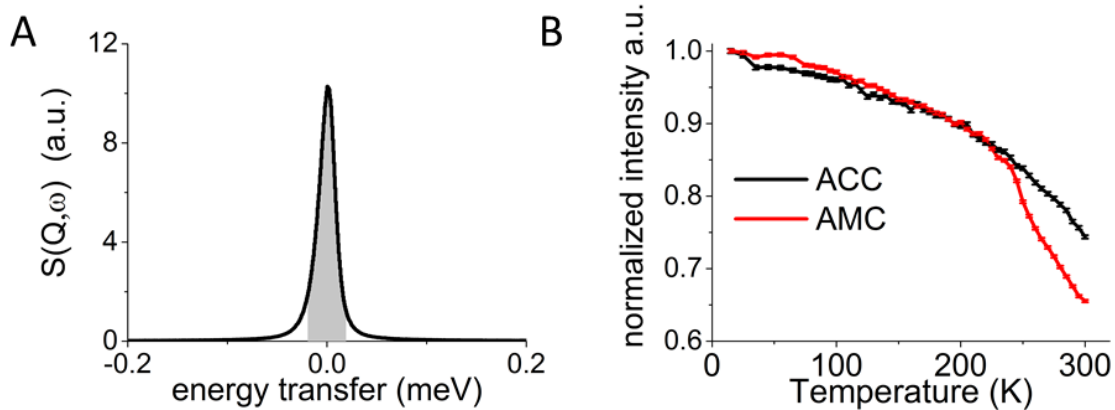
Figure 3.34: A) single temperature spectrum measurement integrated for all Q with the elastic line marked in grey. B) Fixed elastic window scan (FEWS) of ACC and AMC obtained from the integrated area of the elastic line (grey area in A) normalized to the integrated intensity of the elastic line at 5 °K.

3.4.1.2 Quasi Elastic Neutron scattering

The IRIS spectrometer features 50 detector/analyzer pairs given 50 Q values in a range of 0.42-1.85 Å^{-1}. To compare the broadening of the elastic line between the samples, the spectra were averaged over all detectors to give a single spectrum for each sample (Figure 3.35). The samples were measured at 5 °K to determine the resolution function of the sample, assuming negligible line broadening from diffusion or confined motion in the sample at this temperature. The ACC and AMC samples were planned to be measured at three elevated temperatures to determine the activation energy of the motion.
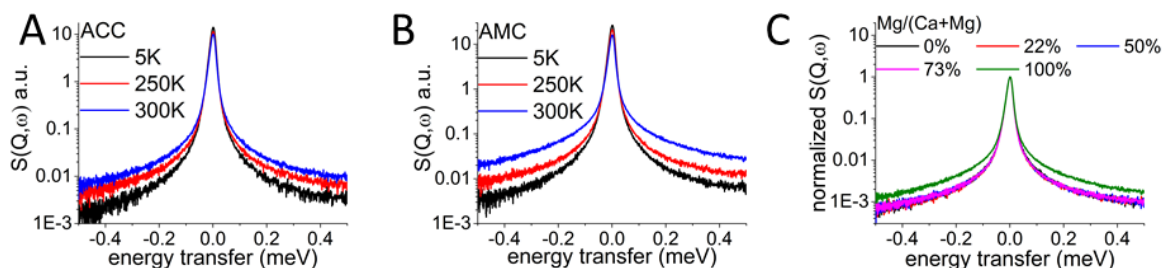
Figure 3.35: Q integrated QENS spectra of ACC (A) and AMC(B) at 5, 250 and 300 °K and QENS spectra at 300 °K for all samples.

However, problems during the beam time meant that only two elevated temperatures could be measured for these samples. ACC and AMC samples both show line

broadening with increasing temperature (figure 3.35 A and B). However, most of the elastic line is still present, showing that most of the H is not mobile on a time scale below the 75 ps resolution limit of the instrument. For ACC (Figure 3.35 A) and AMC (Figure 3.35 B) the line broadening increases with temperature as expected since molecular mobility generally increases with temperature. For AMC the increase from 250 °K to 300 °K is significantly higher than for ACC as expected from the FEWS measurement (Figure 3.34). To compare the line broadening between the samples the spectra were normalized to the height of the elastic line. Since this is proportional to the scattering power of the sample and the amount of sample in the beam this is essentially equivalent to normalizing to the amount of hydrogen as H is by far the strongest scatterer in the system. From the normalized spectra (Figure 3.35 C) it is clear that the ACC and ACMC samples have similar line broadening while the AMC sample has significantly more line broadening, indicating faster motion of the hydrogen and a higher fraction of hydrogen exhibiting this motion in AMC compared to the other samples.

To determine the geometry of the hydrogen motion, the Q dependent QENS spectra was used. The 50 detector banks were grouped into 10 groups to increase the statistics of the weak QENS signal. The FWHM of the line broadening was determined by a convolution of the elastic line and a single lorentzian peak. A fit using two lorentzian peaks was also done but without any improvement to the fit, indicating that only a single type of motion is observed in all samples. This was done for each Q value for all samples (Figure 3.36 A). In the case of translational diffusion an increased FWHM with Q[136] is expected according to equation 2.21, while for confined motion the FWHM should be independent of Q[135]. Despite the noise in the data (Figure 3.36 A) it is clear that there is no increase in line broadening for ACC and the three ACMC samples with Q indicating that the motion observed is confined. A small increase is observed in the AMC sample for Q values from 0.5 to 1 Å^{-1}. By fitting the FWHM(Q) with a jump diffusion model (equation 2.21)[136], a jump distance of 6.4 Å was found. Given that the longest jump distance we found in literature is 3.9 Å for confined water in Li-montmorillonite[159], this distance is considered too large to be physically meaningful. It is likely that the two low Q point are outliers and, like for the other samples, the motion found in AMC is also confined. From the FWHM, the residence time(t) for this confined motion was calculated for each sample as $t = 2\hbar/HWHM$. Where $HWHM$ is the half width as half maximum and $\hbar$ is the reduced Planck constant. The resulting residence time vs. magnesium concentration is shown in figure 3.36 B.
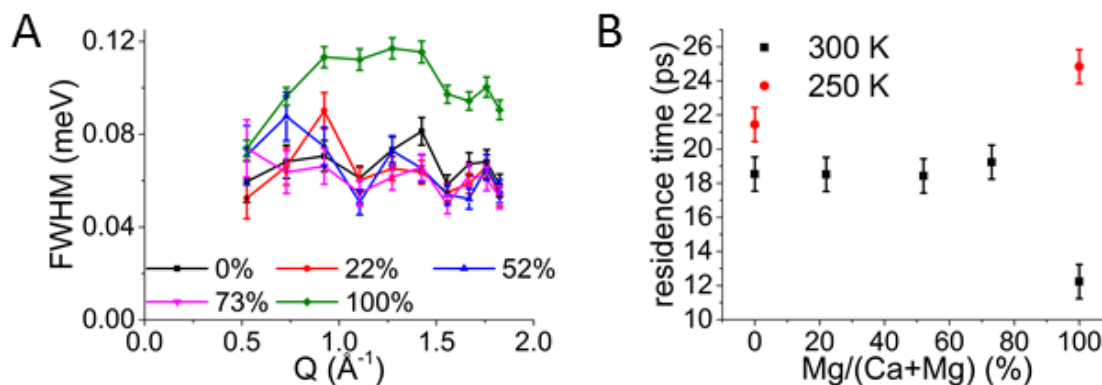
Figure 3.36: A) FWHM of the lorentzian used to fit the QENS spectra as a function of Q for all samples. B) The residence time of the confined motion of H calculated from the FWHM shown in A.

3.4.2 Discussion

The confined motion probed by the QENS measurement of the water molecules and possibly the hydroxides is most likely a reorientation of the O-H bond between hydrogen bonding sites (i.e. with the hydrogen pointing towards oxygen from water, carbonate or hydroxides) in the local environment. This confined motion implies that hydrous species keep bound for ~10-20 ps to one of the available oxygens in its near vicinity before switching to an adjacent site. The residence time of 10-20 ps found for confined motion in ACC/AMC is similar to the reported values for reorientational motion of water in other hydrated minerals (e.g. clays[159] and zeolites[135]) and an order of magnitude slower then what is found in liquid water at room temperature[136]. The shorter residence time found in AMC is surprising, as the residence time for ACC and the three ACMC samples are all very similar. We have not been able to unequivocally determine the cause of the difference between AMC and ACC/ACMC samples. However, it can be speculated that this is likely to be caused by a difference in the hydrogen bonding strength or geometry, as the reorientational motion of the H involves breaking a hydrogen bond and reforming it with an acceptor in a neighboring site. The difference between the AMC and the ACC/ACMC samples seems to occur in the range between $0.73 < x \leq 1$. At low Mg^{2+} contents, H_W are likely to be preferentially hydrogen bonded to carbonate molecules as we have previously shown for ACC (chapter 3.2). At higher Mg^{2+} contents this situation could be perturbed: once enough CO_3^{2-} are replaced by OH^-, because the different sizes and electronic properties of these two anions, the distance between bonding sites and/or the strength of the H-bond interactions can change significantly. The existence of liquid like water in amorphous carbonates has been suggested by several NMR studies[56, 59]. The presence of this kind of water within the materials studied here seems however unlikely. Residence times and jump distances for confined H_2O molecules in clays and mesoporous compounds have been reported between 2 and 43 ps between 1.1 and 3.9 Å, respectively [137, 159]. Bulk liquid water has much faster diffusion with a residence time of 1.25 ps and a jump distance of 1.29 Å[136]. Translational diffusion of water in ACC/AMC has residence times >75 ps (the resolution limit of the IRIS instrument). This indicates that

the large majority of water in these materials is structural. Although structural, water can still slowly diffuse through the material, as it has been predicted by MD simulation[70]. Assuming a long jump distances as high as 4 Å (the highest jump distance reported in literature to the best of our knowledge[159]) and using equation 2.21 one can calculate an upper limit for the diffusion coefficient(D) of $3.56 \cdot 10^{-10}$ $m^2 s^{-1}$, and MD simulations have suggested that it may be as much as 5 orders of magnitude lower[70]. Given the relatively slow diffusion of water in these systems it is unlikely that mobility of the internal water plays a large role in initiating ACC crystallization compared to the much higher mobility of bulk water at the surface of the ACC that may be present. Consistent with the long life time of ACC in vacuum (>6 months)[74] or in confinement[56] compared to the lifetime in solution (minutes)[72, 80].

3.4.3   Conclusion

We have shown that the motion of hydrous species in ACC/AMC is spatially confined in the time range below 75 ps ruling out motion characteristic of liquid or confined water as have been suggested to be present in ACC[59]. We determined that fast mobility of hydrogen arise from a reorientation of H between different hydrogen bonding sites occurring with a residence time around 20 ps for ACC and ACMC (with $0 \leq x \leq 0.73$) while this occurs faster in AMC with a residence time of 12 ps. Since no translational diffusion was found we could only determine an upper limit for the diffusion coefficient for all samples of $D_{max}=3.56 \cdot 10^{-10}$ $m^2 s^{-1}$ based on the instrument resolution and assuming a maximum jump distance of 4 Å, indicating that the water diffusion coefficient for these amorphous phases are at least an order magnitude lower than that of bulk water[136-137]. Consistent with molecular dynamics simulation that suggests a diffusion coefficient as low as $42 \cdot 10^{-15}$ $m^2 s^{-1}$.

3.4.4   Materials and methods

Materials synthesis: ACC/AMC was synthesized by rapid mixing of 20 mL 1 M (Ca/Mg)Cl$_2$ (CaCl$_2 \cdot$2H$_2$O ≥99%, MgCl$_2 \cdot$6H$_2$O 99-102%, Sigma Aldrich) solution with 480 mL Na$_2$CO$_3$ (Na$_2$CO$_3 \cdot$10H$_2$O 99.999%, Sigma Aldrich) to get an initial concentration of 40 mM of both the carbonate and Ca/Mg ions. The solution was filtered, after which the solid was washed with cold ethanol (99.8%, Sigma Aldrich) and dried in a vacuum desiccator for a minimum of 24 h.

QENS: Quasi elastic neutron scattering was performed on the IRIS instrument[125] at ISIS-TS1 using a pyrolytic graphite 002 analyser (STFC Rutherford Appleton Laboratory, Didcot, UK). The samples were measured from -0.4 to 0.4 meV in ω and from 0.42 to 1.85 Å^{-1} in Q. ~2 grams of sample was place in a annular aluminium can with 2 mm sample thickness. ACC and AMC was measured at 5 K, 250 K and 300 K for 6 hours while ACMC with Mg/(Ca+Mg)=0.22, 0.52 and 0.73 was measured at 300 K for 6 hours. Fixed elastic window scan was performed on ACC and AMC from 5 K

to 300 K with 5 K resolution and 20 min exposure per step. Data reduction and analysis was performed in Mantid[160].

4   Summary and Conclusion

In chapter 3.1 it was shown that ACC and AMC samples can be made in quantities necessary for neutron diffraction studies and even for inelastic neutron diffraction experiments. The synthesis route was optimized to obtain samples with a high reproducibility in composition and equipment was designed to ensure that samples could remain stable for the time necessary to travel to the neutron sources and to perform the measurements (approximately 2-3 weeks). With a production rate of ~15 grams/day this opens the opportunity perform parametric studies on ACC covering a large number of samples, potentially as many as 20 samples for a full week of beam time, although the maximum reached in this study was 13 samples in 5 days at the sandals instrument. We also showed that magnesium coprecipitates with hydroxide ions when synthesizing AMC or ACMC by a combined analysis using FTIR, ICP-OES and TGA given a composition of:

$$Ca_{1-x}Mg_x(CO_3)_{1-0.32(4)x}(OH)_{0.64(8)x} \cdot nH_2O \ \ with \ n = 1.1 - 1.2$$
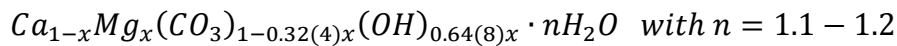
In chapter 3.2 an EPSR model of ACC was presented with a hydration level of n=1.1 and 0.5. This showed that dehydration does not cause large changes to the pdf for both neutron and x-ray measurements. However, a detailed EPSR structural analysis showed that large structural changes did take place during dehydration, but without changing the interactions between the molecules/ions and without increasing the order of the system. The structural analysis showed that there is a high diversity in the binding site available in ACC for all the components evident by the broad distribution of coordination numbers for the various atomic pairs (figure 3.9 and 3.11). By comparing the coordi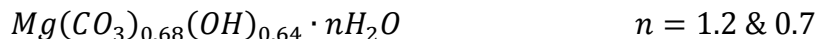nation number distribution before and after the dehydration a shift was seen to higher coordination numbers in most of the distributions. Of special interest was the distribution of nearest neighbouring oxygen around calcium. This showed that during dehydration, water molecules are stripped off the calcium ion and that the carbonate ions reorientate to compensate for the loss of water oxygens giving a mean coordination number of 7.2 oxygens around calcium for both hydration levels. Analysis of the angular distribution of oxygens around calcium showed that the wide range of coordination number result in no preferred angle above 100° and with a 70° angle between adjacent oxygens indicating that there is no preferred coordination geometry, consistent with the wide range of reported coordination geometries present in the crystalline calcium carbonate minerals[50-54]. The angular distribution of oxygens from water around calcium showed two preferred angles of 70° and 140°, characteristic of the local environment of calcium ions in solution, suggesting that the hydration shell of the ion in solution may be partially preserved during the precipitation reaction. The addition of the n-pdf allows for the evaluation for the hydrogen related ppdfs and showed that the water molecules are highly structural in ACC. This is seen by the large fraction of water molecules binding to the ions, 90% and 100% of the water molecules binding to calcium and carbonate respectively while only 10% of the water molecules form hydrogen bonds with other water molecules. The presence of large pores in the ACC structure was also evaluated as this has been discussed in several previous studies[43, 59, 63, 69]. This showed that water molecules are in close proximity of other water molecules but
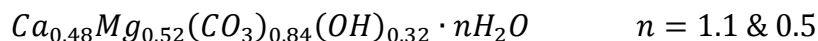
that they are only infrequently hydrogen bonded together and as such may match the definition of water percolation as stated by Bushuev et al[69].

In chapter 3.3 the analysis of the local structure in AMC and ACMC was presented with the following composition for AMC:

$$Mg(CO_3)_{0.68}(OH)_{0.64} \cdot nH_2O \qquad\qquad n = 1.2 \ \& \ 0.7$$

And for ACMC:

$$Ca_{0.48}Mg_{0.52}(CO_3)_{0.84}(OH)_{0.32} \cdot nH_2O \qquad\qquad n = 1.1 \ \& \ 0.5$$

Similar to the ACC pdfs only small changes were observed in the pdfs of ACMC and AMC upon dehydration.

For the AMC sample, the EPSR analysis showed that there was almost no change in the local coordination geometry of the magnesium upon dehydration. This is consistent with more of the water in AMC not coordinating to the cation compared to the ACC, suggesting that the water is mainly being removed from binding sites related only to the anions in the AMC. Only 2/3 of the water in the AMC are binding to the cation compared to the 90% in ACC, but they are all forming hydrogen bonds to either carbonate or hydroxide ions. The coordination number distributions show similar broad distribution as seen in ACC (figure 3.21), indicating a high diversity in the various binding sites. From the first peak in the cation-C ppdf also showed that magnesium is less inclined to form bidentate binding with carbonate compared to calcium. Analyses of the angular distribution of nearest neighbouring oxygens to the magnesium showed a high probability for forming 90° and 180° angles between oxygens, indicating a strong preference for octahedral coordination geometry in the first coordination sphere of magnesium. Consistent with the structure reported for magnesium in the various crystalline phases that all show octahedral coordination of magnesium[50, 91-94, 156] with monodentate binding to the carbonate except for nesquehonite that show a mixture of bidentate and monodentate[92]. Analysis of the hydrogen bonding showed that both hydrogen from water and hydroxide contribute to hydrogen bonding as is also evident from the FTIR measurements (figure 3.32). It was also clear that all three types of oxygen contribute as hydrogen bond acceptors. By comparing the peak at 1.8 in the O-H ppdfs a ranking for the preferred hydrogen donors and acceptors could be made for donors:

$$H_w > H_h$$

And for hydrogen bond acceptors:

$$O_h > O_c > O_w$$

The ACMC model showed that the local environment of calcium and magnesium is very similar to the local environment for the cations in ACC and AMC with the addition of hydroxide ions also binding to the calcium ion. Analysis of the cation-cation nearest and next nearest neighbour showed that there was no preference for magnesium to be near other magnesium ions over other calcium ions and vice versa (figure 3.26) indicating a well-mixed but highly inhomogeneous phase as evident by the broad distribution of coordination

numbers. Dehydration of the ACMC phase also showed that magnesium can undergo structural changes upon dehydration similar to what was observed for calcium in ACC with a lowering of the coordination number of water binding to the cation compensated for by a reorientation of the carbonate ion to coordination more cations on average, keeping the same mean coordination number for the cation before and after dehydration. However, the hydroxide ion does not seem to take part in this reorientation event as seen by both the lack of change for the coordination number distribution of O_h around calcium and magnesium before and after dehydration (figure 3.26). Despite the O-H ppdf in ACMC indicating a similar ranking of the hydrogen bond donor and acceptors as seen in the AMC, the sheer number of carbonate present in the system result in most of the hydrogen bonds forming between water and carbonate ions.

In chapter 3.4 the dynamics of hydrous species in ACC, AMC and ACMC are investigated this analysis confirmed the results of the EPSR analysis that water is highly structural and therefore does not show translational diffusion on the timescale expected for bulk or confined water as have been postulated in previous studies[59, 63]. Instead a confined motion was observed indicating that the hydrous species can reorientate between sites where the hydrogen atoms can form bonds to oxygen from hydroxide, carbonate or water molecules/ions with a residence time of 10-20 ps. Some difference was found between the AMC and ACMC(x=0 to 0.73) samples, indicating a faster confined motion in AMC, likely connected to the more mixed hydrogen bonding present in AMC caused by the high concentration of hydroxide ions.

In conclusion we have shown that amorphous carbonate samples can be formed in quantities allowing for neutron measurements to be made without the presence of stabilizing additives that have been used in previous studies[43, 66]. We have also showed that EPSR can be used to generate physically relevant structure to interpret the local environment of the amorphous phase given that accurate reference potentials, composition and density can be determined. The structural analysis showed that the amorphous phases are well mixed but highly inhomogeneous phase with a broad distribution in coordination numbers around the various species. We have shown that the hydrogen bonding mainly occur between carbonate and water for samples containing ≤ 50 % magnesium (maybe ≤ 72% magnesium as indicated from the QENS analysis) and in AMC the main hydrogen bond acceptors are carbonate and hydroxide ions resulting in faster confined motion for the hydrous species. The lack of translational diffusion at the fast time scales and the hydrogen bond analysis from ESPR showed that water in ACC/ACMC and AMC is highly structural.

Analysis of the local environment of the cations showed that the calcium environment is highly flexible and can adopt many different local geometries, while magnesium strongly favours the octahedral geometry making the local structure of magnesium highly constrained compared to calcium. However, this constraint does not translate to the calcium environment in the mixed phase ACMC as there is enough flexibility in the carbonate/hydroxide environment to accommodate both the diverse calcium centres and the highly ordered magnesium centres at the same time without requiring a phase separated system of magnesium and calcium rich domains. By analysing the local structure both before and after partial dehydration it was shown that the main structural change arise from the stripping of

water molecules away from the cations compensated for by a rearrangement of the carbonate ions that results in a fixed mean coordination number of ~7.3 for Ca and ~5.2 for Mg[n] for both hydration levels. However, this effect is much smaller for magnesium compared to calcium and in AMC this effect is almost absent as a large amount of the water molecules do not interact directly with the cation and hence the dehydration mainly affects the hydrogen bonding to the anions.

---

[n] The mean coordination number here is taking from the average found in ACC, ACMC and AMC

5   Outlook

The optimization of the ACC synthesis now allows for a relatively large number of samples to be prepared for a single neutron diffraction experiment. This gives some new opportunities to perform parametric neutron diffraction studies both in pdf analysis that are highly sensitive to local structure and in inelastic measurements that is more sensitive to hydrous species.

5.1   Possible for future parametric studies based on neutron diffraction

In this study magnesium and hydration level has been the main focus, but there are several other important additives that warrant this more elaborate analysis (i.e. EPSR fitting). A larger number of samples for each parameter would also greatly help to get a better understanding of the local structure as ACMC studied in this work:

$$Ca_{1-x}Mg_x(CO_3)_{1-0.32(4)x}(OH)_{0.64(8)x} \cdot nH_2O$$
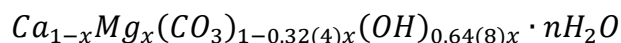
we have only studied three x values and two n for each x *in the pdf analysis,* which is very minimal compared to what could be possible if instruments of a higher intensity was used (i.e. shorter measurement times). This could be either INOVA at J-PARC (Tokai, Japan) or NIMROD at ISIS (Oxford, UK) but could also be done at SANDALS if enough time is available. This would also place more pressure on computation time and data treatment, but if several models can be analyzed in parallel this would be possible[o].

The other inorganic additives that would be of interest could be the Strontium and barium if amorphous samples can be made. The other divalent ions would also be of great interest as the relationship between cation size and structural parameters could then elucidated similar to what has been available for decades for the crystalline phases. Anions of different geometry and charge would also be interesting to study, to deconvolute how the different parameters affect the local environment. E.g. perchlorate (ClO_4^-), sulfate (SO_4^{2-}) and phosphate (PO_4^{3-}) all have a tetrahedral geometry but different charges. However, it is not clear if all of the interesting anions will form an amorphous phase with calcium or if it possible to get similar hydration level for each phase, which would be a prerequisite for any comparison. Given the biological relevance for the amorphous phase, structural studies including proteins, sugars, lipids and small organic molecules are also relevant to study, but extensive deuteration may be necessary to gain enough sensitivity in the experimental data to perform the EPSR modeling without relying too much on the reference potential alone. If e.g. proteins become too large there may also be limitations in the computation time it would take to fully analyze the structure. Another drawback of this approach is the sensitivity of the pdf to additives of low concentration as seen in figure 3.4, making analysis of mixed phases at low concentrations difficult without access to additional data from techniques that are more selective, such as NMR, vibrational spectroscopy or EXAFS.

---

[o] The disordered materials group also host a EPSR workshop at their annual user meeting which is highly recommended for anyone wanting to learn how to use ESPR

5.2 Translational diffusion of water in ACC

In the QENS study that is described in chapter 3.4, the main drawback was that the translational diffusion was not measured as evident by the high intensity of the elastic peak even at room temperature of the QENS measurement (figure 3.35). This was a result of a choice that had to be made about which instrument to use, either a spectrometer that could have covered the time scale suggested by Malini et al. from MD simulation[70] or as was chosen a spectrometer that was sensitive to the time scale reported for translational motion in liquid water and confined liquid water as had been suggested to be present based on NMR studies[59]. The IRIS instrument clearly showed that the internal water in ACC is not in a liquid state and that magnesium only has a minor effect on the confined motion of hydrous species in ACC, but it does not tell us anything about how the diffusion occurs in the system or the effect that magnesium may have on the diffusion mechanics. But there are several other high resolution inelastic spectrometers available to analysis the longer time scale such as the IN16B instrument at the ILL (Grenoble, France) which can probe time scale from ~40 ps to 1.7 ns. Even longer time scale are accessible using spin echo neutron spectroscopy (SENS) at e.g. IN15 which has a very wide energy transfer range of 0.2 neV to 200 µeV. However, the measurement time necessary for such an experiment may make it difficult to analyze several samples using SENS.

The argument can also be made that if the dynamics of the water is very slow, the diffusion of water may not be relevant for ACC crystallizes and as such would provide only a limited insight into the properties of the amorphous phase. In that case it may not warrant the use of such expensive analysis techniques as SENS.

6   Acknowledgements

7   References

1.   Mann, S., *Biomineralization: principles and concepts in bioinorganic materials chemistry*. Oxford University Press: 2001; Vol. 5.
2.   Swann, G. E. A.; Leng, M. J., A review of diatom δ18O in palaeoceanography. *Quaternary Science Reviews* **2009,** *28* (5), 384-398.
3.   Blakemore, R. P., Magnetotactic bacteria. *Science* **1975,** *190* (4212), 377-379.
4.   Mann, S.; Perry, C. C.; Webb, J.; Luke, B.; Williams, R. J. P., Structure, Morphology, Composition and Organization of Biogenic Minerals in Limpet Teeth. *Proceedings of the Royal Society of London. Series B. Biological Sciences* **1986,** *227* (1247), 179-190.
5.   Leemreize, H.; Almer, J. D.; Stock, S. R.; Birkedal, H., Three-dimensional distribution of polymorphs and magnesium in a calcified underwater attachment system by diffraction tomography. *Journal of The Royal Society Interface* **2013,** *10* (86), 20130319.
6.   Hasse, B.; Ehrenberg, H.; Marxen, J. C.; Becker, W.; Epple, M., Calcium carbonate modifications in the mineralized shell of the freshwater snail Biomphalaria glabrata. *Chem. Eur. J.* **2000,** *6* (*20*), *3679-3685*.
7.   Setoguchi, H.; Okazaki, M.; Suga, S., Calcification in Higher Plants with Special Reference to Cystoliths. In *Origin, Evolution, and Modern Aspects of Biomineralization in Plants and Animals*, Crick, R. E., Ed. Springer US: Boston, MA, 1989; pp 409-418.
8.   Carlstr; xf; m, D., A Crystallographic Study of Vertebrate Otoliths. *Biological Bulletin* **1963,** *125* (3), 441-463.
9.   Gauldie, R. W.; Sharma, S. K.; Volk, E., Micro-raman spectral study of vaterite and aragonite otoliths of the coho salmon, Oncorhynchus kisutch. *Comparative Biochemistry and Physiology Part A: Physiology* **1997,** *118* (3), 753-757.
10.   Reith, F.; Lengke, M. F.; Falconer, D.; Craw, D.; Southam, G., The geomicrobiology of gold. *The ISME Journal* **2007,** *1* (7), 567.
11.   Macaskie, L. E.; Empson, R. M.; Cheetham, A. K.; Grey, C. P.; Skarnulis, A. J., Uranium Bioaccumulation by a Citrobacter sp. as a Result of Enzymically Mediated Growth of Polycrystalline HUO$_2$PO$_4$. *Science* **1992,** *257* (5071), 782-784.
12.   Habraken, W. J. E. M.; Masic, A.; Bertinetti, L.; Al-Sawalmih, A.; Glazer, L.; Bentov, S.; Fratzl, P.; Sagi, A.; Aichmayer, B.; Berman, A., Layered growth of crayfish gastrolith: About the stability of amorphous calcium carbonate and role of additives. *Journal of Structural Biology* **2015,** *189* (1), 28-36.
13.   Kabalah-Amitai, L.; Mayzel, B.; Zaslansky, P.; Kauffmann, Y.; Clotens, P.; Pokroy, B., Unique crystallographic pattern in the macro to atomic structure of Herdmania momus vateritic spicules. *Journal of Structural Biology* **2013,** *183* (2), 191-198.
14.   Weiss, I. M.; Tuross, N.; Addadi, L.; Weiner, S., Mollusc larval shell formation: amorphous calcium carbonate is a precursor phase for aragonite. *Journal of Experimental Zoology* **2002,** *293* (5), 478-491.
15.   Cartwright, J. H. E.; Checa, A. G.; Gale, J. D.; Gebauer, D.; Sainz-Díaz, C. I., Calcium Carbonate Polyamorphism and Its Role in Biomineralization: How Many Amorphous Calcium Carbonates Are There? *Angew. Chem. Int. Ed.* **2012,** *51* (*48*), *11960-11970*.
16.   Robach, J. S.; Stock, S. R.; Veis, A., Mapping of magnesium and of different protein fragments in sea urchin teeth via secondary ion mass spectroscopy. *Journal of Structural Biology* **2006,** *155* (1), 87-95.
17.   Politi, Y.; Arad, T.; Klein, E.; Weiner, S.; Addadi, L., Sea urchin spine calcite forms via a transient amorphous calcium carbonate phase. *Science* **2004,** *306* (5699), 1161-1164.
18.   Killian, C. E.; Metzler, R. A.; Gong, Y. U. T.; Olson, I. C.; Aizenberg, J.; Politi, Y.; Wilt, F. H.; Scholl, A.; Young, A.; Doran, A.; Kunz, M.; Tamura, N.; Coppersmith, S. N.;

Gilbert, P. U. P. A., Mechanism of Calcite Co-Orientation in the Sea Urchin Tooth. *Journal of the American Chemical Society* **2009,** *131* (51), 18404-18409.

19.   Su, X.; Kamat, S.; Heuer, A., The structure of sea urchin spines, large biogenic single crystals of calcite. *Journal of materials science* **2000,** *35* (22), 5545-5551.

20.   Gilbert, P. U. P. A.; Metzler, R. A.; Zhou, D.; Scholl, A.; Doran, A.; Young, A.; Kunz, M.; Tamura, N.; Coppersmith, S. N., Gradual Ordering in Red Abalone Nacre. *Journal of the American Chemical Society* **2008,** *130* (51), 17519-17527.

21.   Addadi, L.; Raz, S.; Weiner, S., Taking Advantage of Disorder: Amorphous Calcium Carbonate and Its Roles in Biomineralization. *Adv. Mater.* **2003,** *15* (*12*), *959-970.*

22.   Weiner, S.; Levi-Kalisman, Y.; Raz, S.; Addadi, L., Biologically Formed Amorphous Calcium Carbonate. *Connect. Tissue Res.* **2003,** *44* (*1*), *214-218.*

23.   Weiner, S.; Sagi, I.; Addadi, L., Choosing the crystallization path less traveled. *Science* **2005,** *309* (*5737*), *1027-1028.*

24.   Sviben, S.; Gal, A.; Hood, M. A.; Bertinetti, L.; Politi, Y.; Bennet, M.; Krishnamoorthy, P.; Schertel, A.; Wirth, R.; Sorrentino, A.; Pereiro, E.; Faivre, D.; Scheffel, A., A vacuole-like compartment concentrates a disordered calcium phase in a key coccolithophorid alga. *Nat Commun* **2016,** *7.*

25.   Gal, A.; Kahil, K.; Vidavsky, N.; DeVol, R. T.; Gilbert, P. U. P. A.; Fratzl, P.; Weiner, S.; Addadi, L., Particle Accretion Mechanism Underlies Biological Crystal Growth from an Amorphous Precursor Phase. *Advanced Functional Materials* **2014,** *24* (34), 5420-5426.

26.   Falini, G.; Fermani, S., Nucleation and Growth from a Biomineralization Perspective. In *New Perspectives on Mineral Nucleation and Growth: From Solution Precursors to Solid Materials*, Van Driessche, A. E. S.; Kellermeier, M.; Benning, L. G.; Gebauer, D., Eds. Springer International Publishing: Cham, 2017; pp 185-197.

27.   Zou, Z.; Bertinetti, L.; Politi, Y.; Jensen, A. C. S.; Weiner, S.; Addadi, L.; Fratzl, P.; Habraken, W. J. E. M., Opposite Particle Size Effect on Amorphous Calcium Carbonate Crystallization in Water and during Heating in Air. *Chem. Mater* **2015,** *27* (*12*), *4237-4246.*

28.   Beniash, E.; Addadi, L.; Weiner, S., Cellular Control Over Spicule Formation in Sea Urchin Embryos: A Structural Approach. *Journal of Structural Biology* **1999,** *125* (1), 50-62.

29.   Politi, Y.; Levi-Kalisman, Y.; Raz, S.; Wilt, F.; Addadi, L.; Weiner, S.; Sagi, I., Structural characterization of the transient amorphous calcium carbonate precursor phase in sea urchin embryos. *Adv. Funct. Mater.* **2006,** *16* (*10*), *1289-1298.*

30.   Gal, A.; Weiner, S.; Addadi, L., A perspective on underlying crystal growth mechanisms in biomineralization: solution mediated growth versus nanosphere particle accretion. *CrystEngComm* **2015,** *17* (13), 2606-2615.

31.   Gal, A.; Brumfeld, V.; Weiner, S.; Addadi, L.; Oron, D., Certain Biominerals in Leaves Function as Light Scatterers. *Advanced Materials* **2012,** *24* (10), OP77-OP83.

32.   Reeder, R. J.; Tang, Y.; Schmidt, M. P.; Kubista, L. M.; Cowan, D. F.; Phillips, B. L., Characterization of Structure in Biogenic Amorphous Calcium Carbonate: Pair Distribution Function and Nuclear Magnetic Resonance Studies of Lobster Gastrolith. *Cryst. Growth & Des.* **2013,** *13* (*5*), *1905-1914*.

33.   Levi-Kalisman, Y.; Raz, S.; Weiner, S.; Addadi, L.; Sagi, I., Structural differences between biogenic amorphous calcium carbonate phases using X-ray absorption spectroscopy. *Adv. Funct. Mater.* **2002,** *12* (*1*), *43-48*.

34.   Fernandez-Martinez, A.; Lopez-Martinez, H.; Wang, D., Structural Characteristics and the Occurrence of Polyamorphism in Amorphous Calcium Carbonate. In *New Perspectives on Mineral Nucleation and Growth: From Solution Precursors to Solid Materials*, Van Driessche, A. E. S.; Kellermeier, M.; Benning, L. G.; Gebauer, D., Eds. Springer International Publishing: Cham, 2017; pp 77-92.

References

35.   Gebauer, D.; Gunawidjaja, P. N.; Ko, J. Y. P.; Bacsik, Z.; Aziz, B.; Liu, L.; Hu, Y.; Bergström, L.; Tai, C.-W.; Sham, T.-K.; Edén, M.; Hedin, N., Proto-Calcite and Proto-Vaterite in Amorphous Calcium Carbonates. *Angewandte Chemie* **2010,** *122* (47), 9073-9075.

36.   Michel, F. M.; MacDonald, J.; Feng, J.; Phillips, B. L.; Ehm, L.; Tarabrella, C.; Parise, J. B.; Reeder, R. J., Structural Characteristics of Synthetic Amorphous Calcium Carbonate. *Chem. Mater* **2008,** *20* (*14*), *4720-4728*.

37.   Farhadi Khouzani, M.; Chevrier, D. M.; Guttlein, P.; Hauser, K.; Zhang, P.; Hedin, N.; Gebauer, D., Disordered amorphous calcium carbonate from direct precipitation. *CrystEngComm* **2015,** *17* (26), 4842-4849.

38.   Radha, A. V.; Fernandez-Martinez, A.; Hu, Y.; Jun, Y.-S.; Waychunas, G. A.; Navrotsky, A., Energetic and structural studies of amorphous Ca1−xMgxCO3·nH2O (0 ⩽ x ⩽ 1). *Geochimica et Cosmochimica Acta* **2012,** *90*, 83-95.

39.   Rodriguez-Blanco, J. D.; Shaw, S.; Bots, P.; Roncal-Herrero, T.; Benning, L. G., The role of pH and Mg on the stability and crystallization of amorphous calcium carbonate. *Journal of Alloys and Compounds* **2012,** *536, Supplement 1* (0), S477-S479.

40.   Rodriguez-Blanco, J. D.; Shaw, S.; Bots, P.; Roncal-Herrero, T.; Benning, L. G., The role of Mg in the crystallization of monohydrocalcite. *Geochimica et Cosmochimica Acta* **2014,** *127*, 204-220.

41.   Nishiyama, R.; Munemoto, T.; Fukushi, K., Formation condition of monohydrocalcite from CaCl2–MgCl2–Na2CO3 solutions. *Geochimica et Cosmochimica Acta* **2013,** *100*, 217-231.

42.   Yang, S.-Y.; Chang, H.-H.; Lin, C.-J.; Huang, S.-J.; Chan, J. C., Is Mg-stabilized amorphous calcium carbonate a homogeneous mixture of amorphous magnesium carbonate and amorphous calcium carbonate? *Chemical Communications* **2016,** *52* (77), 11527-11530.

43.   Cobourne, G.; Mountjoy, G.; Rodriguez-Blanco, J. D.; Benning, L. G.; Hannon, A. C.; Plaisier, J. R., Neutron and X-ray diffraction and empirical potential structure refinement modelling of magnesium stabilised amorphous calcium carbonate. *J. Non-Cryst. Solids* **2014,** *401, 154-158*.

44.   Loste, E.; Wilson, R. M.; Seshadri, R.; Meldrum, F. C., The role of magnesium in stabilising amorphous calcium carbonate and controlling calcite morphologies. *Journal of Crystal Growth* **2003,** *254* (1), 206-218.

45.   Taylor, M. G.; Simkiss, K.; Greaves, G.; Okazaki, M.; Mann, S., An X-ray absorption spectroscopy study of the structure and transformation of amorphous calcium carbonate from plant cystoliths. *Proc. Royal Soc. B* **1993,** *252* (*1333*), *75-80*.

46.   Levi-Kalisman, Y.; Raz, S.; Weiner, S.; Addadi, L.; Sagi, I., X-Ray absorption spectroscopy studies on the structure of a biogenic "amorphous" calcium carbonate phase. *Dalton Trans.* **2000,** (*21*), *3977-3982*.

47.   Politi, Y.; Batchelor, D. R.; Zaslansky, P.; Chmelka, B. F.; Weaver, J. C.; Sagi, I.; Weiner, S.; Addadi, L., Role of Magnesium Ion in the Stabilization of Biogenic Amorphous Calcium Carbonate: A Structure−Function Investigation. *Chemistry of Materials* **2010,** *22* (1), 161-166.

48.   Becker, A.; Ziegler, A.; Epple, M., The mineral phase in the cuticles of two species of Crustacea consists of magnesium calcite, amorphous calcium carbonate, and amorphous calcium phosphate. *Dalton Trans.* **2005,** (*10*), 1814-1820.

49.   Marxen, J. C.; Becker, W.; Finke, D.; Hasse, B.; Epple, M., Early mineralization in biomphalaria glabrata: microscopic and structural results. *J. Molluscan Stud.* **2003,** *69* (*2*), *113-121*.

50.   Graf, D., Crystallographic tables for the rhombohedral carbonates. *Am. Mineral* **1961,** *46* (*11-2*), *1283-1316*.

51.   De Villiers, J. P. R., Crystal structures of aragonite, strontianite and witherite. *Am. Mineral* **1971,** *56*, *758-767*.

References

52.   Hesse, K.; Küppers, H.; Suess, E., Refinement of the structure of Ikaite, CaCO3-6H2O. *Z. Kristallogr. Cryst. Mater.* **1983,** *163* (*1-4*), *227-232*.

53.   Swainson, I. P., The structure of monohydrocalcite and the phase composition of the beachrock deposits of Lake Butler and Lake Fellmongery, South Australia. *Am. Mineral* **2008,** *93* (*7*), *1014-1018*.

54.   Kamhi, S., On the structure of vaterite CaCO3. *Acta Cryst.* **1963,** *16* (*8*), *770-772*.

55.   Becker, A.; Bismayer, U.; Epple, M.; Fabritius, H.; Hasse, B.; Shi, J.; Ziegler, A., Structural characterisation of X-ray amorphous calcium carbonate (ACC) in sternal deposits of the crustacea Porcellio scaber. *Dalton Trans.* **2003,** (*4*), *551-555*.

56.   Ihli, J.; Wong, W. C.; Noel, E. H.; Kim, Y.-Y.; Kulak, A. N.; Christenson, H. K.; Duer, M. J.; Meldrum, F. C., Dehydration and crystallization of amorphous calcium carbonate in solution and in air. *Nat Commun* **2014,** *5*, *3169*.

57.   Kababya, S.; Gal, A.; Kahil, K.; Weiner, S.; Addadi, L.; Schmidt, A., Phosphate–Water Interplay Tunes Amorphous Calcium Carbonate Metastability: Spontaneous Phase Separation and Crystallization vs Stabilization Viewed by Solid State NMR. *J. Am. Chem. Soc.* **2015,** *137* (*2*), *990-998*.

58.   Nebel, H.; Neumann, M.; Mayer, C.; Epple, M., On the structure of amorphous calcium carbonate · A detailed study by solid-state NMR spectroscopy. *Inorg. Chem.* **2008,** *47* (*17*), *7874-7879*.

59.   Schmidt, M. P.; Ilott, A. J.; Phillips, B. L.; Reeder, R. J., Structural Changes upon Dehydration of Amorphous Calcium Carbonate. *Cryst. Growth & Des.* **2014,** *14* (*3*), *938-951*.

60.   Henry, E. F.; Adrian, C. B.; Philip, S. S., Neutron and x-ray diffraction studies of liquids and glasses. *Reports on Progress in Physics* **2006,** *69* (1), 233.

61.   Soper, A. K., Partial structure factors from disordered materials diffraction data: An approach using empirical potential structure refinement. *Phys. Rev. B* **2005,** *72* (*10*), *104204*.

62.   Egami, T.; Billinge, S. J., *Underneath the Bragg peaks: structural analysis of complex materials*. Elsevier: 2003; Vol. 16.

63.   Goodwin, A. L.; Michel, F. M.; Phillips, B. L.; Keen, D. A.; Dove, M. T.; Reeder, R. J., Nanoporous Structure and Medium-Range Order in Synthetic Amorphous Calcium Carbonate. *Chem. Mater* **2010,** *22* (*10*), *3197-3205*.

64.   Singer, J. W.; Yazaydin, A. Ö.; Kirkpatrick, R. J.; Bowers, G. M., Structure and Transformation of Amorphous Calcium Carbonate: A Solid-State 43Ca NMR and Computational Molecular Dynamics Investigation. *Chem. Mater* **2012,** *24* (*10*), *1828-1836*.

65.   Tobler, D. J.; Rodriguez Blanco, J. D.; Sørensen, H. O.; Stipp, S. L. S.; Dideriksen, K., Effect of pH on Amorphous Calcium Carbonate Structure and Transformation. *Cryst. Growth & Des.* **2016,** *16* (*8*), *4500-4508*.

66.   Wang, H.-W.; Daemen, L. L.; Cheshire, M. C.; Kidder, M. K.; Stack, A. G.; Allard, L. F.; Neuefeind, J.; Olds, D.; Liu, J.; Page, K., Synthesis and structure of synthetically pure and deuterated amorphous (basic) calcium carbonates. *Chemical Communications* **2017,** *53* (20), 2942-2945.

67.   Tomono, H.; Nada, H.; Zhu, F.; Sakamoto, T.; Nishimura, T.; Kato, T., Effects of Magnesium Ions and Water Molecules on the Structure of Amorphous Calcium Carbonate: A Molecular Dynamics Study. *The Journal of Physical Chemistry B* **2013,** *117* (47), 14849-14856.

68.   Saharay, M.; James Kirkpatrick, R., Onset of Orientational Order in Amorphous Calcium Carbonate (ACC) upon Dehydration. *Chem. Phys. Lett.* **2014,** *591* (*0*), *287-291*.

69.   Bushuev, Y. G.; Finney, A. R.; Rodger, P. M., Stability and Structure of Hydrated Amorphous Calcium Carbonate. *Cryst. Growth & Des.* **2015,** *15* (*11*), *5269-5279*.

70.   Innocenti Malini, R.; Bushuev, Y. G.; Hall, S. A.; Freeman, C. L.; Rodger, P. M.; Harding, J. H., Using simulation to understand the structure and properties of hydrated amorphous calcium carbonate. *CrystEngComm* **2016,** *18* (1), 92-101.

References

71.   Raiteri, P.; Gale, J. D., Water Is the Key to Nonclassical Nucleation of Amorphous Calcium Carbonate. *Journal of the American Chemical Society* **2010,** *132* (49), 17623-17634.

72.   Rodriguez-Blanco, J. D.; Shaw, S.; Benning, L. G., The kinetics and mechanisms of amorphous calcium carbonate (ACC) crystallization to calcite, viavaterite. *Nanoscale* **2011,** *3* (1), 265-271.

73.   Bots, P.; Benning, L. G.; Rodriguez-Blanco, J.-D.; Roncal-Herrero, T.; Shaw, S., Mechanistic Insights into the Crystallization of Amorphous Calcium Carbonate (ACC). *Crystal Growth & Design* **2012,** *12* (7), 3806-3814.

74.   Konrad, F.; Gallien, F.; Gerard, D. E.; Dietzel, M., Transformation of Amorphous Calcium Carbonate in Air. *Crystal Growth & Design* **2016,** *16* (11), 6310-6317.

75.   Koga, N.; Nakagoe, Y.; Tanaka, H., Crystallization of amorphous calcium carbonate. *Thermochimica Acta* **1998,** *318* (1–2), 239-244.

76.   Yoshino, T.; Maruyama, K.; Kagi, H.; Nara, M.; Kim, J. C., Pressure-Induced Crystallization from Amorphous Calcium Carbonate. *Crystal Growth & Design* **2012,** *12* (7), 3357-3361.

77.   Maruyama, K.; Kagi, H.; Inoue, T.; Ohfuji, H.; Yoshino, T., In Situ Observation of Pressure-induced Crystallization from Amorphous Calcium Carbonate by Time-resolved X-ray Diffraction. *Chemistry Letters* **2015,** *44* (4), 434-436.

78.   Rodriguez-Blanco, J. D.; Shaw, S.; Benning, L. G., How to make 'stable' ACC: protocol and preliminary structural characterization. *Mineralogical Magazine* **2008,** *72* (1), 283-286.

79.   Wolf, S. L. P.; Jahme, K.; Gebauer, D., Synergy of Mg2+ and poly(aspartic acid) in additive-controlled calcium carbonate precipitation. *CrystEngComm* **2015**.

80.   Jensen, A. C. S.; Hinge, M.; Birkedal, H., Calcite nucleation on the surface of PNIPAM-PAAc micelles studied by time resolved in situ PXRD. *CrystEngComm* **2015,** *17* (36), 6940-6946.

81.   Ihli, J.; Kim, Y.-Y.; Noel, E. H.; Meldrum, F. C., The Effect of Additives on Amorphous Calcium Carbonate (ACC): Janus Behavior in Solution and the Solid State. *Advanced Functional Materials* **2013,** *23* (12), 1575-1585.

82.   Sun, S.; Gebauer, D.; Colfen, H., A solvothermal method for synthesizing monolayer protected amorphous calcium carbonate clusters. *Chemical Communications* **2016**.

83.   Kimura, T.; Koga, N., Monohydrocalcite in Comparison with Hydrated Amorphous Calcium Carbonate: Precipitation Condition and Thermal Behavior. *Crystal Growth & Design* **2011,** *11* (9), 3877-3884.

84.   White, C. E.; Henson, N. J.; Daemen, L. L.; Hartl, M.; Page, K., Uncovering the True Atomic Structure of Disordered Materials: The Structure of a Hydrated Amorphous Magnesium Carbonate (MgCO3·3D2O). *Chemistry of Materials* **2014,** *26* (8), 2693-2702.

85.   Davis, K. J.; Dove, P. M.; De Yoreo, J. J., The role of Mg2+ as an impurity in calcite growth. *Science* **2000,** *290* (5494), 1134-1137.

86.   Lin, C.-J.; Yang, S.-Y.; Huang, S.-J.; Chan, J. C. C., Structural Characterization of Mg-Stabilized Amorphous Calcium Carbonate by Mg-25 Solid-State NMR Spectroscopy. *The Journal of Physical Chemistry C* **2015,** *119* (13), 7225-7233.

87.   Xu, J.; Yan, C.; Zhang, F.; Konishi, H.; Xu, H.; Teng, H. H., Testing the cation-hydration effect on the crystallization of Ca–Mg–CO(3) systems. *Proceedings of the National Academy of Sciences of the United States of America* **2013,** *110* (44), 17750-17755.

88.   De Yoreo, J.; Zepeda-Ruiz, L.; Friddle, R.; Qiu, S.; Wasylenki, L.; Chernov, A.; Gilmer, G.; Dove, P., Rethinking classical crystal growth models through molecular scale insights: consequences of kink-limited kinetics. *Crystal Growth & Design* **2009,** *9* (12), 5135-5144.

89.   Lippmann, F., *Sedimentary carbonate minerals*. Springer Science & Business Media: 2012; Vol. 6.

90.   Munemoto, T.; Fukushi, K., Transformation kinetics of monohydrocalcite to aragonite in aqueous solutions. *Journal of Mineralogical and Petrological Sciences* **2008,** *103* (5), 345-349.

91.   Akao, M.; Iwai, S., The hydrogen bonding of hydromagnesite. *Acta Crystallographica Section B: Structural Crystallography and Crystal Chemistry* **1977,** *33* (4), 1273-1275.

92.   Giester, G.; Lengauer, C.; Rieck, B., The crystal structure of nesquehonite, MgCO 3· 3H 2 O, from Lavrion, Greece. *Mineralogy and Petrology* **2000,** *70* (3), 153-163.

93.   Akao, M.; Iwai, S., The hydrogen bonding of artinite. *Acta Crystallographica Section B: Structural Crystallography and Crystal Chemistry* **1977,** *33* (12), 3951-3953.

94.   BAI-NIAN, L.; XIANG-TING, Z.; XIU-SHAN, C.; JI-GANG, T., Synthesis of lansfordite MgCO 3· 5H 2 O and its crystal structure investigation. *Science in China Series B-Chemistry, Life Sciences & Earth Sciences* **1990,** *33* (11), 1350-1356.

95.   Lei, Z.; Sun, S.; Wu, P., Ultrafast, Scale-Up Synthesis of Pure and Stable Amorphous Carbonate Mineral Nanoparticles. *ACS Sustainable Chemistry & Engineering* **2017,** *5* (6), 4499-4504.

96.   Giacovazzo, C., *Fundamentals of crystallography*. Oxford university press, USA: 2002; Vol. 7.

97.   Bowron, D. T., Building Monte Carlo Models of Glasses Using Neutron and/or X-ray Diffraction Data. *Procedia Materials Science* **2014,** *7*, 38-52.

98.   Henderson, D.; Gutowsky, H. *A nuclear magnetic resonance determination of the hydrogen positions in Ca (OH) 2*; ILLINOIS UNIV URBANA NOYES CHEMICAL LAB: 1962.

99.   Barnes, A.; Lague, S.; Salmon, P.; Fischer, H., A determination of the structure of liquid using neutron diffraction and isotopic substitution. *Journal of Physics: Condensed Matter* **1997,** *9* (29), 6159.

100.   Mi, J.-L.; Jensen, K. M. O.; Tyrsted, C.; Bremholm, M.; Iversen, B. B., In situ total X-ray scattering study of the formation mechanism and structural defects in anatase TiO2 nanoparticles under hydrothermal conditions. *CrystEngComm* **2015**.

101.   Farrow, C.; Juhas, P.; Liu, J.; Bryndin, D.; Božin, E.; Bloch, J.; Proffen, T.; Billinge, S., PDFfit2 and PDFgui: computer programs for studying nanostructure in crystals. *Journal of Physics: Condensed Matter* **2007,** *19* (33), 335219.

102.   Tyrsted, C.; Lock, N.; Jensen, K. M. O.; Christensen, M.; Bojesen, E. D.; Emerich, H.; Vaughan, G.; Billinge, S. J. L.; Iversen, B. B., Evolution of atomic structure during nanoparticle formation. *IUCrJ* **2014,** *1* (3), 165-171.

103.   Tyrsted, C.; Ørnsbjerg Jensen, K. M.; Bøjesen, E. D.; Lock, N.; Christensen, M.; Billinge, S. J. L.; Brummerstedt Iversen, B., Understanding the Formation and Evolution of Ceria Nanoparticles Under Hydrothermal Conditions. *Angewandte Chemie International Edition* **2012,** *51* (36), 9030-9033.

104.   De Yoreo, J. J.; Gilbert, P. U. P. A.; Sommerdijk, N. A. J. M.; Penn, R. L.; Whitelam, S.; Joester, D.; Zhang, H.; Rimer, J. D.; Navrotsky, A.; Banfield, J. F.; Wallace, A. F.; Michel, F. M.; Meldrum, F. C.; Cölfen, H.; Dove, P. M., Crystallization by particle attachment in synthetic, biogenic, and geologic environments. *Science* **2015,** *349* (6247).

105.   McGreevy, R.; Pusztai, L., Reverse Monte Carlo simulation: a new technique for the determination of disordered structures. *Molecular Simulation* **1988,** *1* (6), 359-367.

106.   Mancinelli, R.; Botti, A.; Bruni, F.; Ricci, M. A.; Soper, A. K., Hydration of Sodium, Potassium, and Chloride Ions in Solution and the Concept of Structure Maker/Breaker. *The Journal of Physical Chemistry B* **2007,** *111* (48), 13570-13577.

107.   Imberti, S.; Botti, A.; Bruni, F.; Cappa, G.; Ricci, M. A.; Soper, A. K., Ions in water: The microscopic structure of concentrated hydroxide solutions. *The Journal of Chemical Physics* **2005,** *122* (19), 194509.

108.   Soper, A. K., The radial distribution functions of water and ice from 220 to 673 K and at pressures up to 400 MPa. *Chem. Phys.* **2000,** *258* (*2–3*), *121-137.*

109.   Alan, K. S., Boroxol rings from diffraction data on vitreous boron trioxide. *Journal of Physics: Condensed Matter* **2011,** *23* (36), 365402.

110.   Soper, A. K., Network structure and concentration fluctuations in a series of elemental, binary, and tertiary liquids and glasses. *J. Phys. Condens Matter* **2010,** *22* (*40*), *404210.*

111.   Soper, A. K., Computer simulation as a tool for the interpretation of total scattering data from glasses and liquids. *Mol. Simul.* **2012,** *38* (*14-15*), *1171-1185.*

112.   Soper, A., On the uniqueness of structure extracted from diffraction experiments on liquids and glasses. *Journal of Physics: Condensed Matter* **2007,** *19* (41), 415108.

113.   Soper, A. K., Tests of the empirical potential structure refinement method and a new method of application to neutron diffraction data on water. *Mol. Phys.* **2001,** *99* (*17*), *1503-1516.*

114.   Soper, A. K., Empirical potential Monte Carlo simulation of fluid structure. *Chemical Physics* **1996,** *202* (2–3), 295-306.

115.   Chupas, P. J.; Qiu, X.; Hanson, J. C.; Lee, P. L.; Grey, C. P.; Billinge, S. J., Rapid-acquisition pair distribution function (RA-PDF) analysis. *Journal of Applied Crystallography* **2003,** *36* (6), 1342-1347.

116.   Keen, D. A., A comparison of various commonly used correlation functions for describing total scattering. *Journal of Applied Crystallography* **2001,** *34* (2), 172-177.

117.   Soper, A., *Rutherford Appleton Laboratory Technical Report RAL-TR-2011-013* **2011**.

118.   Hannon, A.; Howells, W.; Soper, A. In *ATLAS: A suite of programs for the analysis of time-of-flight neutron diffraction data from liquid and amorphous samples*, Inst. Phys. Conf. Ser, 1990; pp 193-211.

119.   Gabriel, J. C., Structure factor determination of amorphous materials by neutron diffraction. *Journal of Physics: Condensed Matter* **2008,** *20* (24), 244109.

120.   Benmore, C.; Soper, A. *The SANDALS manual. A guide to performing experiments on the small angle neutron diffractometer for amorphous and liquid samples at ISIS*; Council for the Central Lab. of the Research Councils (CLRC): 1998.

121.   Fischer, H.; Cuello, G.; Palleau, P.; Feltin, D.; Barnes, A.; Badyal, Y.; Simonson, J., D4c: A very high precision diffractometer for disordered materials. *Applied Physics A: Materials Science & Processing* **2002,** *74*, s160-s162.

122.   Jones, C. J., *d-and f-Block Chemistry*. 2001.

123.   Hudson, B. S., Vibrational spectroscopy using inelastic neutron scattering: Overview and outlook. *Vibrational Spectroscopy* **2006,** *42* (1), 25-32.

124.   Stewart, F. P.; Felix, F.-A.; Anibal, J. R.-C.; John, T.; Svemir, R.; Roberto, S. P.; Giuseppe, G.; Javier Fernández, C., Recent and future developments on TOSCA at ISIS. *J. Phys. Conf. Ser.* **2014,** *554* (*1*), *012003.*

125.   Campbell, S. I.; Telling, M. T. F.; Carlile, C. J., The optimisation of analyser geometry in near-backscattering spectrometers – IRIS on the ISIS-pulsed source. *Physica B: Condensed Matter* **2000,** *276–278*, 206-207.

126.   Li, J., Inelastic neutron scattering studies of hydrogen bonding in ices. *J. Chem. Phys.* **1996,** *105* (*16*), *6733-6755.*

127.   Baddour-Hadjean, R.; Fillaux, F.; Floquet, N.; Belushkin, S.; Natkaniec, I.; Desgranges, L.; Grebille, D., Inelastic neutron scattering study of proton dynamics in $Ca(OH)_2$ at 20 K. *Chemical Physics* **1995,** *197* (1), 81-90.

128.   Line, C. M. B.; Kearley, G. J., An inelastic incoherent neutron scattering study of water in small-pored zeolites and other water-bearing minerals. *J. Chem. Phys.* **2000,** *112* (*20*), *9058-9067.*

References

129. Line, C. M. B.; Kearley, G. J.; Suard, E.; Fitch, A.; Swainson, I., Water in wairakite: A water-zeolite model system. *Physica B: Condensed Matter* **1997**, *234–236*, 79-81.

130. Li, J.; Kolesnikov, A. I., Neutron spectroscopic investigation of dynamics of water ice. *Journal of Molecular Liquids* **2002**, *100* (1), 1-39.

131. G. Taylor, M.; Simkiss, K.; F. Parker, S.; C. H. Mitchell, P., Inelastic neutron scattering studies of synthetic calcium phosphates. *Physical Chemistry Chemical Physics* **1999**, *1* (13), 3141-3144.

132. Mitchell, P. C. H.; Parker, S. F.; Simkiss, J.; Simmons, J.; Taylor, M. G., Hydrated sites in biogenic amorphous calcium phosphates: An infrared, Raman, and inelastic neutron scattering study. *J. Inorg. Biochem.* **1996**, *62* (*3*), *183-197*.

133. Parker, S. F.; Refson, K.; Hannon, A. C.; Barney, E. R.; Robertson, S. J.; Albers, P., Characterization of Hydrous Palladium Oxide: Implications for Low-Temperature Carbon Monoxide Oxidation. *J. Phys. Chem. C* **2010**, *114* (*33*), *14164-14172*.

134. Taylor, M. G.; Parker, S. F.; Simkiss, K.; Mitchell, P. C. H., Bone mineral: evidence for hydroxy groups by inelastic neutron scattering. *Physical Chemistry Chemical Physics* **2001**, *3* (8), 1514-1517.

135. Shepherd, P. D.; Kagunya, W. W.; Campbell, S. I.; Chapple, A. P.; Dreyer, J. W.; Humphreys, R. J.; Kemali, M.; Mercer, M.; Ross, D. K., Water dynamics in Na zeolite P by QENS. *Physica B: Condensed Matter* **1997**, *234–236*, 914-916.

136. Teixeira, J.; Bellissent-Funel, M. C.; Chen, S. H.; Dianoux, A. J., Experimental determination of the nature of diffusive motions of water molecules at low temperatures. *Physical Review A* **1985**, *31* (3), 1913-1917.

137. Skipper, N. T.; Lock, P. A.; Titiloye, J. O.; Swenson, J.; Mirza, Z. A.; Howells, W. S.; Fernandez-Alonso, F., The structure and dynamics of 2-dimensional fluids in swelling clays. *Chemical Geology* **2006**, *230* (3–4), 182-196.

138. Mamontov, E.; Cole, D. R.; Dai, S.; Pawel, M. D.; Liang, C. D.; Jenkins, T.; Gasparovic, G.; Kintzel, E., Dynamics of water in LiCl and CaCl2 aqueous solutions confined in silica matrices: A backscattering neutron spectroscopy study. *Chemical Physics* **2008**, *352* (1–3), 117-124.

139. Bénézeth, P.; Saldi, G. D.; Dandurand, J.-L.; Schott, J., Experimental determination of the solubility product of magnesite at 50 to 200 °C. *Chemical Geology* **2011**, *286* (1–2), 21-31.

140. De Visscher, A.; Vanderdeelen, J., Estimation of the Solubility Constant of Calcite, Aragonite, and Vaterite at 25°C Based on Primary Data Using the Pitzer Ion Interaction Approach. *Monatshefte für Chemie / Chemical Monthly* **2003**, *134* (5), 769-775.

141. Pokrovsky, O. S.; Schott, J., Experimental study of brucite dissolution and precipitation in aqueous solutions: surface speciation and chemical affinity control. *Geochimica et Cosmochimica Acta* **2004**, *68* (1), 31-45.

142. Lambert, I.; Clever, H. L., *Alkaline earth hydroxides in water and aqueous solutions*. Elsevier: 2013; Vol. 52.

143. Sen, S.; Kaseman, D. C.; Colas, B.; Jacob, D. E.; Clark, S. M., Hydrogen bonding induced distortion of CO3 units and kinetic stabilization of amorphous calcium carbonate: results from 2D 13C NMR spectroscopy. *Physical Chemistry Chemical Physics* **2016**.

144. Van Coung, P. K., Bjørn Kuznetsova, Tatiana Jensen, Bjørnar, *The impact of short-range force field parameters and temperature effect on selective adsorption of water and CO2 on calcite*. wseas: 2012; Vol. 1.

145. Bruni, F.; Imberti, S.; Mancinelli, R.; Ricci, M. A., Aqueous solutions of divalent chlorides: Ions hydration shell and water structure. *J. Chem. Phys.* **2012**, *136* (*6*), *064520*.

146. Hiemstra, T.; Rahnemaie, R.; van Riemsdijk, W. H., Surface complexation of carbonate on goethite: IR spectroscopy, structure and charge distribution. *J. Colloid Interface Sci.* **2004**, *278* (*2*), *282-290*.

References

147.   Williams, D. F., I., *Spectroscopic method in organic chemistry*. 6th ed.; McGraw Hill: 2008.

148.   Neumann, M.; Epple, M., Monohydrocalcite and Its Relationship to Hydrated Amorphous Calcium Carbonate in Biominerals. *Eur. J. Inorg. Chem.* **2007,** *2007* (*14*), *1953-1957*.

149.   Rez, P.; Blackwell, A., Ca L23 Spectrum in Amorphous and Crystalline Phases of Calcium Carbonate. *J. Phys. Chem. B* **2011,** *115* (*38*), *11193-11198*.

150.   Rez, P.; Sinha, S.; Gal, A., Nanocrystallite model for amorphous calcium carbonate. *J. Appl. Cryst.* **2014,** *47* (*5*), *1651-1657*.

151.   Kohagen, M.; Mason, P. E.; Jungwirth, P., Accurate Description of Calcium Solvation in Concentrated Aqueous Solutions. *J. Phys. Chem. B* **2014,** *118* (*28*), *7902-7909*.

152.   Zou, Z.; Habraken, W. J. E. M.; Bertinetti, L.; Politi, Y.; Gal, A.; Weiner, S.; Addadi, L.; Fratzl, P., On the Phase Diagram of Calcium Carbonate Solutions. *Adv. Mater. Interfaces* **2016,** *4* (*1*), *1600076*.

153.   Faatz, M.; Gröhn, F.; Wegner, G., Amorphous Calcium Carbonate: Synthesis and Potential Intermediate in Biomineralization. *Adv. Mater.* **2004,** *16* (*12*), *996-1000*.

154.   Wallace, A. F.; Hedges, L. O.; Fernandez-Martinez, A.; Raiteri, P.; Gale, J. D.; Waychunas, G. A.; Whitelam, S.; Banfield, J. F.; De Yoreo, J. J., Microscopic Evidence for Liquid-Liquid Separation in Supersaturated CaCO3 Solutions. *Science* **2013,** *341* (*6148*), *885-889*.

155.   Poduska, K. M.; Regev, L.; Boaretto, E.; Addadi, L.; Weiner, S.; Kronik, L.; Curtarolo, S., Decoupling Local Disorder and Optical Effects in Infrared Spectra: Differentiating Between Calcites with Different Origins. *Advanced Materials* **2011,** *23* (4), 550-554.

156.   Zigan, F.; Rothbauer, R., Neutronenbeugungsmessungen am brucit. *Neues Jahrbuch für Mineralogie Monatshefte* **1967,** *1967*, 137À143.

157.   Hazen, R. M., Effects of temperature and pressure on the cell dimension and X-ray temperature factors of periclase. *American Mineralogist* **1976,** *61* (3), 266-71.

158.   Wang, D.; Hamm, L. M.; Bodnar, R. J.; Dove, P. M., Raman spectroscopic characterization of the magnesium content in amorphous calcium carbonates. *Journal of Raman Spectroscopy* **2012,** *43* (4), 543-548.

159.   Swenson, J.; Bergman, R.; Howells, W. S., Quasielastic neutron scattering of two-dimensional water in a vermiculite clay. *The Journal of Chemical Physics* **2000,** *113* (7), 2873-2879.

160.   Arnold, O.; Bilheux, J.-C.; Borreguero, J.; Buts, A.; Campbell, S. I.; Chapon, L.; Doucet, M.; Draper, N.; Leal, R. F.; Gigg, M., Mantid—data analysis and visualization package for neutron scattering and μ SR experiments. *Nuclear Instruments and Methods in Physics Research Section A: Accelerators, Spectrometers, Detectors and Associated Equipment* **2014,** *764*, 156-166.

8 Appendix

The following pages contains the permissions to reprint the figures presented in chapter 1

Copyright
Clearance
Center

RightsLink®

Home   Create Account   Help

ACS Publications
Most Trusted. Most Cited. Most Read.

Title: Structural Characteristics of Synthetic Amorphous Calcium Carbonate

Author: F. Marc Michel, Jason MacDonald, Jian Feng, et al

Publication: Chemistry of Materials

Publisher: American Chemical Society

Date: Jul 1, 2008

Copyright © 2008, American Chemical Society

PERMISSION/LICENSE IS GRANTED FOR YOUR ORDER AT NO CHARGE

This type of permission/license, instead of the standard Terms & Conditions, is sent to you because no fee is being charged for your order. Please note the following:

- Permission is granted for your request in both print and electronic formats, and translations.
- If figures and/or tables were requested, they may be adapted or used in part.
- Please print this page for your records and send a copy of it to your publisher/graduate school.
- Appropriate credit for the requested material should be given as follows: "Reprinted (adapted) with permission from (COMPLETE REFERENCE CITATION). Copyright (YEAR) American Chemical Society." Insert appropriate information in place of the capitalized words.
- One-time permission is granted only for the use specified in your request. No additional uses are granted (such as derivative works or other editions). For any other uses, please submit a new request.

If credit is given to another source for the material you requested, permission must be obtained from that source.

BACK   CLOSE WINDOW

Copyright Clearance Center

RightsLink®

Home   Create Account   Help

ACS Publications
Most Trusted. Most Cited. Most Read.

Title: Nanoporous Structure and Medium-Range Order in Synthetic Amorphous Calcium Carbonate

Author: Andrew L. Goodwin, F. Marc Michel, Brian L. Phillips, et al

Publication: Chemistry of Materials

Publisher: American Chemical Society

Date: May 1, 2010

Copyright © 2010, American Chemical Society

LOGIN

If you're a copyright.com user, you can login to RightsLink using your copyright.com credentials. Already **a RightsLink user** or want to learn more?

PERMISSION/LICENSE IS GRANTED FOR YOUR ORDER AT NO CHARGE

This type of permission/license, instead of the standard Terms & Conditions, is sent to you because no fee is being charged for your order. Please note the following:

- Permission is granted for your request in both print and electronic formats, and translations.
- If figures and/or tables were requested, they may be adapted or used in part.
- Please print this page for your records and send a copy of it to your publisher/graduate school.
- Appropriate credit for the requested material should be given as follows: "Reprinted (adapted) with permission from (COMPLETE REFERENCE CITATION). Copyright (YEAR) American Chemical Society." Insert appropriate information in place of the capitalized words.
- One-time permission is granted only for the use specified in your request. No additional uses are granted (such as derivative works or other editions). For any other uses, please submit a new request.

If credit is given to another source for the material you requested, permission must be obtained from that source.

BACK   CLOSE WINDOW

ELSEVIER LICENSE
TERMS AND CONDITIONS

Jan 02, 2018

This Agreement between Mr. Anders jensen ("You") and Elsevier ("Elsevier") consists of your license details and the terms and conditions provided by Elsevier and Copyright Clearance Center.

License Number	4260801447493
License date	Jan 02, 2018
Licensed Content Publisher	Elsevier
Licensed Content Publication	Journal of Non-Crystalline Solids
Licensed Content Title	Neutron and X-ray diffraction and empirical potential structure refinement modelling of magnesium stabilised amorphous calcium carbonate
Licensed Content Author	G. Cobourne,G. Mountjoy,J.D. Rodriguez-Blanco,L.G. Benning,A.C. Hannon,J.R. Plaisier
Licensed Content Date	Oct 1, 2014
Licensed Content Volume	401
Licensed Content Issue	n/a
Licensed Content Pages	5
Start Page	154
End Page	158
Type of Use	reuse in a thesis/dissertation
Portion	figures/tables/illustrations
Number of figures/tables /illustrations	1
Format	both print and electronic
Are you the author of this Elsevier article?	No
Will you be translating?	No
Original figure numbers	1
Title of your thesis/dissertation	Structure and dynamics of amorphous carbonates related to biomineralization
Expected completion date	Jan 2018
Estimated size (number of pages)	100
Requestor Location	Mr. Anders jensen Carl dahne str. 11 0.02 Potsdam, 14469 Germany Attn: Mr. Anders jensen
Publisher Tax ID	GB 494 6272 12
Total	0.00 USD
Terms and Conditions	

INTRODUCTION

1. The publisher for this copyrighted material is Elsevier. By clicking "accept" in connection with completing this licensing transaction, you agree that the following terms and conditions apply to this transaction (along with the Billing and Payment terms and conditions established by Copyright Clearance Center, Inc. ("CCC"), at the time that you opened your Rightslink account and that are available at any time at http://myaccount.copyright.com).

GENERAL TERMS

2. Elsevier hereby grants you permission to reproduce the aforementioned material subject to the terms and conditions indicated.

3. Acknowledgement: If any part of the material to be used (for example, figures) has appeared in our publication with credit or acknowledgement to another source, permission must also be sought from that source. If such permission is not obtained then that material may not be included in your publication/copies. Suitable acknowledgement to the source must be made, either as a footnote or in a reference list at the end of your publication, as follows:

"Reprinted from Publication title, Vol /edition number, Author(s), Title of article / title of chapter, Pages No., Copyright (Year), with permission from Elsevier [OR APPLICABLE SOCIETY COPYRIGHT OWNER]." Also Lancet special credit - "Reprinted from The Lancet, Vol. number, Author(s), Title of article, Pages No., Copyright (Year), with permission from Elsevier."

4. Reproduction of this material is confined to the purpose and/or media for which permission is hereby given.

5. Altering/Modifying Material: Not Permitted. However figures and illustrations may be altered/adapted minimally to serve your work. Any other abbreviations, additions, deletions and/or any other alterations shall be made only with prior written authorization of Elsevier Ltd. (Please contact Elsevier at permissions@elsevier.com). No modifications can be made to any Lancet figures/tables and they must be reproduced in full.

6. If the permission fee for the requested use of our material is waived in this instance, please be advised that your future requests for Elsevier materials may attract a fee.

7. Reservation of Rights: Publisher reserves all rights not specifically granted in the combination of (i) the license details provided by you and accepted in the course of this licensing transaction, (ii) these terms and conditions and (iii) CCC's Billing and Payment terms and conditions.

8. License Contingent Upon Payment: While you may exercise the rights licensed immediately upon issuance of the license at the end of the licensing process for the transaction, provided that you have disclosed complete and accurate details of your proposed use, no license is finally effective unless and until full payment is received from you (either by publisher or by CCC) as provided in CCC's Billing and Payment terms and conditions. If full payment is not received on a timely basis, then any license preliminarily granted shall be deemed automatically revoked and shall be void as if never granted. Further, in the event that you breach any of these terms and conditions or any of CCC's Billing and Payment terms and conditions, the license is automatically revoked and shall be void as if never granted. Use of materials as described in a revoked license, as well as any use of the materials beyond the scope of an unrevoked license, may constitute copyright infringement and publisher reserves the right to take any and all action to protect its copyright in the materials.

9. Warranties: Publisher makes no representations or warranties with respect to the licensed material.

10. Indemnity: You hereby indemnify and agree to hold harmless publisher and CCC, and their respective officers, directors, employees and agents, from and against any and all

claims arising out of your use of the licensed material other than as specifically authorized pursuant to this license.

11. No Transfer of License: This license is personal to you and may not be sublicensed, assigned, or transferred by you to any other person without publisher's written permission.

12. No Amendment Except in Writing: This license may not be amended except in a writing signed by both parties (or, in the case of publisher, by CCC on publisher's behalf).

13. Objection to Contrary Terms: Publisher hereby objects to any terms contained in any purchase order, acknowledgment, check endorsement or other writing prepared by you, which terms are inconsistent with these terms and conditions or CCC's Billing and Payment terms and conditions. These terms and conditions, together with CCC's Billing and Payment terms and conditions (which are incorporated herein), comprise the entire agreement between you and publisher (and CCC) concerning this licensing transaction. In the event of any conflict between your obligations established by these terms and conditions and those established by CCC's Billing and Payment terms and conditions, these terms and conditions shall control.

14. Revocation: Elsevier or Copyright Clearance Center may deny the permissions described in this License at their sole discretion, for any reason or no reason, with a full refund payable to you. Notice of such denial will be made using the contact information provided by you. Failure to receive such notice will not alter or invalidate the denial. In no event will Elsevier or Copyright Clearance Center be responsible or liable for any costs, expenses or damage incurred by you as a result of a denial of your permission request, other than a refund of the amount(s) paid by you to Elsevier and/or Copyright Clearance Center for denied permissions.

LIMITED LICENSE

The following terms and conditions apply only to specific license types:

15. **Translation**: This permission is granted for non-exclusive world **English** rights only unless your license was granted for translation rights. If you licensed translation rights you may only translate this content into the languages you requested. A professional translator must perform all translations and reproduce the content word for word preserving the integrity of the article.

16. **Posting licensed content on any Website**: The following terms and conditions apply as follows: Licensing material from an Elsevier journal: All content posted to the web site must maintain the copyright information line on the bottom of each image; A hyper-text must be included to the Homepage of the journal from which you are licensing at http://www.sciencedirect.com/science/journal/xxxxx or the Elsevier homepage for books at http://www.elsevier.com; Central Storage: This license does not include permission for a scanned version of the material to be stored in a central repository such as that provided by Heron/XanEdu.

Licensing material from an Elsevier book: A hyper-text link must be included to the Elsevier homepage at http://www.elsevier.com . All content posted to the web site must maintain the copyright information line on the bottom of each image.

Posting licensed content on Electronic reserve: In addition to the above the following clauses are applicable: The web site must be password-protected and made available only to bona fide students registered on a relevant course. This permission is granted for 1 year only. You may obtain a new license for future website posting.

17. **For journal authors:** the following clauses are applicable in addition to the above:
Preprints:
A preprint is an author's own write-up of research results and analysis, it has not been peer-reviewed, nor has it had any other value added to it by a publisher (such as formatting, copyright, technical enhancement etc.).

Authors can share their preprints anywhere at any time. Preprints should not be added to or enhanced in any way in order to appear more like, or to substitute for, the final versions of articles however authors can update their preprints on arXiv or RePEc with their Accepted Author Manuscript (see below).

If accepted for publication, we encourage authors to link from the preprint to their formal publication via its DOI. Millions of researchers have access to the formal publications on ScienceDirect, and so links will help users to find, access, cite and use the best available version. Please note that Cell Press, The Lancet and some society-owned have different preprint policies. Information on these policies is available on the journal homepage.

Accepted Author Manuscripts: An accepted author manuscript is the manuscript of an article that has been accepted for publication and which typically includes author-incorporated changes suggested during submission, peer review and editor-author communications.

Authors can share their accepted author manuscript:

- immediately
  - via their non-commercial person homepage or blog
  - by updating a preprint in arXiv or RePEc with the accepted manuscript
  - via their research institute or institutional repository for internal institutional uses or as part of an invitation-only research collaboration work-group
  - directly by providing copies to their students or to research collaborators for their personal use
  - for private scholarly sharing as part of an invitation-only work group on commercial sites with which Elsevier has an agreement
- After the embargo period
  - via non-commercial hosting platforms such as their institutional repository
  - via commercial sites with which Elsevier has an agreement

In all cases accepted manuscripts should:

- link to the formal publication via its DOI
- bear a CC-BY-NC-ND license - this is easy to do
- if aggregated with other manuscripts, for example in a repository or other site, be shared in alignment with our hosting policy not be added to or enhanced in any way to appear more like, or to substitute for, the published journal article.

Published journal article (JPA): A published journal article (PJA) is the definitive final record of published research that appears or will appear in the journal and embodies all value-adding publishing activities including peer review co-ordination, copy-editing, formatting, (if relevant) pagination and online enrichment.

Policies for sharing publishing journal articles differ for subscription and gold open access articles:

Subscription Articles: If you are an author, please share a link to your article rather than the full-text. Millions of researchers have access to the formal publications on ScienceDirect, and so links will help your users to find, access, cite, and use the best available version. Theses and dissertations which contain embedded PJAs as part of the formal submission can be posted publicly by the awarding institution with DOI links back to the formal publications on ScienceDirect.

If you are affiliated with a library that subscribes to ScienceDirect you have additional private sharing rights for others' research accessed under that agreement. This includes use for classroom teaching and internal training at the institution (including use in course packs

and courseware programs), and inclusion of the article for grant funding purposes.
Gold Open Access Articles: May be shared according to the author-selected end-user
license and should contain a CrossMark logo, the end user license, and a DOI link to the
formal publication on ScienceDirect.
Please refer to Elsevier's posting policy for further information.
18. **For book authors** the following clauses are applicable in addition to the above:
Authors are permitted to place a brief summary of their work online only. You are not
allowed to download and post the published electronic version of your chapter, nor may you
scan the printed edition to create an electronic version. **Posting to a repository:** Authors are
permitted to post a summary of their chapter only in their institution's repository.
19. **Thesis/Dissertation**: If your license is for use in a thesis/dissertation your thesis may be
submitted to your institution in either print or electronic form. Should your thesis be
published commercially, please reapply for permission. These requirements include
permission for the Library and Archives of Canada to supply single copies, on demand, of
the complete thesis and include permission for Proquest/UMI to supply single copies, on
demand, of the complete thesis. Should your thesis be published commercially, please
reapply for permission. Theses and dissertations which contain embedded PJAs as part of
the formal submission can be posted publicly by the awarding institution with DOI links
back to the formal publications on ScienceDirect.

Elsevier Open Access Terms and Conditions

You can publish open access with Elsevier in hundreds of open access journals or in nearly
2000 established subscription journals that support open access publishing. Permitted third
party re-use of these open access articles is defined by the author's choice of Creative
Commons user license. See our open access license policy for more information.
Terms & Conditions applicable to all Open Access articles published with Elsevier:
Any reuse of the article must not represent the author as endorsing the adaptation of the
article nor should the article be modified in such a way as to damage the author's honour or
reputation. If any changes have been made, such changes must be clearly indicated.
The author(s) must be appropriately credited and we ask that you include the end user
license and a DOI link to the formal publication on ScienceDirect.
If any part of the material to be used (for example, figures) has appeared in our publication
with credit or acknowledgement to another source it is the responsibility of the user to
ensure their reuse complies with the terms and conditions determined by the rights holder.
Additional Terms & Conditions applicable to each Creative Commons user license:
CC BY: The CC-BY license allows users to copy, to create extracts, abstracts and new
works from the Article, to alter and revise the Article and to make commercial use of the
Article (including reuse and/or resale of the Article by commercial entities), provided the
user gives appropriate credit (with a link to the formal publication through the relevant
DOI), provides a link to the license, indicates if changes were made and the licensor is not
represented as endorsing the use made of the work. The full details of the license are
available at http://creativecommons.org/licenses/by/4.0.
CC BY NC SA: The CC BY-NC-SA license allows users to copy, to create extracts,
abstracts and new works from the Article, to alter and revise the Article, provided this is not
done for commercial purposes, and that the user gives appropriate credit (with a link to the
formal publication through the relevant DOI), provides a link to the license, indicates if
changes were made and the licensor is not represented as endorsing the use made of the
work. Further, any new works must be made available on the same conditions. The full
details of the license are available at http://creativecommons.org/licenses/by-nc-sa/4.0.
CC BY NC ND: The CC BY-NC-ND license allows users to copy and distribute the Article,
provided this is not done for commercial purposes and further does not permit distribution of

the Article if it is changed or edited in any way, and provided the user gives appropriate credit (with a link to the formal publication through the relevant DOI), provides a link to the license, and that the licensor is not represented as endorsing the use made of the work. The full details of the license are available at http://creativecommons.org/licenses/by-nc-nd/4.0. Any commercial reuse of Open Access articles published with a CC BY NC SA or CC BY NC ND license requires permission from Elsevier and will be subject to a fee. Commercial reuse includes:

- Associating advertising with the full text of the Article
- Charging fees for document delivery or access
- Article aggregation
- Systematic distribution via e-mail lists or share buttons

Posting or linking by commercial companies for use by customers of those companies.

20. **Other Conditions**:

v1.9

Questions? customercare@copyright.com or +1-855-239-3415 (toll free in the US) or +1-978-646-2777.

Copyright Clearance Center

RightsLink®

Home   Create Account   Help

ACS Publications
Most Trusted. Most Cited. Most Read.

Title: Stability and Structure of Hydrated Amorphous Calcium Carbonate

Author: Yuriy G. Bushuev, Aaron R. Finney, P. Mark Rodger

Publication: Crystal Growth and Design

Publisher: American Chemical Society

Date: Nov 1, 2015

Copyright © 2015, American Chemical Society

LOGIN

If you're a copyright.com user, you can login to RightsLink using your copyright.com credentials. Already **a RightsLink user** or want to learn more?

PERMISSION/LICENSE IS GRANTED FOR YOUR ORDER AT NO CHARGE

This type of permission/license, instead of the standard Terms & Conditions, is sent to you because no fee is being charged for your order. Please note the following:

- Permission is granted for your request in both print and electronic formats, and translations.
- If figures and/or tables were requested, they may be adapted or used in part.
- Please print this page for your records and send a copy of it to your publisher/graduate school.
- Appropriate credit for the requested material should be given as follows: "Reprinted (adapted) with permission from (COMPLETE REFERENCE CITATION). Copyright (YEAR) American Chemical Society." Insert appropriate information in place of the capitalized words.
- One-time permission is granted only for the use specified in your request. No additional uses are granted (such as derivative works or other editions). For any other uses, please submit a new request.

If credit is given to another source for the material you requested, permission must be obtained from that source.

BACK   CLOSE WINDOW

Copyright Clearance Center

RightsLink®

ACS Publications
Most Trusted. Most Cited. Most Read.

Title: Effect of pH on Amorphous Calcium Carbonate Structure and Transformation

Author: Dominique J. Tobler, Juan Diego Rodriguez Blanco, Henning O. S rensen, et al

Publication: Crystal Growth and Design

Publisher: American Chemical Society

Date: Aug 1, 2016

Copyright © 2016, American Chemical Society

PERMISSION/LICENSE IS GRANTED FOR YOUR ORDER AT NO CHARGE

This type of permission/license, instead of the standard Terms & Conditions, is sent to you because no fee is being charged for your order. Please note the following:

- Permission is granted for your request in both print and electronic formats, and translations.
- If figures and/or tables were requested, they may be adapted or used in part.
- Please print this page for your records and send a copy of it to your publisher/graduate school.
- Appropriate credit for the requested material should be given as follows: "Reprinted (adapted) with permission from (COMPLETE REFERENCE CITATION). Copyright (YEAR) American Chemical Society." Insert appropriate information in place of the capitalized words.
- One-time permission is granted only for the use specified in your request. No additional uses are granted (such as derivative works or other editions). For any other uses, please submit a new request.

If credit is given to another source for the material you requested, permission must be obtained from that source.

BACK   CLOSE WINDOW

ELSEVIER LICENSE
TERMS AND CONDITIONS

Jan 02, 2018

This Agreement between Mr. Anders jensen ("You") and Elsevier ("Elsevier") consists of your license details and the terms and conditions provided by Elsevier and Copyright Clearance Center.

License Number	4260810189237
License date	Jan 02, 2018
Licensed Content Publisher	Elsevier
Licensed Content Publication	Thermochimica Acta
Licensed Content Title	Crystallization of amorphous calcium carbonate
Licensed Content Author	Nobuyoshi Koga,Yuzou Nakagoe,Haruhiko Tanaka
Licensed Content Date	Sep 7, 1998
Licensed Content Volume	318
Licensed Content Issue	1-2
Licensed Content Pages	6
Start Page	239
End Page	244
Type of Use	reuse in a thesis/dissertation
Intended publisher of new work	other
Portion	figures/tables/illustrations
Number of figures/tables /illustrations	1
Format	both print and electronic
Are you the author of this Elsevier article?	No
Will you be translating?	No
Original figure numbers	figure 3
Title of your thesis/dissertation	Structure and dynamics of amorphous carbonates related to biomineralization
Expected completion date	Jan 2018
Estimated size (number of pages)	100
Requestor Location	Mr. Anders jensen Carl dahne str. 11 0.02 Potsdam, 14469 Germany Attn: Mr. Anders jensen
Publisher Tax ID	GB 494 6272 12
Total	0.00 USD
Terms and Conditions	

INTRODUCTION

1. The publisher for this copyrighted material is Elsevier. By clicking "accept" in connection with completing this licensing transaction, you agree that the following terms and conditions apply to this transaction (along with the Billing and Payment terms and conditions established by Copyright Clearance Center, Inc. ("CCC"), at the time that you opened your Rightslink account and that are available at any time at http://myaccount.copyright.com).

GENERAL TERMS

2. Elsevier hereby grants you permission to reproduce the aforementioned material subject to the terms and conditions indicated.

3. Acknowledgement: If any part of the material to be used (for example, figures) has appeared in our publication with credit or acknowledgement to another source, permission must also be sought from that source. If such permission is not obtained then that material may not be included in your publication/copies. Suitable acknowledgement to the source must be made, either as a footnote or in a reference list at the end of your publication, as follows:

"Reprinted from Publication title, Vol /edition number, Author(s), Title of article / title of chapter, Pages No., Copyright (Year), with permission from Elsevier [OR APPLICABLE SOCIETY COPYRIGHT OWNER]." Also Lancet special credit - "Reprinted from The Lancet, Vol. number, Author(s), Title of article, Pages No., Copyright (Year), with permission from Elsevier."

4. Reproduction of this material is confined to the purpose and/or media for which permission is hereby given.

5. Altering/Modifying Material: Not Permitted. However figures and illustrations may be altered/adapted minimally to serve your work. Any other abbreviations, additions, deletions and/or any other alterations shall be made only with prior written authorization of Elsevier Ltd. (Please contact Elsevier at permissions@elsevier.com). No modifications can be made to any Lancet figures/tables and they must be reproduced in full.

6. If the permission fee for the requested use of our material is waived in this instance, please be advised that your future requests for Elsevier materials may attract a fee.

7. Reservation of Rights: Publisher reserves all rights not specifically granted in the combination of (i) the license details provided by you and accepted in the course of this licensing transaction, (ii) these terms and conditions and (iii) CCC's Billing and Payment terms and conditions.

8. License Contingent Upon Payment: While you may exercise the rights licensed immediately upon issuance of the license at the end of the licensing process for the transaction, provided that you have disclosed complete and accurate details of your proposed use, no license is finally effective unless and until full payment is received from you (either by publisher or by CCC) as provided in CCC's Billing and Payment terms and conditions. If full payment is not received on a timely basis, then any license preliminarily granted shall be deemed automatically revoked and shall be void as if never granted. Further, in the event that you breach any of these terms and conditions or any of CCC's Billing and Payment terms and conditions, the license is automatically revoked and shall be void as if never granted. Use of materials as described in a revoked license, as well as any use of the materials beyond the scope of an unrevoked license, may constitute copyright infringement and publisher reserves the right to take any and all action to protect its copyright in the materials.

9. Warranties: Publisher makes no representations or warranties with respect to the licensed material.

10. Indemnity: You hereby indemnify and agree to hold harmless publisher and CCC, and their respective officers, directors, employees and agents, from and against any and all

claims arising out of your use of the licensed material other than as specifically authorized pursuant to this license.

11. No Transfer of License: This license is personal to you and may not be sublicensed, assigned, or transferred by you to any other person without publisher's written permission.

12. No Amendment Except in Writing: This license may not be amended except in a writing signed by both parties (or, in the case of publisher, by CCC on publisher's behalf).

13. Objection to Contrary Terms: Publisher hereby objects to any terms contained in any purchase order, acknowledgment, check endorsement or other writing prepared by you, which terms are inconsistent with these terms and conditions or CCC's Billing and Payment terms and conditions. These terms and conditions, together with CCC's Billing and Payment terms and conditions (which are incorporated herein), comprise the entire agreement between you and publisher (and CCC) concerning this licensing transaction. In the event of any conflict between your obligations established by these terms and conditions and those established by CCC's Billing and Payment terms and conditions, these terms and conditions shall control.

14. Revocation: Elsevier or Copyright Clearance Center may deny the permissions described in this License at their sole discretion, for any reason or no reason, with a full refund payable to you. Notice of such denial will be made using the contact information provided by you. Failure to receive such notice will not alter or invalidate the denial. In no event will Elsevier or Copyright Clearance Center be responsible or liable for any costs, expenses or damage incurred by you as a result of a denial of your permission request, other than a refund of the amount(s) paid by you to Elsevier and/or Copyright Clearance Center for denied permissions.

LIMITED LICENSE

The following terms and conditions apply only to specific license types:

15. **Translation**: This permission is granted for non-exclusive world **English** rights only unless your license was granted for translation rights. If you licensed translation rights you may only translate this content into the languages you requested. A professional translator must perform all translations and reproduce the content word for word preserving the integrity of the article.

16. **Posting licensed content on any Website**: The following terms and conditions apply as follows: Licensing material from an Elsevier journal: All content posted to the web site must maintain the copyright information line on the bottom of each image; A hyper-text must be included to the Homepage of the journal from which you are licensing at http://www.sciencedirect.com/science/journal/xxxxx or the Elsevier homepage for books at http://www.elsevier.com; Central Storage: This license does not include permission for a scanned version of the material to be stored in a central repository such as that provided by Heron/XanEdu.

Licensing material from an Elsevier book: A hyper-text link must be included to the Elsevier homepage at http://www.elsevier.com . All content posted to the web site must maintain the copyright information line on the bottom of each image.

Posting licensed content on Electronic reserve: In addition to the above the following clauses are applicable: The web site must be password-protected and made available only to bona fide students registered on a relevant course. This permission is granted for 1 year only. You may obtain a new license for future website posting.

17. **For journal authors:** the following clauses are applicable in addition to the above:
Preprints:
A preprint is an author's own write-up of research results and analysis, it has not been peer-reviewed, nor has it had any other value added to it by a publisher (such as formatting, copyright, technical enhancement etc.).

Authors can share their preprints anywhere at any time. Preprints should not be added to or enhanced in any way in order to appear more like, or to substitute for, the final versions of articles however authors can update their preprints on arXiv or RePEc with their Accepted Author Manuscript (see below).

If accepted for publication, we encourage authors to link from the preprint to their formal publication via its DOI. Millions of researchers have access to the formal publications on ScienceDirect, and so links will help users to find, access, cite and use the best available version. Please note that Cell Press, The Lancet and some society-owned have different preprint policies. Information on these policies is available on the journal homepage.

Accepted Author Manuscripts: An accepted author manuscript is the manuscript of an article that has been accepted for publication and which typically includes author-incorporated changes suggested during submission, peer review and editor-author communications.

Authors can share their accepted author manuscript:

- immediately
    - via their non-commercial person homepage or blog
    - by updating a preprint in arXiv or RePEc with the accepted manuscript
    - via their research institute or institutional repository for internal institutional uses or as part of an invitation-only research collaboration work-group
    - directly by providing copies to their students or to research collaborators for their personal use
    - for private scholarly sharing as part of an invitation-only work group on commercial sites with which Elsevier has an agreement
- After the embargo period
    - via non-commercial hosting platforms such as their institutional repository
    - via commercial sites with which Elsevier has an agreement

In all cases accepted manuscripts should:

- link to the formal publication via its DOI
- bear a CC-BY-NC-ND license - this is easy to do
- if aggregated with other manuscripts, for example in a repository or other site, be shared in alignment with our hosting policy not be added to or enhanced in any way to appear more like, or to substitute for, the published journal article.

Published journal article (JPA): A published journal article (PJA) is the definitive final record of published research that appears or will appear in the journal and embodies all value-adding publishing activities including peer review co-ordination, copy-editing, formatting, (if relevant) pagination and online enrichment.

Policies for sharing publishing journal articles differ for subscription and gold open access articles:

Subscription Articles: If you are an author, please share a link to your article rather than the full-text. Millions of researchers have access to the formal publications on ScienceDirect, and so links will help your users to find, access, cite, and use the best available version. Theses and dissertations which contain embedded PJAs as part of the formal submission can be posted publicly by the awarding institution with DOI links back to the formal publications on ScienceDirect.

If you are affiliated with a library that subscribes to ScienceDirect you have additional private sharing rights for others' research accessed under that agreement. This includes use for classroom teaching and internal training at the institution (including use in course packs

and courseware programs), and inclusion of the article for grant funding purposes.
Gold Open Access Articles: May be shared according to the author-selected end-user license and should contain a CrossMark logo, the end user license, and a DOI link to the formal publication on ScienceDirect.
Please refer to Elsevier's posting policy for further information.
18. **For book authors** the following clauses are applicable in addition to the above: Authors are permitted to place a brief summary of their work online only. You are not allowed to download and post the published electronic version of your chapter, nor may you scan the printed edition to create an electronic version. **Posting to a repository:** Authors are permitted to post a summary of their chapter only in their institution's repository.
19. **Thesis/Dissertation**: If your license is for use in a thesis/dissertation your thesis may be submitted to your institution in either print or electronic form. Should your thesis be published commercially, please reapply for permission. These requirements include permission for the Library and Archives of Canada to supply single copies, on demand, of the complete thesis and include permission for Proquest/UMI to supply single copies, on demand, of the complete thesis. Should your thesis be published commercially, please reapply for permission. Theses and dissertations which contain embedded PJAs as part of the formal submission can be posted publicly by the awarding institution with DOI links back to the formal publications on ScienceDirect.

Elsevier Open Access Terms and Conditions

You can publish open access with Elsevier in hundreds of open access journals or in nearly 2000 established subscription journals that support open access publishing. Permitted third party re-use of these open access articles is defined by the author's choice of Creative Commons user license. See our open access license policy for more information.
Terms & Conditions applicable to all Open Access articles published with Elsevier:
Any reuse of the article must not represent the author as endorsing the adaptation of the article nor should the article be modified in such a way as to damage the author's honour or reputation. If any changes have been made, such changes must be clearly indicated.
The author(s) must be appropriately credited and we ask that you include the end user license and a DOI link to the formal publication on ScienceDirect.
If any part of the material to be used (for example, figures) has appeared in our publication with credit or acknowledgement to another source it is the responsibility of the user to ensure their reuse complies with the terms and conditions determined by the rights holder.
Additional Terms & Conditions applicable to each Creative Commons user license:
CC BY: The CC-BY license allows users to copy, to create extracts, abstracts and new works from the Article, to alter and revise the Article and to make commercial use of the Article (including reuse and/or resale of the Article by commercial entities), provided the user gives appropriate credit (with a link to the formal publication through the relevant DOI), provides a link to the license, indicates if changes were made and the licensor is not represented as endorsing the use made of the work. The full details of the license are available at http://creativecommons.org/licenses/by/4.0.
CC BY NC SA: The CC BY-NC-SA license allows users to copy, to create extracts, abstracts and new works from the Article, to alter and revise the Article, provided this is not done for commercial purposes, and that the user gives appropriate credit (with a link to the formal publication through the relevant DOI), provides a link to the license, indicates if changes were made and the licensor is not represented as endorsing the use made of the work. Further, any new works must be made available on the same conditions. The full details of the license are available at http://creativecommons.org/licenses/by-nc-sa/4.0.
CC BY NC ND: The CC BY-NC-ND license allows users to copy and distribute the Article, provided this is not done for commercial purposes and further does not permit distribution of

the Article if it is changed or edited in any way, and provided the user gives appropriate credit (with a link to the formal publication through the relevant DOI), provides a link to the license, and that the licensor is not represented as endorsing the use made of the work. The full details of the license are available at http://creativecommons.org/licenses/by-nc-nd/4.0. Any commercial reuse of Open Access articles published with a CC BY NC SA or CC BY NC ND license requires permission from Elsevier and will be subject to a fee. Commercial reuse includes:

- Associating advertising with the full text of the Article
- Charging fees for document delivery or access
- Article aggregation
- Systematic distribution via e-mail lists or share buttons

Posting or linking by commercial companies for use by customers of those companies.

20. **Other Conditions**:

v1.9

Questions? customercare@copyright.com or +1-855-239-3415 (toll free in the US) or +1-978-646-2777.

<div align="center">

ELSEVIER LICENSE
TERMS AND CONDITIONS

Jan 02, 2018

</div>

This Agreement between Mr. Anders jensen ("You") and Elsevier ("Elsevier") consists of your license details and the terms and conditions provided by Elsevier and Copyright Clearance Center.

License Number	4260810375312
License date	Jan 02, 2018
Licensed Content Publisher	Elsevier
Licensed Content Publication	Geochimica et Cosmochimica Acta
Licensed Content Title	Formation condition of monohydrocalcite from CaCl2–MgCl2–Na2CO3 solutions
Licensed Content Author	Risa Nishiyama,Takashi Munemoto,Keisuke Fukushi
Licensed Content Date	Jan 1, 2013
Licensed Content Volume	100
Licensed Content Issue	n/a
Licensed Content Pages	15
Start Page	217
End Page	231
Type of Use	reuse in a thesis/dissertation
Intended publisher of new work	other
Portion	figures/tables/illustrations
Number of figures/tables /illustrations	1
Format	both print and electronic
Are you the author of this Elsevier article?	No
Will you be translating?	No
Original figure numbers	figure 8
Title of your thesis/dissertation	Structure and dynamics of amorphous carbonates related to biomineralization
Expected completion date	Jan 2018
Estimated size (number of pages)	100
Requestor Location	Mr. Anders jensen Carl dahne str. 11 0.02 Potsdam, 14469 Germany Attn: Mr. Anders jensen
Publisher Tax ID	GB 494 6272 12
Total	0.00 USD

Terms and Conditions

INTRODUCTION

1. The publisher for this copyrighted material is Elsevier. By clicking "accept" in connection with completing this licensing transaction, you agree that the following terms and conditions apply to this transaction (along with the Billing and Payment terms and conditions established by Copyright Clearance Center, Inc. ("CCC"), at the time that you opened your Rightslink account and that are available at any time at http://myaccount.copyright.com).

GENERAL TERMS

2. Elsevier hereby grants you permission to reproduce the aforementioned material subject to the terms and conditions indicated.

3. Acknowledgement: If any part of the material to be used (for example, figures) has appeared in our publication with credit or acknowledgement to another source, permission must also be sought from that source. If such permission is not obtained then that material may not be included in your publication/copies. Suitable acknowledgement to the source must be made, either as a footnote or in a reference list at the end of your publication, as follows:

"Reprinted from Publication title, Vol /edition number, Author(s), Title of article / title of chapter, Pages No., Copyright (Year), with permission from Elsevier [OR APPLICABLE SOCIETY COPYRIGHT OWNER]." Also Lancet special credit - "Reprinted from The Lancet, Vol. number, Author(s), Title of article, Pages No., Copyright (Year), with permission from Elsevier."

4. Reproduction of this material is confined to the purpose and/or media for which permission is hereby given.

5. Altering/Modifying Material: Not Permitted. However figures and illustrations may be altered/adapted minimally to serve your work. Any other abbreviations, additions, deletions and/or any other alterations shall be made only with prior written authorization of Elsevier Ltd. (Please contact Elsevier at permissions@elsevier.com). No modifications can be made to any Lancet figures/tables and they must be reproduced in full.

6. If the permission fee for the requested use of our material is waived in this instance, please be advised that your future requests for Elsevier materials may attract a fee.

7. Reservation of Rights: Publisher reserves all rights not specifically granted in the combination of (i) the license details provided by you and accepted in the course of this licensing transaction, (ii) these terms and conditions and (iii) CCC's Billing and Payment terms and conditions.

8. License Contingent Upon Payment: While you may exercise the rights licensed immediately upon issuance of the license at the end of the licensing process for the transaction, provided that you have disclosed complete and accurate details of your proposed use, no license is finally effective unless and until full payment is received from you (either by publisher or by CCC) as provided in CCC's Billing and Payment terms and conditions. If full payment is not received on a timely basis, then any license preliminarily granted shall be deemed automatically revoked and shall be void as if never granted. Further, in the event that you breach any of these terms and conditions or any of CCC's Billing and Payment terms and conditions, the license is automatically revoked and shall be void as if never granted. Use of materials as described in a revoked license, as well as any use of the materials beyond the scope of an unrevoked license, may constitute copyright infringement and publisher reserves the right to take any and all action to protect its copyright in the materials.

9. Warranties: Publisher makes no representations or warranties with respect to the licensed material.

10. Indemnity: You hereby indemnify and agree to hold harmless publisher and CCC, and their respective officers, directors, employees and agents, from and against any and all

claims arising out of your use of the licensed material other than as specifically authorized pursuant to this license.

11. No Transfer of License: This license is personal to you and may not be sublicensed, assigned, or transferred by you to any other person without publisher's written permission.

12. No Amendment Except in Writing: This license may not be amended except in a writing signed by both parties (or, in the case of publisher, by CCC on publisher's behalf).

13. Objection to Contrary Terms: Publisher hereby objects to any terms contained in any purchase order, acknowledgment, check endorsement or other writing prepared by you, which terms are inconsistent with these terms and conditions or CCC's Billing and Payment terms and conditions. These terms and conditions, together with CCC's Billing and Payment terms and conditions (which are incorporated herein), comprise the entire agreement between you and publisher (and CCC) concerning this licensing transaction. In the event of any conflict between your obligations established by these terms and conditions and those established by CCC's Billing and Payment terms and conditions, these terms and conditions shall control.

14. Revocation: Elsevier or Copyright Clearance Center may deny the permissions described in this License at their sole discretion, for any reason or no reason, with a full refund payable to you. Notice of such denial will be made using the contact information provided by you. Failure to receive such notice will not alter or invalidate the denial. In no event will Elsevier or Copyright Clearance Center be responsible or liable for any costs, expenses or damage incurred by you as a result of a denial of your permission request, other than a refund of the amount(s) paid by you to Elsevier and/or Copyright Clearance Center for denied permissions.

LIMITED LICENSE

The following terms and conditions apply only to specific license types:

15. **Translation**: This permission is granted for non-exclusive world **English** rights only unless your license was granted for translation rights. If you licensed translation rights you may only translate this content into the languages you requested. A professional translator must perform all translations and reproduce the content word for word preserving the integrity of the article.

16. **Posting licensed content on any Website**: The following terms and conditions apply as follows: Licensing material from an Elsevier journal: All content posted to the web site must maintain the copyright information line on the bottom of each image; A hyper-text must be included to the Homepage of the journal from which you are licensing at http://www.sciencedirect.com/science/journal/xxxxx or the Elsevier homepage for books at http://www.elsevier.com; Central Storage: This license does not include permission for a scanned version of the material to be stored in a central repository such as that provided by Heron/XanEdu.

Licensing material from an Elsevier book: A hyper-text link must be included to the Elsevier homepage at http://www.elsevier.com . All content posted to the web site must maintain the copyright information line on the bottom of each image.

Posting licensed content on Electronic reserve: In addition to the above the following clauses are applicable: The web site must be password-protected and made available only to bona fide students registered on a relevant course. This permission is granted for 1 year only. You may obtain a new license for future website posting.

17. **For journal authors:** the following clauses are applicable in addition to the above:
Preprints:
A preprint is an author's own write-up of research results and analysis, it has not been peer-reviewed, nor has it had any other value added to it by a publisher (such as formatting, copyright, technical enhancement etc.).

Authors can share their preprints anywhere at any time. Preprints should not be added to or enhanced in any way in order to appear more like, or to substitute for, the final versions of articles however authors can update their preprints on arXiv or RePEc with their Accepted Author Manuscript (see below).

If accepted for publication, we encourage authors to link from the preprint to their formal publication via its DOI. Millions of researchers have access to the formal publications on ScienceDirect, and so links will help users to find, access, cite and use the best available version. Please note that Cell Press, The Lancet and some society-owned have different preprint policies. Information on these policies is available on the journal homepage.

Accepted Author Manuscripts: An accepted author manuscript is the manuscript of an article that has been accepted for publication and which typically includes author-incorporated changes suggested during submission, peer review and editor-author communications.

Authors can share their accepted author manuscript:

- immediately
    - via their non-commercial person homepage or blog
    - by updating a preprint in arXiv or RePEc with the accepted manuscript
    - via their research institute or institutional repository for internal institutional uses or as part of an invitation-only research collaboration work-group
    - directly by providing copies to their students or to research collaborators for their personal use
    - for private scholarly sharing as part of an invitation-only work group on commercial sites with which Elsevier has an agreement
- After the embargo period
    - via non-commercial hosting platforms such as their institutional repository
    - via commercial sites with which Elsevier has an agreement

In all cases accepted manuscripts should:

- link to the formal publication via its DOI
- bear a CC-BY-NC-ND license - this is easy to do
- if aggregated with other manuscripts, for example in a repository or other site, be shared in alignment with our hosting policy not be added to or enhanced in any way to appear more like, or to substitute for, the published journal article.

Published journal article (JPA): A published journal article (PJA) is the definitive final record of published research that appears or will appear in the journal and embodies all value-adding publishing activities including peer review co-ordination, copy-editing, formatting, (if relevant) pagination and online enrichment.

Policies for sharing publishing journal articles differ for subscription and gold open access articles:

Subscription Articles: If you are an author, please share a link to your article rather than the full-text. Millions of researchers have access to the formal publications on ScienceDirect, and so links will help your users to find, access, cite, and use the best available version. Theses and dissertations which contain embedded PJAs as part of the formal submission can be posted publicly by the awarding institution with DOI links back to the formal publications on ScienceDirect.

If you are affiliated with a library that subscribes to ScienceDirect you have additional private sharing rights for others' research accessed under that agreement. This includes use for classroom teaching and internal training at the institution (including use in course packs

and courseware programs), and inclusion of the article for grant funding purposes.
Gold Open Access Articles: May be shared according to the author-selected end-user license and should contain a CrossMark logo, the end user license, and a DOI link to the formal publication on ScienceDirect.
Please refer to Elsevier's posting policy for further information.
18. **For book authors** the following clauses are applicable in addition to the above:
Authors are permitted to place a brief summary of their work online only. You are not allowed to download and post the published electronic version of your chapter, nor may you scan the printed edition to create an electronic version. **Posting to a repository:** Authors are permitted to post a summary of their chapter only in their institution's repository.
19. **Thesis/Dissertation**: If your license is for use in a thesis/dissertation your thesis may be submitted to your institution in either print or electronic form. Should your thesis be published commercially, please reapply for permission. These requirements include permission for the Library and Archives of Canada to supply single copies, on demand, of the complete thesis and include permission for Proquest/UMI to supply single copies, on demand, of the complete thesis. Should your thesis be published commercially, please reapply for permission. Theses and dissertations which contain embedded PJAs as part of the formal submission can be posted publicly by the awarding institution with DOI links back to the formal publications on ScienceDirect.

Elsevier Open Access Terms and Conditions

You can publish open access with Elsevier in hundreds of open access journals or in nearly 2000 established subscription journals that support open access publishing. Permitted third party re-use of these open access articles is defined by the author's choice of Creative Commons user license. See our open access license policy for more information.
Terms & Conditions applicable to all Open Access articles published with Elsevier:
Any reuse of the article must not represent the author as endorsing the adaptation of the article nor should the article be modified in such a way as to damage the author's honour or reputation. If any changes have been made, such changes must be clearly indicated.
The author(s) must be appropriately credited and we ask that you include the end user license and a DOI link to the formal publication on ScienceDirect.
If any part of the material to be used (for example, figures) has appeared in our publication with credit or acknowledgement to another source it is the responsibility of the user to ensure their reuse complies with the terms and conditions determined by the rights holder.
Additional Terms & Conditions applicable to each Creative Commons user license:
CC BY: The CC-BY license allows users to copy, to create extracts, abstracts and new works from the Article, to alter and revise the Article and to make commercial use of the Article (including reuse and/or resale of the Article by commercial entities), provided the user gives appropriate credit (with a link to the formal publication through the relevant DOI), provides a link to the license, indicates if changes were made and the licensor is not represented as endorsing the use made of the work. The full details of the license are available at http://creativecommons.org/licenses/by/4.0.
CC BY NC SA: The CC BY-NC-SA license allows users to copy, to create extracts, abstracts and new works from the Article, to alter and revise the Article, provided this is not done for commercial purposes, and that the user gives appropriate credit (with a link to the formal publication through the relevant DOI), provides a link to the license, indicates if changes were made and the licensor is not represented as endorsing the use made of the work. Further, any new works must be made available on the same conditions. The full details of the license are available at http://creativecommons.org/licenses/by-nc-sa/4.0.
CC BY NC ND: The CC BY-NC-ND license allows users to copy and distribute the Article, provided this is not done for commercial purposes and further does not permit distribution of

the Article if it is changed or edited in any way, and provided the user gives appropriate credit (with a link to the formal publication through the relevant DOI), provides a link to the license, and that the licensor is not represented as endorsing the use made of the work. The full details of the license are available at http://creativecommons.org/licenses/by-nc-nd/4.0. Any commercial reuse of Open Access articles published with a CC BY NC SA or CC BY NC ND license requires permission from Elsevier and will be subject to a fee. Commercial reuse includes:

- Associating advertising with the full text of the Article
- Charging fees for document delivery or access
- Article aggregation
- Systematic distribution via e-mail lists or share buttons

Posting or linking by commercial companies for use by customers of those companies.

20. **Other Conditions**:

v1.9

Questions? customercare@copyright.com or +1-855-239-3415 (toll free in the US) or +1-978-646-2777.

ROYAL SOCIETY OF CHEMISTRY LICENSE
TERMS AND CONDITIONS

Jan 02, 2018

This Agreement between Mr. Anders jensen ("You") and Royal Society of Chemistry ("Royal Society of Chemistry") consists of your license details and the terms and conditions provided by Royal Society of Chemistry and Copyright Clearance Center.

License Number	4260810620087
License date	Jan 02, 2018
Licensed Content Publisher	Royal Society of Chemistry
Licensed Content Publication	CrystEngComm
Licensed Content Title	In situ total X-ray scattering study of the formation mechanism and structural defects in anatase TiO2 nanoparticles under hydrothermal conditions
Licensed Content Author	Jian-Li Mi,Kirsten M. . Jensen,Christoffer Tyrsted,Martin Bremholm,Bo B. Iversen
Licensed Content Date	Apr 20, 2015
Licensed Content Volume	17
Licensed Content Issue	36
Type of Use	Thesis/Dissertation
Requestor type	academic/educational
Portion	figures/tables/images
Number of figures/tables /images	1
Format	print and electronic
Distribution quantity	10
Will you be translating?	no
Order reference number	
Title of the thesis/dissertation	Structure and dynamics of amorphous carbonates related to biomineralization
Expected completion date	Jan 2018
Estimated size	100
Requestor Location	Mr. Anders jensen Carl dahne str. 11 0.02 Potsdam, 14469 Germany Attn: Mr. Anders jensen
Billing Type	Invoice
Billing Address	Mr. Anders jensen Carl dahne str. 11 0.02 Potsdam, Germany 14469 Attn: Mr. Anders jensen
Total	0.00 USD

This License Agreement is between {Requestor Name} ("You") and The Royal Society of Chemistry ("RSC") provided by the Copyright Clearance Center ("CCC"). The license consists of your order details, the terms and conditions provided by the Royal Society of Chemistry, and the payment terms and conditions.

RSC / TERMS AND CONDITIONS

INTRODUCTION

The publisher for this copyrighted material is The Royal Society of Chemistry. By clicking "accept" in connection with completing this licensing transaction, you agree that the following terms and conditions apply to this transaction (along with the Billing and Payment terms and conditions established by CCC, at the time that you opened your RightsLink account and that are available at any time at .

LICENSE GRANTED

The RSC hereby grants you a non-exclusive license to use the aforementioned material anywhere in the world subject to the terms and conditions indicated herein. Reproduction of the material is confined to the purpose and/or media for which permission is hereby given.

RESERVATION OF RIGHTS

The RSC reserves all rights not specifically granted in the combination of (i) the license details provided by your and accepted in the course of this licensing transaction; (ii) these terms and conditions; and (iii) CCC's Billing and Payment terms and conditions.

REVOCATION

The RSC reserves the right to revoke this license for any reason, including, but not limited to, advertising and promotional uses of RSC content, third party usage, and incorrect source figure attribution.

THIRD-PARTY MATERIAL DISCLAIMER

If part of the material to be used (for example, a figure) has appeared in the RSC publication with credit to another source, permission must also be sought from that source. If the other source is another RSC publication these details should be included in your RightsLink request. If the other source is a third party, permission must be obtained from the third party. The RSC disclaims any responsibility for the reproduction you make of items owned by a third party.

PAYMENT OF FEE

If the permission fee for the requested material is waived in this instance, please be advised that any future requests for the reproduction of RSC materials may attract a fee.

ACKNOWLEDGEMENT

The reproduction of the licensed material must be accompanied by the following acknowledgement:

Reproduced ("Adapted" or "in part") from {Reference Citation} (or Ref XX) with permission of The Royal Society of Chemistry.

If the licensed material is being reproduced from New Journal of Chemistry (NJC), Photochemical & Photobiological Sciences (PPS) or Physical Chemistry Chemical Physics (PCCP) you must include one of the following acknowledgements:

For figures originally published in NJC:

Reproduced ("Adapted" or "in part") from {Reference Citation} (or Ref XX) with permission of The Royal Society of Chemistry (RSC) on behalf of the European Society for Photobiology, the European Photochemistry Association and the RSC.

For figures originally published in PPS:

Reproduced ("Adapted" or "in part") from {Reference Citation} (or Ref XX) with permission of The Royal Society of Chemistry (RSC) on behalf of the Centre National de la Recherche Scientifique (CNRS) and the RSC.

For figures originally published in PCCP:

Reproduced ("Adapted" or "in part") from {Reference Citation} (or Ref XX) with permission of the PCCP Owner Societies.

HYPERTEXT LINKS

With any material which is being reproduced in electronic form, you must include a hypertext link to the original RSC article on the RSC's website. The recommended form for the hyperlink is http://dx.doi.org/10.1039/DOI suffix, for example in the link http://dx.doi.org/10.1039/b110420a the DOI suffix is 'b110420a'. To find the relevant DOI suffix for the RSC article in question, go to the Journals section of the website and locate the article in the list of papers for the volume and issue of your specific journal. You will find the DOI suffix quoted there.

LICENSE CONTINGENT ON PAYMENT

While you may exercise the rights licensed immediately upon issuance of the license at the end of the licensing process for the transaction, provided that you have disclosed complete and accurate details of your proposed use, no license is finally effective unless and until full payment is received from you (by CCC) as provided in CCC's Billing and Payment terms and conditions. If full payment is not received on a timely basis, then any license preliminarily granted shall be deemed automatically revoked and shall be void as if never granted. Further, in the event that you breach any of these terms and conditions or any of CCC's Billing and Payment terms and conditions, the license is automatically revoked and shall be void as if never granted. Use of materials as described in a revoked license, as well as any use of the materials beyond the scope of an unrevoked license, may constitute copyright infringement and the RSC reserves the right to take any and all action to protect its copyright in the materials.

WARRANTIES

The RSC makes no representations or warranties with respect to the licensed material.

INDEMNITY

You hereby indemnify and agree to hold harmless the RSC and the CCC, and their respective officers, directors, trustees, employees and agents, from and against any and all claims arising out of your use of the licensed material other than as specifically authorized pursuant to this licence.

NO TRANSFER OF LICENSE

This license is personal to you or your publisher and may not be sublicensed, assigned, or transferred by you to any other person without the RSC's written permission.

NO AMENDMENT EXCEPT IN WRITING

This license may not be amended except in a writing signed by both parties (or, in the case of "Other Conditions, v1.2", by CCC on the RSC's behalf).

OBJECTION TO CONTRARY TERMS

You hereby acknowledge and agree that these terms and conditions, together with CCC's Billing and Payment terms and conditions (which are incorporated herein), comprise the entire agreement between you and the RSC (and CCC) concerning this licensing transaction, to the exclusion of all other terms and conditions, written or verbal, express or implied (including any terms contained in any purchase order, acknowledgment, check endorsement or other writing prepared by you). In the event of any conflict between your obligations established by these terms and conditions and those established by CCC's Billing and Payment terms and conditions, these terms and conditions shall control.

JURISDICTION

This license transaction shall be governed by and construed in accordance with the laws of the District of Columbia. You hereby agree to submit to the jurisdiction of the courts located in the District of Columbia for purposes of resolving any disputes that may arise in connection with this licensing transaction.

LIMITED LICENSE

The following terms and conditions apply to specific license types:

Translation

This permission is granted for non-exclusive world English rights only unless your license was granted for translation rights. If you licensed translation rights you may only translate this content into the languages you requested. A professional translator must perform all translations and reproduce the content word for word preserving the integrity of the article.

Intranet

If the licensed material is being posted on an Intranet, the Intranet is to be password-protected and made available only to bona fide students or employees only. All content posted to the Intranet must maintain the copyright information line on the bottom of each image. You must also fully reference the material and include a hypertext link as specified above.

Copies of Whole Articles

All copies of whole articles must maintain, if available, the copyright information line on the bottom of each page.

Other Conditions

v1.2

Gratis licenses (referencing $0 in the Total field) are free. Please retain this printable license for your reference. No payment is required.

If you would like to pay for this license now, please remit this license along with yourpayment made payable to "COPYRIGHT CLEARANCE CENTER" otherwise you will be invoiced within 48 hours of the license date. Payment should be in the form of a check or money order referencing your account number and this invoice number {Invoice Number}. Once you receive your invoice for this order, you may pay your invoice by credit card. Please follow instructions provided at that time.

Make Payment To:

Copyright Clearance Center

29118 Network Place

Chicago, IL 60673-1291

For suggestions or comments regarding this order, contact Rightslink Customer Support: customercare@copyright.com or +1-855-239-3415 (toll free in the US) or +1-978-646-2777.

Questions? customercare@copyright.com or +1-855-239-3415 (toll free in the US) or +1-978-646-2777.